NEW DEVELOPMENTS IN THE FINITE ELEMENT
ANALYSIS OF SHELLS

G.M. Lindberg, M.D. Olson and G.R. Cowper

Structures and Materials Laboratory

National Aeronautical Establishment

1.0 INTRODUCTION

Considerable progress has been made in the past few years in applying the finite element method to the analysis of shell structures. The initial work in this area was devoted to shells of revolution in which closed rings or conical shell segments were used to model complete structures. Much of this work is reviewed by Jones and Strome[1].

Attempts to develop a finite element method for general shell structures have generally followed two different courses. In the first approach, the shell is replaced by an assemblage of flat plate elements that are either triangular or quadrilateral in shape. Each plate element is connected in some fashion to those surrounding it, and undergoes both bending and stretching deformations. This approach has been successfully employed for cylindrical geometry by Hrennikoff and Tezcan[2] and for general shell shapes by Zienkiewicz and Cheung[3], Clough and Johnson[4], and Carr[5]. However, the method has the disadvantage that there is no coupling between bending and stretching within each element, and consequently a large number of elements must be used to achieve satisfactory accuracy.

The second approach, which ultimately should yield better results, is to develop curved shell elements that permit closer geometrical representations of a shell structure. Such an approach has been followed with good results for the case of cylindrical shells where rectangular elements are generally adequate. Successful cylindrical shell elements have been developed by Bogner, Fox and Schmit[6], Cantin and Clough[7], and Olson and Lindberg[8].

On the other hand, attempts to develop rectangular or quadrilateral elements for general shells have been only partially successful. For example, Connor and Brebbia[9] have introduced a rectangular element based on shallow shell theory, and Gallagher[10] has developed a quadrilateral element for translational shells. However, both elements use only linear distributions for the tangential displacements and consequently do not incorporate all the required rigid body modes. Although this does not preclude convergence to the correct answer, it does mean that the elements are far too stiff and therefore are quite inefficient.

Several curved shallow shell elements of arbitrary triangular shape have now been developed. Utku and Melosh[11] have introduced a shallow curved triangular element based only on linear displacement distributions. This element is consequently too stiff. More recently, Strickland and Loden[12] have presented another shallow curved triangular element based on a cubic variation for the normal displacement and linear variations for the tangential displacements. This element is a distinct advancement over the

FOREWORD

The Quarterly Bulletin is designed primarily for the information of Canadian industry, Universities, and Government Departments and agencies. It provides a regular review of the interests and current activities of two Divisions of the National Research Council of Canada:

The Division of Mechanical Engineering
The National Aeronautical Establishment

Some of the work of the two Divisions comprises classified projects that may not be freely reported and contractual projects of limited general interest. Other work, not generally reported herein, includes calibrations, routine analysis and the testing of proprietary products.

Comments or enquiries relating to any matter published in this Bulletin should be addressed to the Editor, DME/NAE Bulletin, National Research Council of Canada, Ottawa, mentioning the number of the Bulletin.

FORCE DE FRAPPE EXECUTING DRY SURFACE
IMPACT TEST AT 47 mph, VIEWED FROM CEN-
TRAL TOWER AND OBSERVATION POST ROCK-
CLIFFE TEST AREA (8-11 POST CENTRES, 25°
ANGLE BARRIER).

STRUCTURES AND MATERIALS LABORATORY
NATIONAL AERONAUTICAL ESTABLISHMENT

CONTENTS

CONTENTS (Cont'd)

ILLUSTRATIONS

ILLUSTRATIONS (Cont'd)

ILLUSTRATIONS (Cont'd)

former one, but appears to offer little improvement in accuracy over the comparable flat plate model of Clough and Johnson[4]. Bonnes, Dhatt, Giroux, and Robichaud[13] have introduced a shallow curved triangular element based on a cubic variation for all three displacement components. They actually present results for two versions of this element, one with 27 degrees of freedom and the other with 36. The latter version incorporates the normal derivatives of u, v, and w at mid-edge nodes as the extra degrees of freedom and, hence, allows the normal derivatives to vary quadratically along an edge, whereas the former one has only a linear variation. Both elements appear to give somewhat better results than the element of Strickland and Loden[12]. However, the 36-degree-of-freedom version has the distinct disadvantage of having mid-edge nodes, and the other model is somewhat limited by having only a linear variation of normal derivatives along each edge.

All the foregoing elements have disadvantages common to triangular plate-bending elements as well, and it is not surprising that the development of a good triangular curved shell element has been impeded by the lack of a satisfactory conforming triangular plate-bending element. Only recently has such a plate-bending element been developed by Cowper, Kosko, Lindberg and Olson,[14-16] and also by Bell[17,18] and Butlin and Ford[19]. This element uses as generalized co-ordinates the transverse displacement and its first and second derivatives at each vertex, a total of 18 in all. The displacement function for the element contains a complete quartic polynomial plus some higher degree terms and allows a cubic variation of the normal slope along each edge. It is shown[15,16] that use of this element leads to strain energy convergence rates approaching n^{-6}, where n is the number of elements per side of a plate. Along with this rapid rate of convergence, it was also found that remarkably accurate displacement and stress predictions were obtained, even with coarse grids of elements.

The following article is concerned with extending this highly successful approach to the analysis of arbitrarily shaped shell structures. As a first step in this direction, the application to shallow shells is investigated, and a shallow shell element of general triangular shape is formulated and tested. This element proves to be exceptionally efficient, yielding displacement and stress predictions of comparable accuracy to that of the plate-bending element discussed above. Finally, the methodology for applying this shallow shell element to arbitrary deep shells is developed and tested with numerical applications.

2.0 A REFINED SHALLOW SHELL FINITE ELEMENT

In this section, a brief derivation of the refined shallow shell element and numerical results from one application are given. A more complete development and additional numerical results are available in Reference 20.

2.1 Theoretical Formulation

2.1.1 Strain Energy

The geometry for an arbitrary triangular shallow shell element is shown in Figure 1. The shell shape is defined by the height $\zeta(\xi, \eta)$ above the base plane, in which ξ, η are taken as local co-ordinates and x, y as global co-ordinates. The dimensions a, b, c of the base triangle 1'2'3', and the rotation angle θ, are easily derived in terms of the global co-ordinates of the vertices[15,16].

Following the shallow shell theory of Novozhilov,[21] the membrane strains in the shell are given by

$$\epsilon_{\xi\xi} = u_\xi - \zeta_{\xi\xi} w$$

$$\epsilon_{\eta\eta} = v_\eta - \zeta_{\eta\eta} w \tag{1}$$

$$\epsilon_{\xi\eta} = u_\eta + v_\xi - 2\zeta_{\xi\eta} w$$

where u and v are the tangential displacements measured parallel to the ξ and η directions, respectively, and w is the normal displacement (Fig. 1). The subscripts on u, v, w and ζ denote differentiation, i.e. $u_\xi = \partial u/\partial\xi$ etc. The bending strains are given by

$$\kappa_{\xi\xi} = - w_{\xi\xi}, \qquad \kappa_{\eta\eta} = - w_{\eta\eta}, \qquad \kappa_{\xi\eta} = - 2w_{\xi\eta} \tag{2}$$

Combining the contributions from the membrane and bending strains yields the strain energy density

$$\frac{dU}{dA} = \frac{Et}{2(1-\nu^2)}\left\{\left[\epsilon_{\xi\xi}{}^2 + \epsilon_{\eta\eta}{}^2 + 2\nu\epsilon_{\xi\xi}\epsilon_{\eta\eta} + \frac{1}{2}(1-\nu)\epsilon_{\xi\eta}{}^2\right]\right.$$
$$\left. + \frac{t^2}{12}\left[\kappa_{\xi\xi}{}^2 + \kappa_{\eta\eta}{}^2 + 2\nu\kappa_{\xi\xi}\kappa_{\eta\eta} + \frac{1}{2}(1-\nu)\kappa_{\xi\eta}{}^2\right]\right\} \tag{3}$$

For shallow shells, the area of the shell surface is approximately equal to its projected area, and hence equation (3) may be integrated over the base plane. Then combining equations (1) to (3) yields the final strain energy expression

$$U = \frac{Et}{2(1-\nu^2)}\iint\left\{\left[u_\xi{}^2 + v_\eta{}^2 + 2\nu u_\xi v_\eta + \frac{1}{2}(1-\nu)(u_\eta + v_\xi)^2\right]\right.$$
$$- 2\left[(\zeta_{\xi\xi} + \nu\zeta_{\eta\eta})u_\xi + (\zeta_{\eta\eta} + \nu\zeta_{\xi\xi})v_\eta + (1-\nu)\zeta_{\xi\eta}(u_\eta + v_\xi)\right]w$$
$$+ \left[\zeta_{\xi\xi}{}^2 + \zeta_{\eta\eta}{}^2 + 2\nu\zeta_{\xi\xi}\zeta_{\eta\eta} + 2(1-\nu)\zeta_{\xi\eta}{}^2\right]w^2$$
$$\left. + \frac{t^2}{12}\left[w_{\xi\xi}{}^2 + w_{\eta\eta}{}^2 + 2\nu w_{\xi\xi}w_{\eta\eta} + 2(1-\nu)w_{\xi\eta}{}^2\right]\right\}d\xi\,d\eta \tag{4}$$

where the integration is over the base triangle 1'2'3' in Figure 1.

In the present work, the function $\zeta(\xi,\eta)$ is assumed to be of quadratic form

$$\zeta(\xi,\eta) = c_1 + c_2\xi + c_3\eta + c_4\xi^2 + c_5\xi\eta + c_6\eta^2 \tag{5}$$

This implies that the shell element has constant curvatures, and this is consistent with the approximations of shallow shell theory. It may be noted from equation (4) that the shell curvatures are the only shape quantities required in calculating strain energy. Therefore, they may be specified for an element directly (which is the approach followed in this Section), or they may be calculated from equation (5) once the constants therein have been determined. One convenient way to do this is to specify the height of the shell at points 1', 2', and 3', and also at the mid-edge points of the element of Figure 1. This is the approach followed in the deep shell applications of the next Section.

2.1.2 Displacements

Special displacement functions are required for the present element in order to ensure conformity and high accuracy. The displacement function developed for the conforming plate-bending element (Ref. 15, 16) is used here for the normal displacement w. In Reference 20, it is shown that the use of complete cubic polynomials for each of the tangential displacements u and v leads to an asymptotic strain energy convergence rate of n^{-6}, where n is the number of elements per side of a shallow shell.

Hence, the starting point for the present shallow shell element is to assume u, v, and w in the form (Fig. 1)

$$u = a_1 + a_2\xi + a_3\eta + a_4\xi^2 + a_5\xi\eta + a_6\eta^2 + a_7\xi^3 + a_8\xi^2\eta + a_9\xi\eta^2 + a_{10}\eta^3 \quad (6a)$$

$$v = a_{11} + a_{12}\xi + a_{13}\eta + a_{14}\xi^2 + a_{15}\xi\eta + a_{16}\eta^2 + a_{17}\xi^3 + a_{18}\xi^2\eta + a_{19}\xi\eta^2 + a_{20}\eta^3 \quad (6b)$$

$$\begin{aligned} w = a_{21} + a_{22}\xi + a_{23}\eta + a_{24}\xi^2 + a_{25}\xi\eta + a_{26}\eta^2 + a_{27}\xi^3 + a_{28}\xi^2\eta \\ + a_{29}\xi\eta^2 + a_{30}\eta^3 + a_{31}\xi^4 + a_{32}\xi^3\eta + a_{33}\xi^2\eta^2 + a_{34}\xi\eta^3 \\ + a_{35}\eta^4 + a_{36}\xi^5 + a_{37}\xi^3\eta^2 + a_{38}\xi^2\eta^3 + a_{39}\xi\eta^4 + a_{40}\eta^5 \quad (6c) \end{aligned}$$

Note that the expression for w (eq. (6c)) does not contain the term $\xi^4\eta$, and therefore automatically satisfies the requirement that the normal slope be only cubic along the element edge 1 - 2. The two conditions that ensure only cubic variations of normal slopes along edges 2 - 3 and 3 - 1 are the same as for the flat plate case[15,16,20]. These constraints are just sufficient to reduce the twenty independent parameters of equation (6c) to only eighteen. The generalized displacements for w are then taken to be w, and its first and second derivatives at each corner of the element, a total of eighteen, which is consistent with the eighteen free parameters available. The generalized displacements for u and v are taken to be u and v and their first derivatives at each corner plus u and v at the element's centroid. This gives a total of twenty, which is consistent with the twenty free parameters of equations (6a) and (6b). All the generalized displacements are assembled into a 38-column vector $\{W_i\}$, first in the local coordinate system ξ, η

$$\{W_i\}^T = (u_1, u_{\xi_1}, u_{\eta_1}, v_1, v_{\xi_1}, v_{\eta_1}, w_1, w_{\xi_1}, w_{\eta_1},$$

$$w_{\xi\xi_1}, w_{\xi\eta_1}, w_{\eta\eta_1}, u_2, \ldots, u_3, \ldots, u_c, v_c) \quad (7)$$

where $u_\xi = \partial u/\partial\xi$, etc. The subscripts 1, 2, 3, c denote the corners 1, 2, and 3 and the centroid of the element, respectively. The coefficients a_i of equations (6) are assembled into a 40-column vector $\{A\}$ where

$$\{A\}^T = (a_1, a_2, \ldots, a_{40}) \tag{8}$$

and combining equations (6) to (8) plus the two constraint equations yields the matrix relation

$$\begin{Bmatrix} W_1 \\ 0 \\ 0 \end{Bmatrix} = [T]\{A\} \tag{9}$$

where the 40×40 transformation matrix $[T]$ is given in Table I.

The determinant of $[T]$ has the value $-64\,c^{34}\,(a+b)^{31}\,(a^2+c^2)\,(b^2+c^2)/729$, which is nonzero for all practical problems. Hence, equation (9) may be inverted to give

$$\{A\} = [T^{-1}]\begin{Bmatrix} W_1 \\ 0 \\ 0 \end{Bmatrix} = [T_1]\{W_1\} \tag{10}$$

where the 40×38 matrix $[T_1]$ consists of the first 38 columns of $[T^{-1}]$.

2.1.3 Stiffness Matrix

The stiffness matrix for the element is obtained from a calculation of strain energy. The displacement functions of equations (6) are substituted in equation (4) and the integration carried out to yield the quadratic strain energy form

$$U = \frac{Et}{2(1-\nu^2)}\,\{A\}^T[k]\{A\} \tag{11}$$

The entries of the stiffness matrix $[k]$ may be determined in closed form just as they were for the plate-bending element[15,16]. This may be carried out most easily by rewriting equations (6) as

$$u = \sum_{i=1}^{10} a_i \xi^{m_i} \eta^{n_i} \tag{12a}$$

$$v = \sum_{i=11}^{20} a_i \xi^{p_i} \eta^{q_i} \tag{12b}$$

$$w = \sum_{i=21}^{40} a_i \xi^{r_i} \eta^{s_i} \tag{12c}$$

Then substituting equations (12) into equation (4) and incorporating the symmetry requirement yields

$$k_{ij} = m_i m_j F(m_i + m_j - 2, n_i + n_j) + q_i q_j F(p_i + p_j, q_i + q_j - 2)$$

$$- \frac{1}{2}(1-\nu)\left[n_i n_j F(m_i + m_j, n_i + n_j - 2) + p_i p_j F(p_i + p_j - 2, q_i + q_j)\right]$$

$$+ \left[\frac{1}{2}(1-\nu) n_i p_j + \nu m_i q_j\right] F(m_i + p_j - 1, n_i + q_j - 1)$$

$$+ \left[\frac{1}{2}(1-\nu) n_j p_i + \nu m_j q_i\right] F(m_j + p_i - 1, n_j + q_i - 1)$$

$$- (\zeta_{\xi\xi} + \nu \zeta_{\eta\eta})\left[m_i F(m_i + r_j - 1, n_i + s_j) + m_j F(m_j + r_i - 1, n_j + s_i)\right]$$

$$- (\zeta_{\eta\eta} + \nu \zeta_{\xi\xi})\left[q_i F(p_i + r_j, q_i + s_j - 1) + q_j F(p_j + r_i, q_j + s_i - 1)\right]$$

$$\text{(13)}$$

$$- (1-\nu) \zeta_{\xi\eta}\left[n_i F(m_i + r_j, n_i + s_j - 1) + n_j F(m_j + r_i, n_j + s_i - 1)\right.$$

$$\left. + p_i F(p_i + r_j - 1, q_i + s_j) + p_j F(p_j + r_i - 1, q_j + s_i)\right]$$

$$+ \left[\zeta_{\xi\xi}^2 + \zeta_{\eta\eta}^2 + 2\nu \zeta_{\xi\xi}\zeta_{\eta\eta} + 2(1-\nu) \zeta_{\xi\eta}^2\right] F(r_i + r_j, s_i + s_j)$$

$$+ (t^2/12)\left\{r_i r_j (r_i - 1)(r_j - 1) F(r_i + r_j - 4, s_i + s_j)\right.$$

$$+ s_i s_j (s_i - 1)(s_j - 1) F(r_i + r_j, s_i + s_j - 4)$$

$$+ \left[2(1-\nu) r_i r_j s_i s_j + \nu r_i s_j (r_i - 1)(s_j - 1)\right.$$

$$\left.\left. + \nu r_j s_i (r_j - 1)(s_i - 1)\right] F(r_i + r_j - 2, s_i + s_j - 2)\right\}$$

where

$$F(m,n) = c^{n+1}\left[a^{m+1} - (-b)^{m+1}\right] \frac{m!\, n!}{(m + n + 2)!} \tag{14}$$

Note that i and j run from 1 to 40, and therefore m_i and n_i are defined to be zero for $i > 10$, p_i and q_i are zero for $i < 11$ and $i > 20$, and r_i and s_i are zero for $i < 21$. All the computations involved in evaluating the k_{ij} from equation (13) are carried out within

the computer once the values of a b, c, m, n, p, q, r, and s, are furnished.

The transformation from local to global co-ordinates is

$$\{W_1\} = [R]\{W_2\} \tag{15}$$

where

$$\{W_2\}^T = (u_1,\ u_{x1},\ u_{y1},\ v_1,\ v_{x1},\ v_{y1},\ w_1,\ w_{x1},\ w_{y1},\ w_{xx1},\ w_{xy1},$$

$$w_{yy1},\ u_2, \ldots,\ u_3, \ldots,\ u_c,\ v_c) \tag{16}$$

is the generalized displacement vector relative to global co-ordinates (u, v in the directions of x, y), and $[R]$ is the rotation matrix given in Table II. Then combining equations (10), (11), and (15) yields the strain energy in terms of $\{W_2\}$ as

$$U = \frac{Et}{2(1-\nu^2)}\ \{W_2\}^T [K_2]\{W_2\} \tag{17}$$

where

$$[K_2] = [R]^T [T_1]^T [k][T_1][R] \tag{18}$$

is the 38 × 38 stiffness matrix relative to global co-ordinates.

2.1.4 Consistent Load Vector

The consistent load vector is obtained by calculating the virtual work done by the applied loads $Q_u(\xi,\eta)$, $Q_v(\xi,\eta)$, and $Q_w(\xi,\eta)$ in the u, v, and w directions, respectively. The transformed load vector becomes

$$\{P\} = [R]^T [T_1]^T \{Q\} \tag{19}$$

where the entries in the column vector $\{Q\}$ are

$$Q_i = \begin{cases} \iint Q_u \xi^{m_i} \eta^{n_i}\ d\xi\ d\eta, & i < 11 \\[2mm] \iint Q_v \xi^{p_i}\ \eta^{q_i}\ d\xi\ d\eta, & 10 < i < 21 \\[2mm] \iint Q_w \xi^{r_i}\ \eta^{s_i}\ d\xi\ d\eta, & i > 20 \end{cases} \tag{20}$$

2.1.5 Condensation of Stiffness Matrix

Before proceeding to use the element just derived, it is convenient to condense out the centroidal displacements u_c and v_c. It may be noted that these displacements, since they lie inside the element, will be unaffected when the elements are joined together to represent a structure. Hence, they may be eliminated before the elements are joined without affecting the final results. The reduction is carried out by minimizing the potential energy in one element. The matrix equation of equilibrium for an element is written in the partitioned form

$$\left[K_2\right]\left\{W_2\right\} = \left[\begin{array}{c|c} K_o & K_{oc} \\ \hline K_{oc}^T & K_c \end{array}\right]\left\{\begin{array}{c} W \\ \hline W_c \end{array}\right\} = \left\{\begin{array}{c} P_o \\ \hline P_c \end{array}\right\} \tag{21}$$

where $\left\{W_c\right\}^T$ is the two-component vector (u_c, v_c), and $\left\{W\right\}$ contains the first 36 components of equation (16). Equation (21) is separated into two equations and $\left\{W_c\right\}$ is eliminated to yield

$$\left[K\right]\left\{W\right\} = \left\{P\right\} \tag{22}$$

where

$$\left[K\right] = \left[K_o\right] - \left[K_{oc}\right]\left[K_c^{-1}\right]\left[K_{oc}\right]^T \tag{23}$$

is the reduced 36 × 36 stiffness matrix, and

$$\left\{P\right\} = \left\{P_o\right\} - \left[K_{oc}\right]\left[K_c^{-1}\right]\left\{P_c\right\} \tag{24}$$

is the reduced 36 consistent load vector for the shell element.

2.2 Numerical Application - Cylindrical Shell Roof Problem

The geometry for this problem is shown in Figure 2. The shell is loaded by its own dead weight and is supported by diaphragms at the ends but is free along the sides. Using symmetry, only one-quarter of the shell was analyzed, and various uniform gridworks of elements were used with orientations as shown. The numerical data given in the Figure were used in the calculations, so that the results could be compared directly with those of other authors.

Some of the most pertinent numerical results are given in Table III and convergence plots for these quantities are given in Figure 3. It is seen that the approximations obtained with even the coarsest gridworks are exceedingly accurate, and the convergence is very rapid. In particular, the slopes of the error curves for displacements and strain energy are all about -5.

The quantity that has been used by many authors for comparison purposes is the vertical deflection of point B (Fig. 2). Such a comparison is given in Figure 4, where the abscissa is the total number of degrees of freedom (before boundary conditions) required with the various finite element representations. It is clear that this comparison favours the present results in that it shows that the present element yields the best accuracy for the minimum number of degrees of freedom. It is interesting to note that the results of References 5 and 13 have not actually converged to the exact solution, even though more than 1000 degrees of freedom were used.

3.0 ANALYSIS OF ARBITRARY DEEP SHELLS

In this Section, a brief description is given of the development necessary to apply the foregoing shallow shell element to arbitrary deep shells. This is followed by some results from two numerical examples. All this work is preliminary in nature, but full details will be presented in an NRC Aeronautical Report when the investigations are completed.

3.1 Theoretical Development

3.1.1 Co-Ordinate Systems

The relevant geometry is shown in Figure 5, where X, Y, Z are cartesian global co-ordinates, ξ, η, ζ are cartesian local co-ordinates, and α, β are curvilinear shell co-ordinates lying in the mid-surface of the shell. At this point, the latter need not be orthogonal. The ξ, η co-ordinates are to be used as the base plane co-ordinates in the shallow shell formulation and are defined to go through the element corner nodes 1, 2, 3 as shown.

Now it is explicitly assumed that a point α, β on the shell may be determined in terms of the global co-ordinates by

$$X = X(\alpha, \beta)$$

$$Y = Y(\alpha, \beta) \tag{25}$$

$$Z = Z(\alpha, \beta)$$

This leads to a natural computation process in which the element corner nodes are located first by specifying their shell co-ordinates α, β, and then their global co-ordinates X, Y, Z are calculated from equations (25). The element geometry may then be determined from these latter co-ordinates.

Some results from analytical geometry follow. The global co-ordinates of the ξ, η, ζ system origin are

$$X_0 = (1-\rho) X_1 + \rho X_2$$

$$Y_0 = (1-\rho) Y_1 + \rho Y_2 \tag{26}$$

$$Z_0 = (1-\rho) Z_1 + \rho Z_2$$

where the parameter ρ is

$$\rho = \frac{(X_3 - X_1)(X_2 - X_1) + (Y_3 - Y_1)(Y_2 - Y_1) + (Z_3 - Z_1)(Z_2 - Z_1)}{(X_2 - X_1)^2 + (Y_2 - Y_1)^2 + (Z_2 - Z_1)^2} \tag{27}$$

The subscripts denote the element corner nodes 1, 2, 3 of Figure 5. The element dimensions a, b, c are then given by

$$a = (1-\rho)\sqrt{(X_2 - X_1)^2 + (Y_2 - Y_1)^2 + (Z_2 - Z_1)^2}$$

$$b = \rho\sqrt{(X_2 - X_1)^2 + (Y_2 - Y_1)^2 + (Z_2 - Z_1)^2} \tag{28}$$

$$c = \sqrt{(X_3 - X_0)^2 + (Y_3 - Y_0)^2 + (Z_3 - Z_0)^2}$$

3.1.2 Relations Between Co-Ordinate Systems

The following relations between the global and local cartesian co-ordinates are obtained

$$\xi = \left[(X_2 - X_1)(X - X_0) + (Y_2 - Y_1)(Y - Y_0) + (Z_2 - Z_1)(Z - Z_0)\right]/(a + b)$$

$$\eta = \left[(X_3 - X_0)(X - X_0) + (Y_3 - Y_0)(Y - Y_0) + (Z_3 - Z_0)(Z - Z_0)\right]/c \tag{29}$$

$$\zeta = b_1(X - X_0) + b_2(Y - Y_0) + b_3(Z - Z_0)$$

where

$$b_1 = \left[(Y_2 - Y_1)(Z_3 - Z_0) - (Z_2 - Z_1)(Y_3 - Y_0)\right]/(a + b)\,c$$

$$b_2 = \left[(Z_2 - Z_1)(X_3 - X_0) - (X_2 - X_1)(Z_3 - Z_0)\right]/(a + b)\,c \tag{30}$$

$$b_3 = \left[(X_2 - X_1)(Y_3 - Y_0) - (Y_2 - Y_1)(X_3 - X_0)\right]/(a + b)\,c$$

Combining equations (25) and (29) yields the base plane co-ordinates as functions of the shell co-ordinates, written symbolically as

$$\xi = \xi(\alpha, \beta)$$

$$\eta = \eta(\alpha, \beta) \tag{31}$$

Now all the derivatives required in transforming the generalized displacements from local co-ordinates to shell co-ordinates may be derived from the above equations. Unfortunately, these derivations soon become unwieldly, and hence a simplifying assumption is introduced here to reduce the complexity. As a first approximation, it is assumed that equations (31) may be expanded to first order about each element node, say

$$\xi = d_1 - e_{11}\alpha - e_{12}\beta$$

$$\eta = d_2 + e_{21}\alpha + e_{22}\beta \tag{32}$$

where

$$e_{11} = \frac{X_2 - X_1}{a - b}\frac{\partial X}{\partial \alpha} + \frac{Y_2 - Y_1}{a - b}\frac{\partial Y}{\partial \alpha} + \frac{Z_2 - Z_1}{a + b}\frac{\partial Z}{\partial \alpha}$$

$$e_{12} = \frac{X_2 - X_1}{a + b}\frac{\partial X}{\partial \beta} + \frac{Y_2 - Y_1}{a + b}\frac{\partial Y}{\partial \beta} + \frac{Z_2 - Z_1}{a - b}\frac{\partial Z}{\partial \beta}$$

$$e_{21} = \frac{X_3 - X_0}{c}\frac{\partial X}{\partial \alpha} + \frac{Y_3 - Y_0}{c}\frac{\partial Y}{\partial \alpha} + \frac{Z_3 - Z_0}{c}\frac{\partial Z}{\partial \alpha} \tag{33}$$

$$e_{22} = \frac{X_3 - X_0}{c}\frac{\partial X}{\partial \beta} + \frac{Y_3 - Y_0}{c}\frac{\partial Y}{\partial \beta} + \frac{Z_3 - Z_0}{c}\frac{\partial Z}{\partial \beta}$$

are to be evaluated at an element node. Equations (32) will be valid approximations within some neighbourhood of this node provided there are no singularities there. As the finite element size is reduced, these neighbourhoods around each node will eventually overlap, and hence provide a uniformly valid approximation over the entire element.

In the following derivations, it will be convenient to have the inverse of equations (32), say

$$\alpha = f_1 - g_{11}\xi + g_{12}\eta \tag{34}$$

$$\beta = f_2 + g_{21}\xi - g_{22}\eta$$

where

$$g_{11} = e_{22}/e$$

$$g_{12} = -e_{12}/e$$

$$g_{21} = -e_{21}/e \tag{35}$$

$$g_{22} = e_{11}/e$$

and

$$e = e_{11}e_{22} - e_{12}e_{21}$$

The shell element curvatures are determined locally by specifying the shell elevations above the ξ, η base plane at the mid-side nodes 4,5,6 (Fig. 5) and using them in the quadratic function, equation (5). Note that the elevations are zero at the corner nodes 1,2,3. The locations of the mid-side nodes are determined first in the shell co-ordinates simply as averages of the corner node co-ordinates, i.e.

$$\alpha_4 = (\alpha_1 + \alpha_2)/2, \qquad \beta_4 = (\beta_1 + \beta_2)/2$$

$$\alpha_5 = (\alpha_2 + \alpha_3)/2, \qquad \beta_5 = (\beta_2 + \beta_3)/2 \qquad (36)$$

$$\alpha_6 = (\alpha_1 + \alpha_3)/2, \qquad \beta_6 = (\beta_1 + \beta_2)/2$$

The global co-ordinates of these nodes are then easily obtained from equations (25) and are substituted into equations (29) to yield the three elevations ζ_i and the corresponding base plane co-ordinates ξ_i, η_i for $i = 4,5,6$. Note that these points do not necessarily coincide with the mid-side points of the base plane triangle. These results, together with the zero elevations at the three corner nodes, are then sufficient to complete the quadratic fit to the shell shape and determine the c_i coefficients of equation (5). Finally, the three shell curvatures required in the strain energy calculation are obtained simply by differentiating equation (5).

3.1.3 Transformation Matrices

The shallow shell formulation of Section 2.0 begins with generalized displacements written relative to the base plane co-ordinates, w, w_ξ, w_η, etc. To use these results in the present formulation, it is merely necessary to transform these base plane generalized displacements to shell co-ordinate ones. The displacement normal to the shell w is a scalar and hence, using equations (34), its derivatives transform simply as

$$\begin{Bmatrix} w \\ w_\xi \\ w_\eta \\ w_{\xi\xi} \\ w_{\xi\eta} \\ w_{\eta\eta} \end{Bmatrix} = \begin{bmatrix} R_6 \end{bmatrix} \begin{Bmatrix} w \\ w_\alpha \\ w_\beta \\ w_{\alpha\alpha} \\ w_{\alpha\beta} \\ w_{\beta\beta} \end{Bmatrix} \qquad (37)$$

where $\begin{bmatrix} R_6 \end{bmatrix}$ is given in Table IV. The linear approximation (34) implies that the second derivatives of α, β with respect to ξ, η are neglected in the transformation (37). The tangential displacements u, v are defined to be parallel to the co-ordinate axes and hence must be transformed as vectors. Again using results from analytical geometry and the element's shallowness, together with equations (34) for derivatives,

leads to the approximation

$$\begin{Bmatrix} u \\ u_\xi \\ u_\eta \\ v \\ v_\xi \\ v_\eta \end{Bmatrix} = \begin{bmatrix} R_5 \end{bmatrix} \begin{Bmatrix} \tilde{u} \\ \tilde{u}_\alpha \\ \tilde{u}_\beta \\ \tilde{v} \\ \tilde{v}_\alpha \\ \tilde{v}_\beta \end{Bmatrix} \tag{38}$$

where $\tilde{u}$ and $\tilde{v}$ are in the directions of α and β, and $\begin{bmatrix} R_5 \end{bmatrix}$ is given in Table IV. Now combining all these results and dropping the "tilda" notation for simplicity, the complete transformation for one element is

$$\{W_1\} = \begin{bmatrix} R_4 \end{bmatrix} \{W_3\} \tag{39}$$

where

$$\{W_3\}^T = (u_1, u_{\alpha 1}, u_{\beta 1}, v_1, v_{\alpha 1}, v_{\beta 1}, w_1, w_{\alpha 1}, w_{\beta 1}, w_{\alpha\alpha 1},$$

$$w_{\alpha\beta 1}, w_{\beta\beta 1}, u_2, \ldots, u_3, \ldots, u_c, v_c) \tag{40}$$

is the generalized displacement vector in shell co-ordinates (u, v in the directions of α, β) and $\begin{bmatrix} R_4 \end{bmatrix}$ is the new "rotation" matrix given in Table IV. The strain energy in the shell element then becomes

$$U = \frac{Et}{2(1-\nu^2)} \{W_3\}^T \begin{bmatrix} K_3 \end{bmatrix} \{W_3\} \tag{41}$$

where

$$\begin{bmatrix} K_3 \end{bmatrix} = \begin{bmatrix} R_4 \end{bmatrix}^T \begin{bmatrix} T_1 \end{bmatrix}^T \begin{bmatrix} k \end{bmatrix} \begin{bmatrix} T_1 \end{bmatrix} \begin{bmatrix} R_4 \end{bmatrix} \tag{42}$$

is he 38 × 38 stiffness matrix relative to shell co-ordinates. Finally, the consistent load vector and stiffness matrix condensation procedures (Sec. 2.1.4 and 2.1.5) follow through just as before with $\begin{bmatrix} R \end{bmatrix}$ replaced by $\begin{bmatrix} R_4 \end{bmatrix}$, etc.

The usual procedure for assembling individual element stiffness and load

matrices into the master matrices for a given finite element gridwork is followed here as well. This means that all corresponding generalized displacements are equated at a node (except when a discontinuous variable is expected, e.g. normal curvatures across a step in shell thickness) and sums of corresponding generalized forces are set equal to the appropriate load components as well. The question of what continuity the former procedure provides here is as yet unanswered and requires further investigation.

3.2 Numerical Applications

Preliminary results have been obtained from applying the foregoing developments to two numerical examples. These initial results are very encouraging and are presented in the following.

3.2.1 Pinched Cylindrical Shell

The problem geometry illustrated in Figure 6 is that of a thin circular cylindrical shell of radius R, thickness t and length L. The cylinder's ends are freely supported (sometimes called diaphragm ends), and it is loaded by two centrally located and diametrically opposed concentrated forces P. Using the double symmetry available, only one-eighth of the cylinder was analyzed.

The obvious choice for shell co-ordinates α, β are the axial and circumferential ones indicated in the Figure. Equal subdivisions of α from 0 to L/2 and β from 0 to $\pi/2$ were used to form 2×2, 3×3, 4×4, and 5×5 uniform grids of elements; the 3×3 grid is shown in Figure 6. A non-uniform 5×5 grid with element width ratios of 1:2:3:4:5 going away from the point load (also shown in Fig. 6) was used as well. Numerical calculations were carried out for a shell with R/t = 100, L/R = 2, and ν = 0.3. Some typical numerical results are presented in Table V and distributions are plotted in Figures 7a to d and 8. The exact results are from a double Fourier series solution of Flügge's equation's[22], using 80 terms in each direction.

Ignoring the non-uniform grid results of Table V for the moment, it appears that the other finite element predictions all converge monotonically towards the exact solutions. On the other hand, this convergence is quite slow. For instance, a plot of the error in w_c, the displacement under the point load, versus n (for an n × n grid) reveals a slope of about -2.5. Now since w_c is linearly related to strain energy, this means that its convergence rate is also -2.5. Although this convergence rate appears low, it is a direct consequence of the severity of the point load. Rates as low as -2 have been observed in some point-loaded plate problems[15,16].

The non-uniform 5×5 grid yields an appreciable improvement in accuracy in the vicinity of the point load, i.e. at C. Even the bending moments M_α and M_β are increased in magnitude there. However, these improvements near C are accompanied by some degradation of accuracy away from the load, i.e. at B.

The plotted distributions of Figures 7a to d provide a clearer picture of the convergence trends in the calculated results. Firstly, the displacements of Figure 7a exhibit a simple improvement with grid refinement. Next, the membrane stress and bending and twisting moment distributions of Figures 7b to d also exhibit noticeable improvements with grid refinements. However, there are a number of noteworthy features. The kinks or slope discontinuities at element nodes first observed in Reference 20 are again in evidence in some of these plots. This shows again the importance

of calculating distributions of membrane stresses and moments rather than relying on only the nodal values. It appears from these figures that N_β near the point load is the most difficult quantity for the finite elements to predict. In particular, the 5 × 5 grid prediction of N_β along DC is still far from the exact result.

Most of the above difficulties are solved by the non-uniform 5 × 5 grid. Typical membrane stress distributions obtained from this grid are shown in Figure 8. The improvement in N_β along DC (which was the poorest prediction from the uniform grids) is clearly outstanding, the major error remaining being that of the small up-turn at C. Similar improvements in all the other distributions were also obtained from the non-uniform 5 × 5 grid.

3.2.2 Pinched Spherical Shell

The second numerical application is the pinched spherical shell shown in Figure 8. The concentrated loading at each pole is transmitted to the shell through an infinitely rigid boss with a half angle of β_0 as shown. The shell is assumed rigidly attached or welded to each boss, and hence the boundary condition there becomes one of constraining v, w, and $\partial w/\partial \beta$ to allow only vertical motion of the boss.

The meridional angle α and colatitude β are the logical choice for shell coordinates for this problem. Using the symmetry about the equator and the poles, only an angular slice of the shell is analyzed (2 × 5 grid shown). Although only one element is needed in the meridional direction, two elements are used here to provide a symmetric grid and hence symmetric numerical results. The meridional width of the gridwork α_0 used in the calculations was $\pi/(2n+2)$, where n is the number of colatitude elements. Calculations were carried out for a shell with R/t = 50, ν = 0.3, and β_0 = 10 degrees, with various values of n. An exact solution for this problem was obtained for comparison purposes by numerical integration of Timoshenko's equations[23].

The calculated results are given in Table VI for various displacements, membrane stress resultants, and bending moments for values of n of 3, 5, 7, and 9. These results must be considered as only preliminary, since there are several factors yet to be investigated. However, they are very encouraging. It is seen that all these results appear to be converging monotonically towards the exact values as the number of elements increases. Further, when the relative errors in the displacements at the boss w_β and v_β are plotted versus n, they exhibit convergence proportional to about $n^{-1.5}$. This implies that the vertical displacement of the boss, and therefore the strain energy in the shell, converge as $n^{-1.5}$ as well.

Distributions of the displacements v and w as obtained from the finite elements are plotted in Figure 10. The excellent accuracy of these predictions is evident from the Figure. At this time, further work is underway to develop a method for calculating the analogous membrane stress resultant and bending moment distributions. It should be noted that the nodal predictions of these quantities appear to be quite accurate.

4.0 CONCLUDING REMARKS

The finite element analysis of shells, as outlined herein, is undergoing further development. Several interesting and fundamental questions that are under critical investigation are as follows. What displacement continuity does the transformation to

deep shell co-ordinates provide? What are the effects of different displacement boundary conditions? What gains may be achieved through the use of a more exact transformation between the local and shell co-ordinates? What gains may be obtained from a more exact deep shell theory rather than shallow shell theory?

The results of this investigation indicate that accurate solutions for a large variety of shell problems can be efficiently obtained. For shallow shells, the present approach using curved elements has proven to be far superior to the alternate flat element approach. Though no comparisons have as yet been made, it is anticipated that the same conclusions will also hold for deep shell problems.

5.0 REFERENCES

1. Jones, R.E.
   Strome, D.R.

   A Survey of Analysis of Shells by the Displacement Method.
   IN Matrix Methods in Structural Mechanics, Wright-Patterson AFB, AFFDL-TR-66-80, 1966.

2. Hrennikoff, A.
   Tezcan, S.S.

   Analysis of Cylindrical Shells by the Finite Element Method.
   Symposium on Problems of Interdependence of Design and Construction of Large-Span Shells for Industrial and Civic Buildings, Leningrad, U.S.S.R., 6-9 September 1966.

3. Zienkiewicz, O.C.
   Cheung, Y.K.

   The Finite Element Method in Structural and Continuum Mechanics.
   McGraw Hill Book Co., London, 1967.

4. Clough, R.W.
   Johnson, R.J.

   A Finite Element Approximation for the Analysis of Thin Shells.
   International Journal for Solids and Structures, Vol.4, 1968, pp. 43-60.

5. Carr, A.J.

   A Refined Finite Element Analysis of Thin Shell Structures Including Dynamic Loadings.
   Ph.D. Thesis, University of California, Berkeley, 1967.

6. Bogner, F.K.
   Fox, R.L.
   Schmit, L.A.

   A Cylindrical Shell Discrete Element.
   AIAA Journal, Vol. 5, 1967, pp. 745-750.

7. Cantin, G.
   Clough, R.W.

   A Curved, Cylindrical Shell, Finite Element.
   AIAA Journal, Vol. 6, 1968, pp. 1057-1062.

8. Olson, M.D.
   Lindberg, G.M.

   Vibration Analysis of Cantilevered Curved Plates Using a New Cylindrical Shell Finite Element.
   Proc. 2nd Conf. on Matrix Methods in Structural Mechanics, Wright-Patterson AFB, Ohio, October 1968.

9. Connor, J.J.
   Brebbia, C.

   Stiffness Matrix for Shallow Rectangular Shell Element.
   Journal of Engineering Mech. Div., A.S.C.E., Vol. 93, No. 5, October 1967.

10. Gallagher, R. H.   The Development and Evaluation of Matrix Methods of
                        Thin Shell Structural Analysis.
                        Ph. D. Thesis, State University of New York at Buffalo,
                        1966.

11. Utku, S.   Behavior of Triangular Shell Element Stiffness Matrices
    Melosh, R. J.   Associated with Polyhedral Deflection Distributions.
                        AIAA Paper No. 67-114, AIAA Sixth Aerospace Sciences
                        Meeting, New York, January 1967. (Also AIAA J., Vol. 6,
                        1968, pp. 374-376.)

12. Strickland, C. E. A Doubly-Curved Triangular Shell Element.
    Loden, W. A.   Proc. 2nd Conf. on Matrix Methods in Structural Mechanics,
                        Wright-Patterson AFB, Ohio, October 1968.

13. Bonnes, G.   Curved Triangular Elements for the Analysis of Shells.
    Dhatt, G.   Proc. 2nd Conf. on Matrix Methods in Structural Mechanics
    Giroux, Y. M   Wright-Patterson AFB, Ohio, October 1968.
    Robichaud, L. P. A.

14. Cowper, G. R.   Formulation of a New Triangular Plate-Bending Element.
    Kosko, E.   Can. Aero Space Inst. Trans., Vol. 1, September 1968,
    Lindberg, G. M.   pp. 86-90.
    Olson, M. D.

15. Cowper, G. R.   A High Precision Triangular Plate-Bending Element.
    Kosko, E.   NRC, NAE Aero. Report LR-514, National Research
    Lindberg, G. M.   Council of Canada, December 1968.
    Olson, M. D.

16. Cowper, G. R.   Static and Dynamic Applications of a High Precision
    Kosko, E.   Triangular Plate-Bending Element.
    Lindberg, G. M.   AIAA Journal, Vol. 7, 1969, pp. 1957-1965.
    Olson, M. D.

17. Bell, K.   Analysis of Thin Plates in Bending Using Triangular
                       Finite Elements.
                       Institutt for Statikk, Norges Tekniske Hogskole, Trondheim,
                       Norway, February 1968.

18. Bell, K.   A Refined Triangular Plate-Bending Finite Element.
                       International Journal of Numerical Methods in Engineering,
                       Vol. 1, 1969, pp. 101-120.

19. Butlin, G. A.   A Compatible Triangular Plate-Bending Finite Element.
    Ford, R.   University of Leicester, Eng. Dept. Report 68-15,
                       October 1968.

20. Cowper, G. R.   A Shallow Shell Element of Triangular Shape.
    Lindberg, G. M.   International Journal of Solids and Structures, 1970.
    Olson, M. D.   (In press).

21. Novozhilov, V.V.   The Theory of Thin Shells. 2nd ed.
                         Noordhoff, P., Groningen, The Netherlands, Sec. 17a,
                         1964.

22. Flugge, W.   Stresses in Shells.
                         Springer-Verlag, Berlin, Sec. 5.2, 1962, p. 221.

23. Timoshenko, S.   Theory of Plates and Shells. 2nd ed.
     Woinowsky-Krieger, S. McGraw-Hill Book Co., Sec. 127, 1959, p.533.

TABLE I
TRANSFORMATION MATRIX $[\mathsf{T}]$

$$[\mathsf{T}] = \begin{bmatrix} S_1 & 0 & 0 \\ 0 & S_1 & 0 \\ 0 & 0 & S_2 \\ S_3 & 0 & 0 \\ 0 & S_3 & 0 \\ 0 & 0 & S_4 \\ S_5 & 0 & 0 \\ 0 & S_5 & 0 \\ 0 & 0 & S_6 \\ S_7 & 0 & 0 \\ 0 & S_7 & 0 \\ 0 & 0 & S_8 \end{bmatrix}$$

$$[S_1] = \begin{bmatrix} 1 & -b & 0 & b^2 & 0 & 0 & -b^3 & 0 & 0 & 0 \\ 0 & 1 & 0 & -2b & 0 & 0 & 3b^2 & 0 & 0 & 0 \\ 0 & 0 & 1 & 0 & -b & 0 & 0 & b^2 & 0 & 0 \end{bmatrix}$$

$$[S_2] = \begin{bmatrix} 1 & -b & 0 & b^2 & 0 & 0 & -b^3 & 0 & 0 & 0 & b^4 & 0 & 0 & 0 & 0 & -b^5 & 0 & 0 & 0 & 0 \\ 0 & 1 & 0 & -2b & 0 & 0 & 3b^2 & 0 & 0 & 0 & -4b^3 & 0 & 0 & 0 & 0 & 5b^4 & 0 & 0 & 0 & 0 \\ 0 & 0 & 1 & 0 & -b & 0 & 0 & b^2 & 0 & 0 & 0 & -b^3 & 0 & 0 & 0 & 0 & 0 & 0 & 0 & 0 \\ 0 & 0 & 0 & 2 & 0 & 0 & -6b & 0 & 0 & 0 & 12b^2 & 0 & 0 & 0 & 0 & -20b^3 & 0 & 0 & 0 & 0 \\ 0 & 0 & 0 & 0 & 1 & 0 & 0 & -2b & 0 & 0 & 0 & 3b^2 & 0 & 0 & 0 & 0 & 0 & 0 & 0 & 0 \\ 0 & 0 & 0 & 0 & 0 & 2 & 0 & 0 & -2b & 0 & 0 & 0 & 2b^2 & 0 & 0 & 0 & -2b^3 & 0 & 0 & 0 \end{bmatrix}$$

$$[S_3] = \begin{bmatrix} 1 & a & 0 & a^2 & 0 & 0 & a^3 & 0 & 0 & 0 \\ 0 & 1 & 0 & 2a & 0 & 0 & 3a^2 & 0 & 0 & 0 \\ 0 & 0 & 1 & 0 & a & 0 & 0 & a^2 & 0 & 0 \end{bmatrix}$$

$$[S_4] = \begin{bmatrix} 1 & a & 0 & a^2 & 0 & 0 & a^3 & 0 & 0 & 0 & a^4 & 0 & 0 & 0 & 0 & a^5 & 0 & 0 & 0 & 0 \\ 0 & 1 & 0 & 2a & 0 & 0 & 3a^2 & 0 & 0 & 0 & 4a^3 & 0 & 0 & 0 & 0 & 5a^4 & 0 & 0 & 0 & 0 \\ 0 & 0 & 1 & 0 & a & 0 & 0 & a^2 & 0 & 0 & 0 & a^3 & 0 & 0 & 0 & 0 & 0 & 0 & 0 & 0 \\ 0 & 0 & 0 & 2 & 0 & 0 & 6a & 0 & 0 & 0 & 12a^2 & 0 & 0 & 0 & 0 & 20a^3 & 0 & 0 & 0 & 0 \\ 0 & 0 & 0 & 0 & 1 & 0 & 0 & 2a & 0 & 0 & 0 & 3a^2 & 0 & 0 & 0 & 0 & 0 & 0 & 0 & 0 \\ 0 & 0 & 0 & 0 & 0 & 2 & 0 & 0 & 2a & 0 & 0 & 0 & 2a^2 & 0 & 0 & 0 & 2a^3 & 0 & 0 & 0 \end{bmatrix}$$

$$[S_5] = \begin{bmatrix} 1 & 0 & c & 0 & 0 & c^2 & 0 & 0 & 0 & c^3 \\ 0 & 1 & 0 & 0 & c & 0 & 0 & 0 & c^2 & 0 \\ 0 & 0 & 1 & 0 & 0 & 2c & 0 & 0 & 0 & 3c^2 \end{bmatrix}$$

$$[S_6] = \begin{bmatrix} 1 & 0 & c & 0 & 0 & c^2 & 0 & 0 & 0 & c^3 & 0 & 0 & 0 & 0 & c^4 & 0 & 0 & 0 & 0 & c^5 \\ 0 & 1 & 0 & 0 & c & 0 & 0 & 0 & c^2 & 0 & 0 & 0 & 0 & c^3 & 0 & 0 & 0 & 0 & c^4 & 0 \\ 0 & 0 & 1 & 0 & 0 & 2c & 0 & 0 & 0 & 3c^2 & 0 & 0 & 0 & 0 & 4c^3 & 0 & 0 & 0 & 0 & 5c^4 \\ 0 & 0 & 0 & 2 & 0 & 0 & 0 & 2c & 0 & 0 & 0 & 0 & 2c^2 & 0 & 0 & 0 & 0 & 2c^3 & 0 & 0 \\ 0 & 0 & 0 & 0 & 1 & 0 & 0 & 0 & 2c & 0 & 0 & 0 & 0 & 3c^2 & 0 & 0 & 0 & 0 & 4c^3 & 0 \\ 0 & 0 & 0 & 0 & 0 & 2 & 0 & 0 & 0 & 6c & 0 & 0 & 0 & 0 & 12c^2 & 0 & 0 & 0 & 0 & 20c^3 \end{bmatrix}$$

$$[S_7] = \begin{bmatrix} 1 & \dfrac{a-b}{3} & \dfrac{c}{3} & \dfrac{(a-b)^2}{9} & \dfrac{(a-b)c}{9} & \dfrac{c^2}{9} & \dfrac{(a-b)^3}{27} & \dfrac{(a-b)^2 c}{27} & \dfrac{(a-b)c^2}{27} & \dfrac{c^3}{27} \end{bmatrix}$$

$$[S_8] = \begin{bmatrix} 0 & 0 & 0 & 0 & 0 & 0 & 0 & 0 & 0 & 0 & 0 & 0 & 0 & 0 & 0 & 5a^4 c, & 3a^2 c^3 & 2a^4 c, & -2ac^4 + 3a^3 c^2, & c^5 - 4a^2 c^3, & 5ac^4 \\ 0 & 0 & 0 & 0 & 0 & 0 & 0 & 0 & 0 & 0 & 0 & 0 & 0 & 0 & 0 & 5b^4 c, & 3b^2 c^3 - 2b^4 c, & 2bc^4 - 3b^3 c^2, & c^5 - 4b^2 c^3, & -5bc^4 \end{bmatrix}$$

TABLE II
ROTATION MATRIX $[R]$

$$[R] = \begin{bmatrix} R_1 & 0 & 0 & 0 & 0 & 0 & 0 \\ 0 & R_2 & 0 & 0 & 0 & 0 & 0 \\ 0 & 0 & R_1 & 0 & 0 & 0 & 0 \\ 0 & 0 & 0 & R_2 & 0 & 0 & 0 \\ 0 & 0 & 0 & 0 & R_1 & 0 & 0 \\ 0 & 0 & 0 & 0 & 0 & R_2 & 0 \\ 0 & 0 & 0 & 0 & 0 & 0 & R_3 \end{bmatrix}$$

where

$$[R_1] = \begin{bmatrix} \cos\theta & 0 & 0 & \sin\theta & 0 & 0 \\ 0 & \cos^2\theta & \sin\theta\cos\theta & 0 & \sin\theta\cos\theta & \sin^2\theta \\ 0 & -\sin\theta\cos\theta & \cos^2\theta & 0 & -\sin^2\theta & \sin\theta\cos\theta \\ -\sin\theta & 0 & 0 & \cos\theta & 0 & 0 \\ 0 & -\sin\theta\cos\theta & -\sin^2\theta & 0 & \cos^2\theta & \sin\theta\cos\theta \\ 0 & \sin^2\theta & -\sin\theta\cos\theta & 0 & -\sin\theta\cos\theta & \cos^2\theta \end{bmatrix}$$

$$[R_2] = \begin{bmatrix} 1 & 0 & 0 & 0 & 0 & 0 \\ 0 & \cos\theta & \sin\theta & 0 & 0 & 0 \\ 0 & -\sin\theta & \cos\theta & 0 & 0 & 0 \\ 0 & 0 & 0 & \cos^2\theta & 2\sin\theta\cos\theta & \sin^2\theta \\ 0 & 0 & 0 & -\sin\theta\cos\theta & \cos^2\theta-\sin^2\theta & \sin\theta\cos\theta \\ 0 & 0 & 0 & \sin^2\theta & -2\sin\theta\cos\theta & \cos^2\theta \end{bmatrix}$$

$$[R_3] = \begin{bmatrix} \cos\theta & \sin\theta \\ -\sin\theta & \cos\theta \end{bmatrix}$$

TABLE III

NUMERICAL RESULTS FOR CYLINDRICAL

SHELL ROOF PROBLEM

Fin. El. Grids	$10\,u_A$ (in)	w_B (in)	$10\,v_B$ (in)	$10\,w_C$ (in)
1 × 1	-0.9158	-1.21672	-3.96349	0.2228
2 × 2	-1.3954	-3.66312	-8.08975	4.5518
3 × 3	-1.49497	-4.03037	-8.65809	5.1446
4 × 4	-1.51050	-4.08388	-8.73995	5.2258
Exact	-1.51325	-4.09916	-8.76147	5.2494

$10^{-3}N_{xxB}$ (lb/in)	$10^{-3}M_{yyC}$ (lb in/in)	$10^{-2}M_{xxC}$ (lb in/in)	$10^{-4}x$ Strain Energy (lb in)
5.3637	1.5437	2.994	2.78548
6.9845	2.3463	4.498	5.37577
6.6313	2.1571	2.127	5.79980
6.5016	2.0871	1.284	5.86511
6.4124	2.0562	0.9272	5.88277

TABLE IV
TRANSFORMATION MATRIX $[R_4]^*$

$$[R_4] = \begin{bmatrix} [R_5]_1 & 0 & 0 & 0 & 0 & 0 & 0 \\ 0 & [R_6]_1 & 0 & 0 & 0 & 0 & 0 \\ 0 & 0 & [R_5]_2 & 0 & 0 & 0 & 0 \\ 0 & 0 & 0 & [R_6]_2 & 0 & 0 & 0 \\ 0 & 0 & 0 & 0 & [R_5]_3 & 0 & 0 \\ 0 & 0 & 0 & 0 & 0 & [R_6]_3 & 0 \\ 0 & 0 & 0 & 0 & 0 & 0 & [R_7]_c \end{bmatrix}$$

where

$$[R_5] = \begin{bmatrix} g_{22}/r_2 & 0 & 0 & -g_{12}/r_1 & 0 & 0 \\ 0 & g_{11}g_{22}/r_2 & g_{21}g_{22}/r_2 & 0 & -g_{11}g_{12}/r_1 & -g_{12}g_{21}/r_1 \\ 0 & g_{12}g_{22}/r_2 & g_{22}^2/r_2 & 0 & -g_{12}^2/r_1 & -g_{12}g_{22}/r_1 \\ -g_{21}/r_2 & 0 & 0 & g_{11}/r_1 & 0 & 0 \\ 0 & -g_{11}g_{21}/r_2 & -g_{21}^2/r_2 & 0 & g_{11}^2/r_1 & g_{11}g_{21}/r_1 \\ 0 & -g_{12}g_{21}/r_2 & -g_{21}g_{22}/r_2 & 0 & g_{11}g_{12}/r_1 & g_{11}g_{22}/r_1 \end{bmatrix}$$

$$[R_6] = \begin{bmatrix} 1 & 0 & 0 & 0 & 0 & 0 \\ 0 & g_{11} & g_{21} & 0 & 0 & 0 \\ 0 & g_{12} & g_{22} & 0 & 0 & 0 \\ 0 & 0 & 0 & g_{11}^2 & 2g_{11}g_{21} & g_{21}^2 \\ 0 & 0 & 0 & g_{11}g_{12} & g_{11}g_{22}+g_{12}g_{21} & g_{21}g_{22} \\ 0 & 0 & 0 & g_{12}^2 & 2g_{12}g_{22} & g_{22}^2 \end{bmatrix}$$

$$[R_7] = \begin{bmatrix} g_{22}/r_2 & -g_{12}/r_1 \\ -g_{21}/r_2 & g_{11}/r_1 \end{bmatrix} \qquad r_1 = \sqrt{g_{11}^2 + g_{12}^2}$$
$$r_2 = \sqrt{g_{22}^2 + g_{21}^2}$$

* SUBSCRIPTS [ ]$_i$ MEAN EVALUATED AT NODE i OR CENTROID c

TABLE V

NUMERICAL RESULTS FOR PINCHED CYLINDRICAL SHELL

$R/t = 100$, $L/R = 2$, $\nu = 0.3$

Fin. El. Grids	Etw_C/P	Etw_s/P	Etu_D/P	$RN_{\alpha C}/P$
2 × 2	-72.95	-11.93	2.870	-5.61
3 × 3	-119.02	-7.52	3.447	-8.24
4 × 4	-141.25	-3.40	3.744	-10.68
5 × 5	-151.10	-2.08	3.902	-12.24
Non-uniform				
5 × 5	-159.23	-4.63	3.954	-16.08
Exact	-164.24	-0.47	4.114	-15.72

$RN_{\beta C}/P$	$RN_{\beta s}/P$	$M_{\alpha C}/P$	$M_{\beta C}/P$
4.86	-0.47	-0.03	-0.04
3.99	-0.56	-0.08	-0.10
1.53	-0.43	-0.12	-0.16
-1.39	-0.29	-0.15	-0.19
-16.42	-0.76	-0.27	-0.31
-18.6	-0.09	$-\infty$	$-\infty$

TABLE VI

NUMERICAL RESULTS FOR PINCHED SPHERICAL SHELL

$R/t = 50, \quad \nu = 0.3$

(SUBSCRIPTS, B = BOSS, E = EQUATOR)

Colatitude Elements, n	Etw_B/P	Etv_B/P	$RN_{\alpha B}/P$	$RN_{\beta B}/P$
3	-2.1654	0.3818	-0.6354	-2.118
5	-2.8443	0.5015	-0.6788	-2.263
7	-3.1488	0.5552	-0.7074	-2.358
9	-3.2879	0.5797	-0.7257	-2.419
Exact	-3.5849	0.6321	-0.7605	-2.535

$10^2 M_{\alpha B}/P$	$10^2 M_{\beta B}/P$	Etw_E/P	$RN_{\alpha E}/P$	$RN_{\beta E}/P$
0.1789	0.596	0.1459	0.1265	-0.1434
0.3645	1.215	0.1700	0.1321	-0.1448
0.5019	1.673	0.1832	0.1414	-0.1497
0.5859	1.953	0.1904	0.1465	-0.1522
0.7663	2.554	0.2069	0.1591	-0.1591
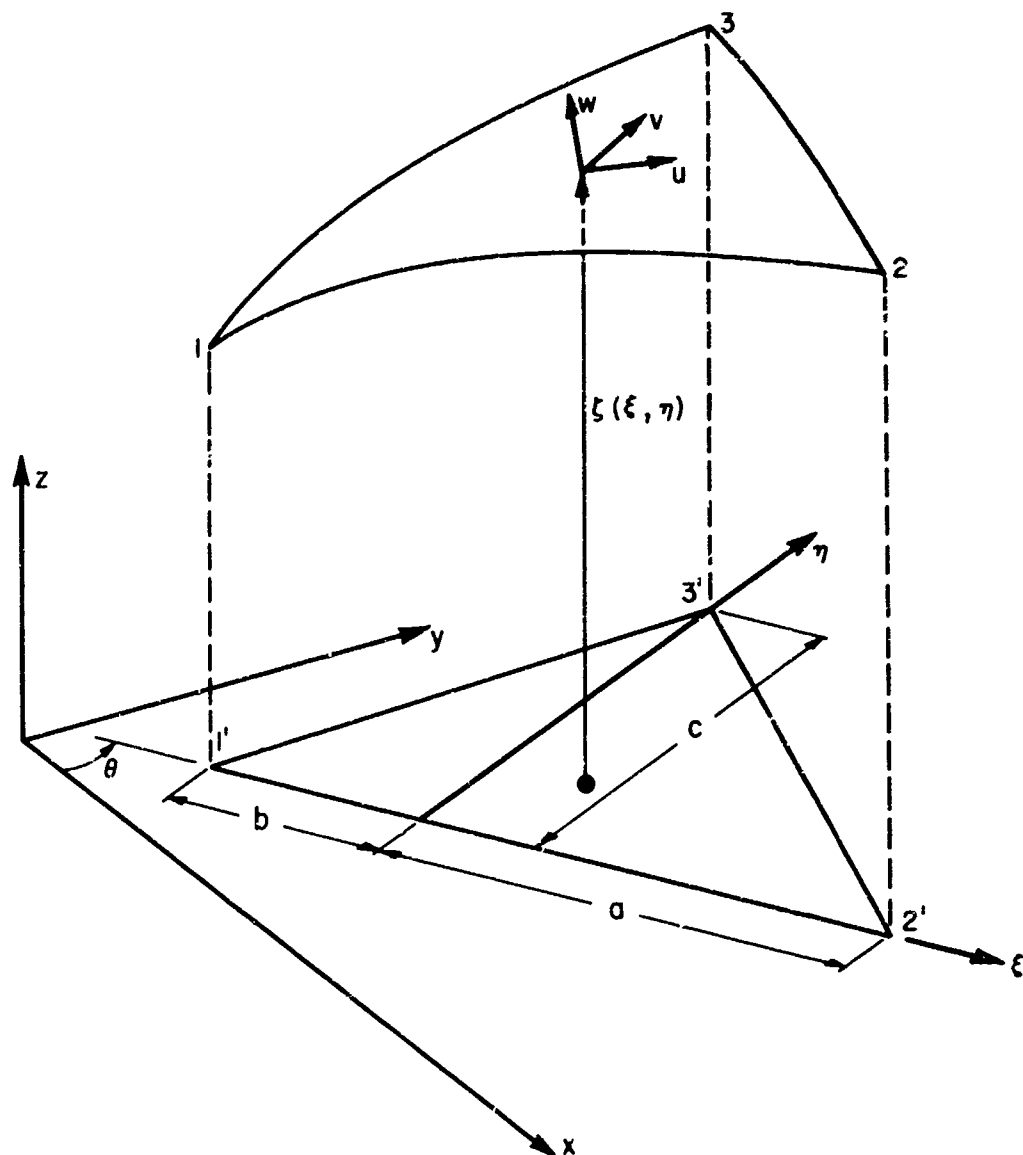
FIG.I: SHALLOW SHELL ELEMENT GEOMETRY AND
CO-ORDINATE SYSTEMS

DIAPHRAGM

FREE EDGE

FREE EDGE

DIAPHRAGM

CROWN

L = 50 FT

R = 25 FT

40°

$E = 3.0 \times 10^6$ psi
$\nu = 0.0$
$t = 3.0$ in

SHELL WEIGHT = 90 LB/SQ. FT.
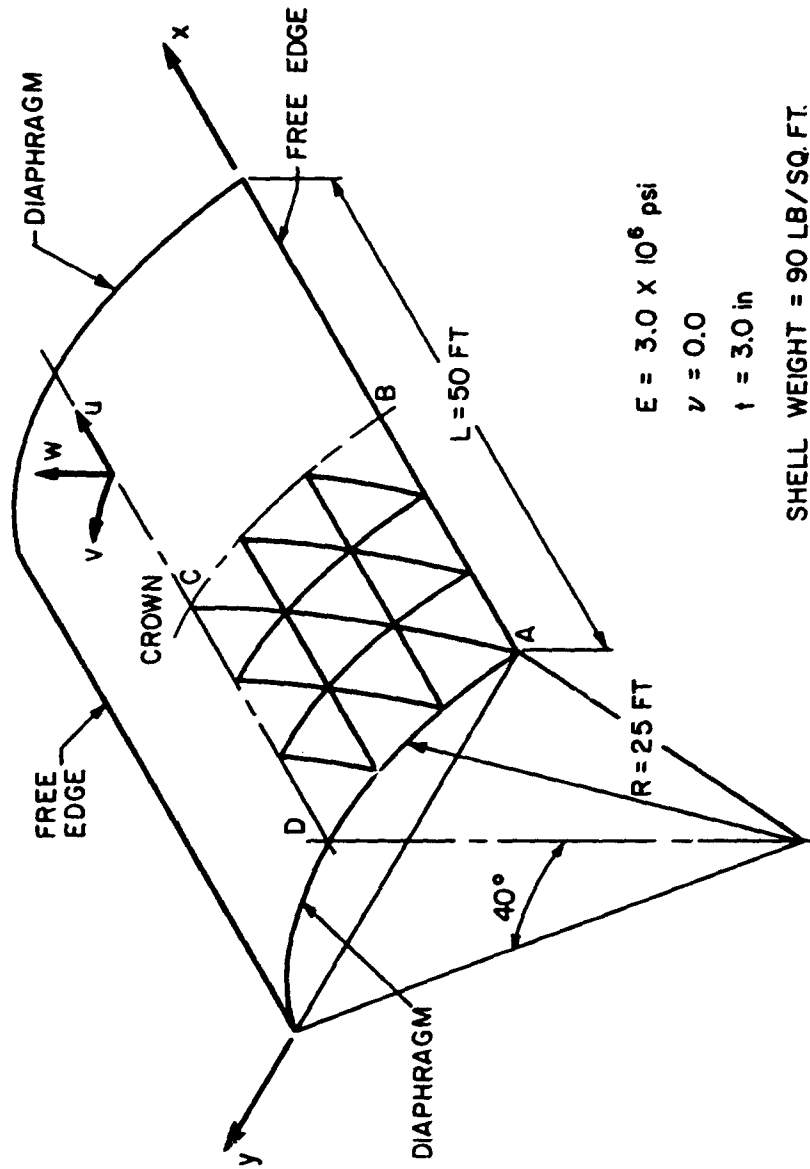
FIG. 2: CYLINDRICAL SHELL ROOF CONFIGURATION
(3 x 3 GRID SHOWN)
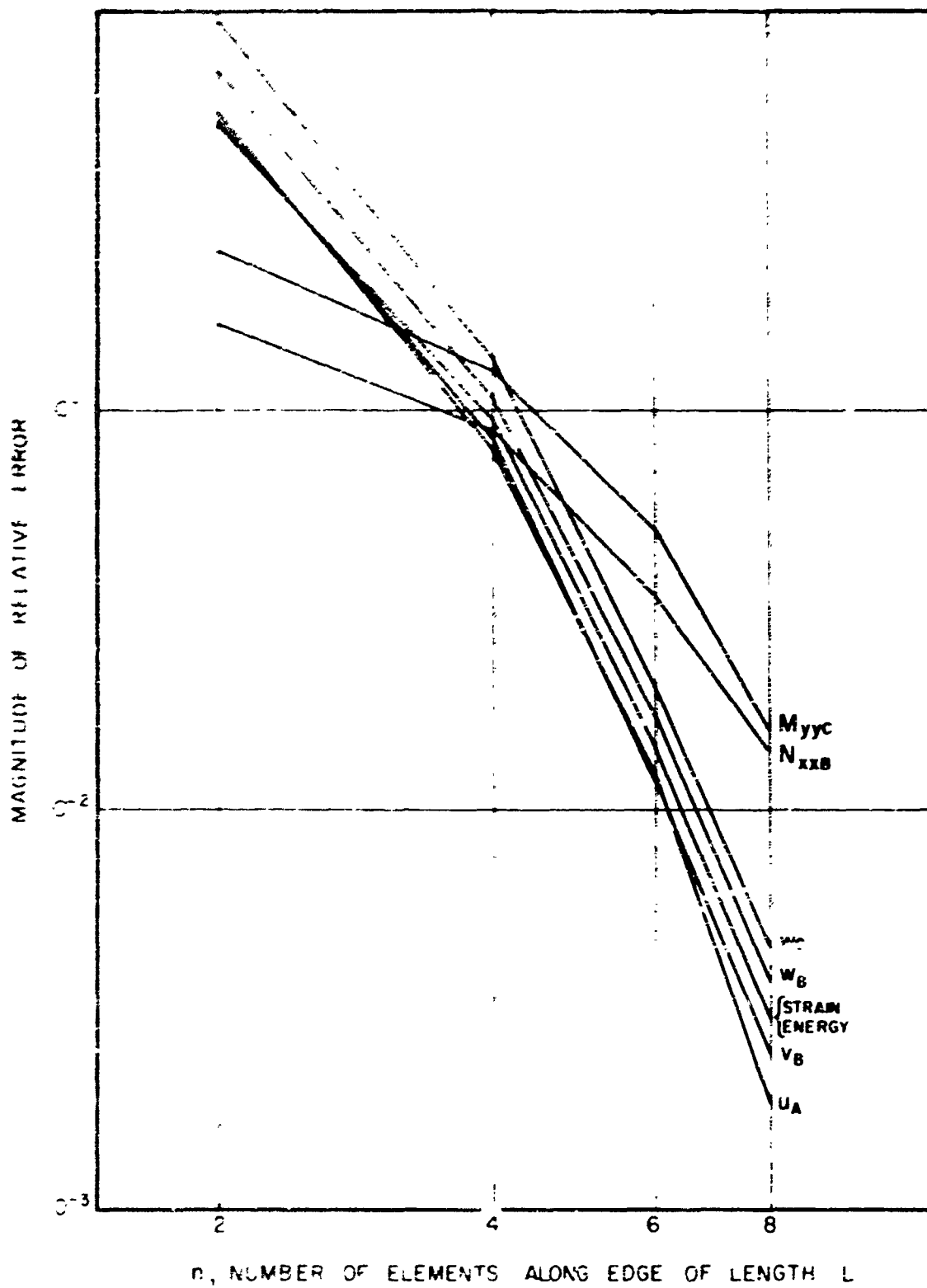
FIG 3: RELATIVE ERROR OF FINITE ELEMENT SOLUTIONS
FOR CYLINDRICAL SHELL ROOF PROBLEM
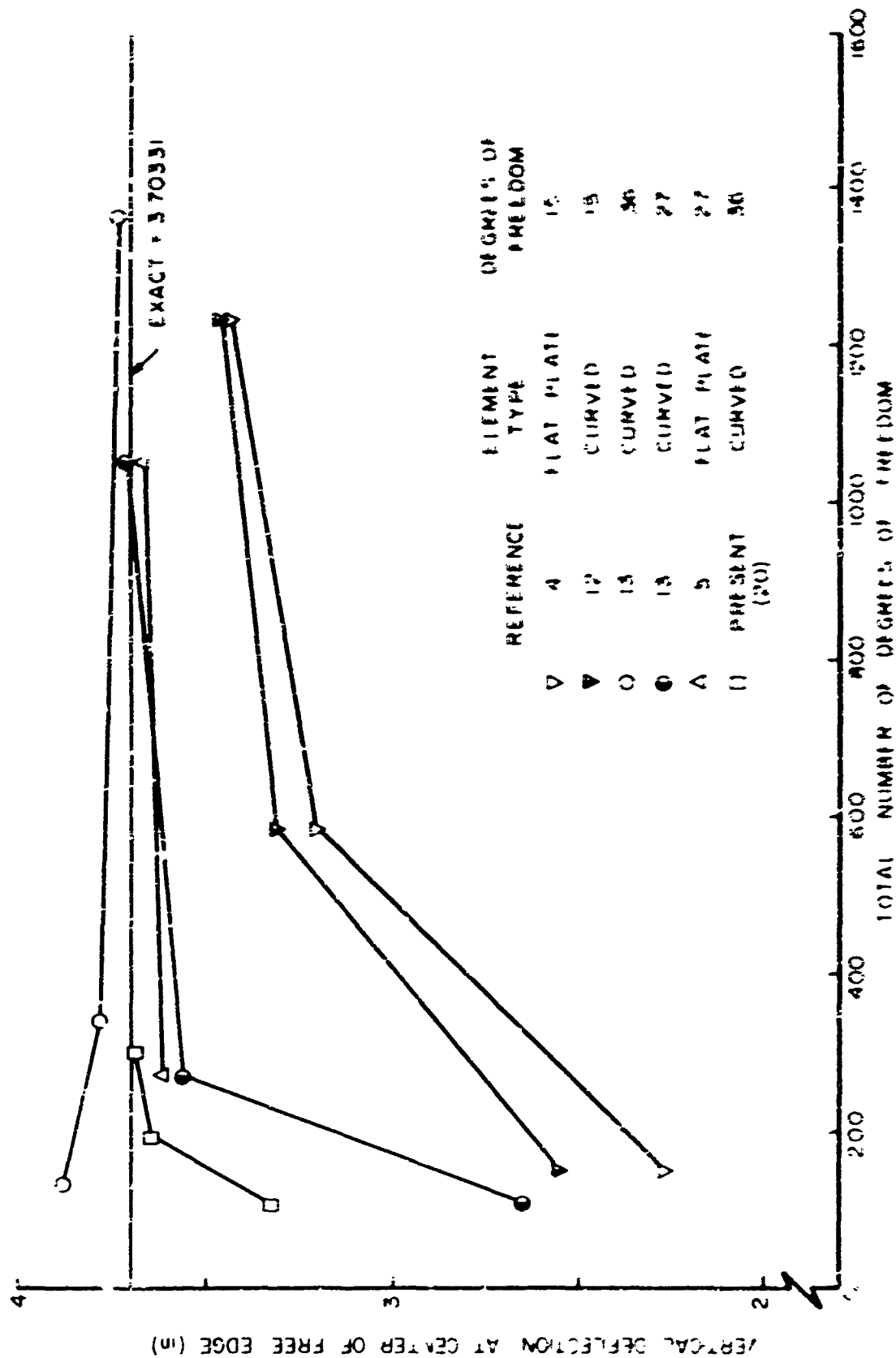
FIG. 4 : CYLINDRICAL SHELL ROOF PROBLEM COMPARISONS
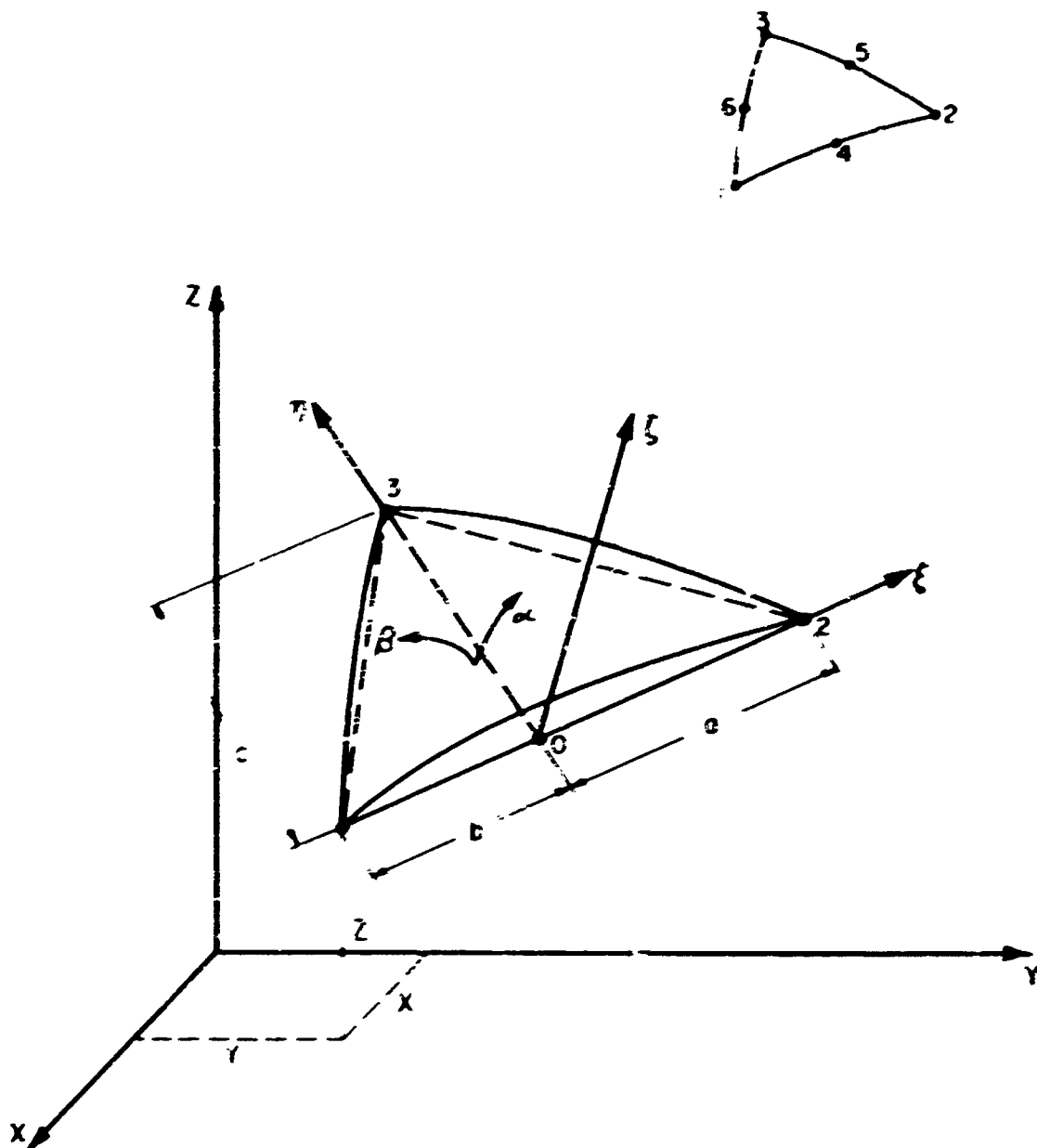
FIG 5. GEOMETRY AND CO-ORDINATE SYSTEMS FOR
DEEP SHELL FORMULATION

NON-UNIFORM 5 x 5 GRID
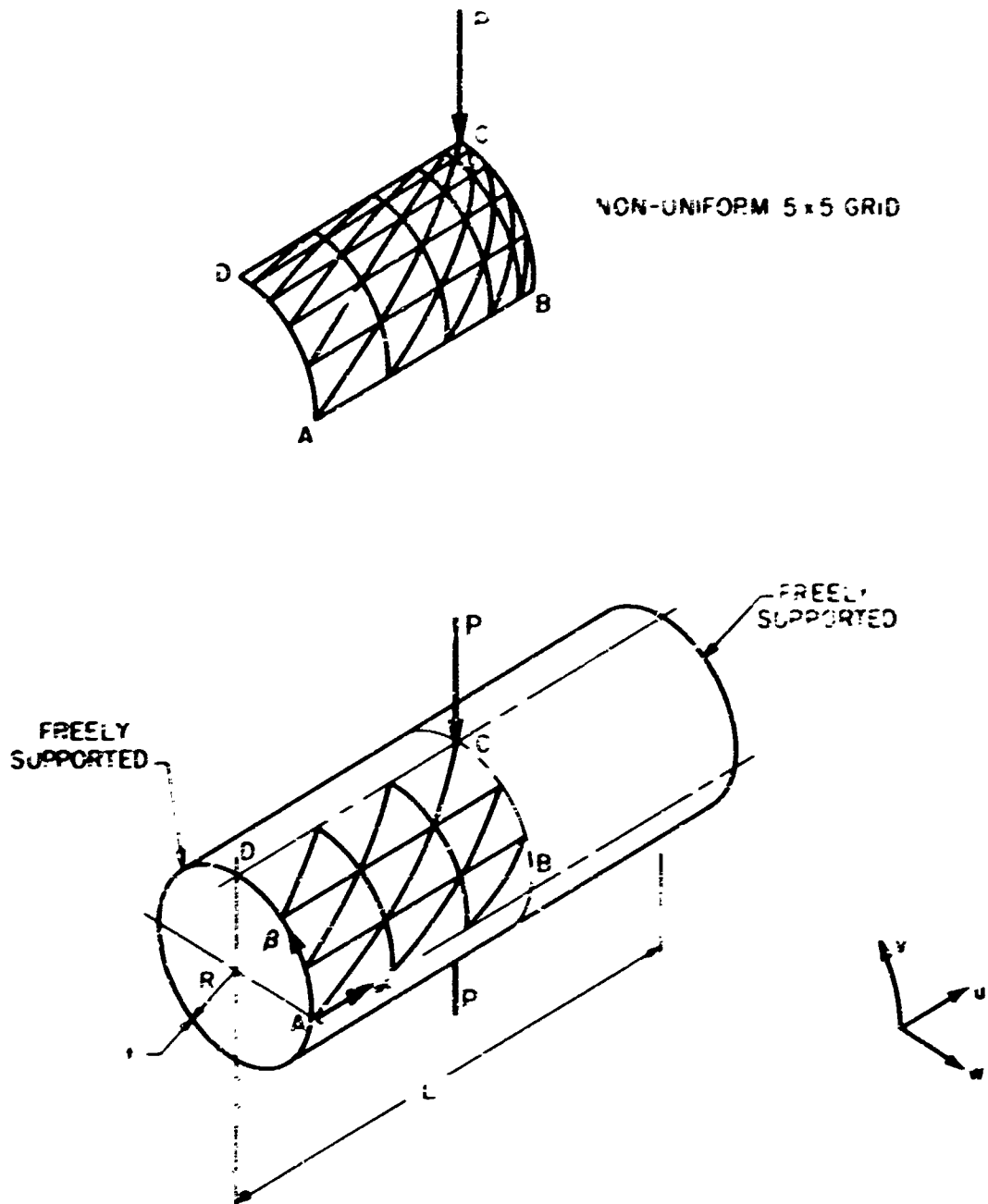
FIG. 6 - PINCHED CYLINDRICAL SHELL CONFIGURATION
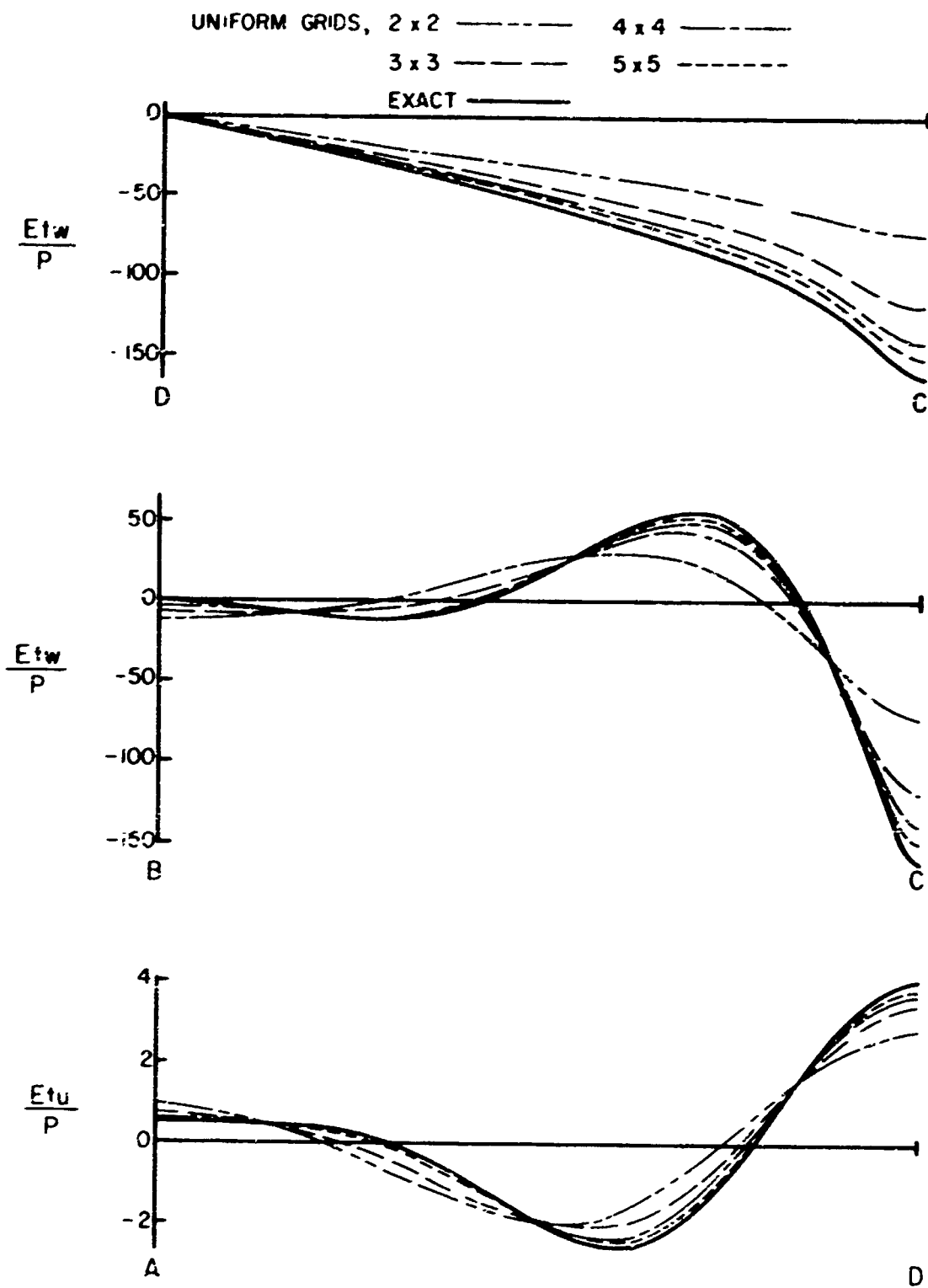
FIG. 7a: DISPLACEMENT DISTRIBUTIONS FOR PINCHED
CYLINDRICAL SHELL
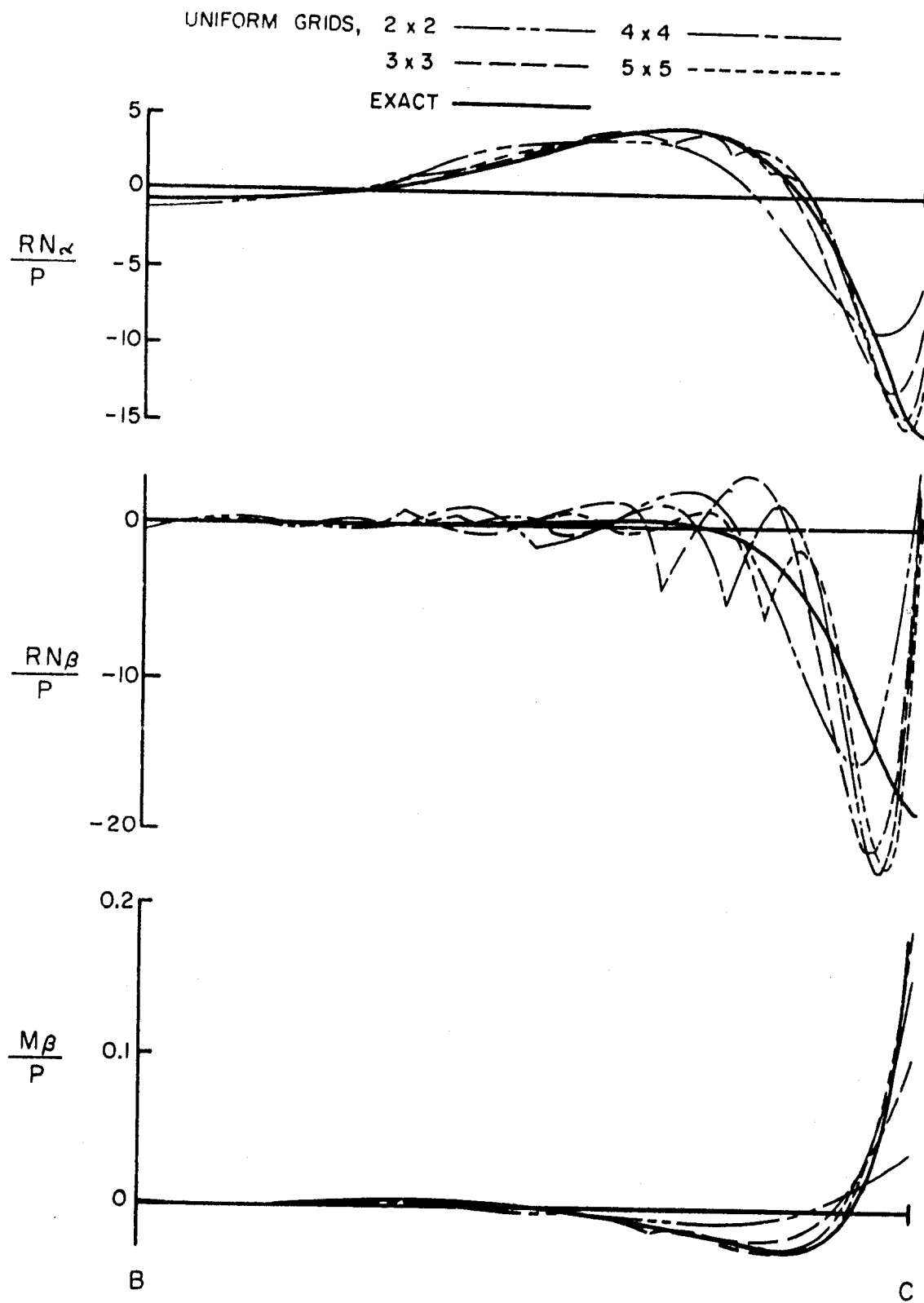
FIG. 7 b: MEMBRANE STRESS AND BENDING MOMENT DISTRIBUTIONS
ALONG BC OF PINCHED CYLINDRICAL SHELL
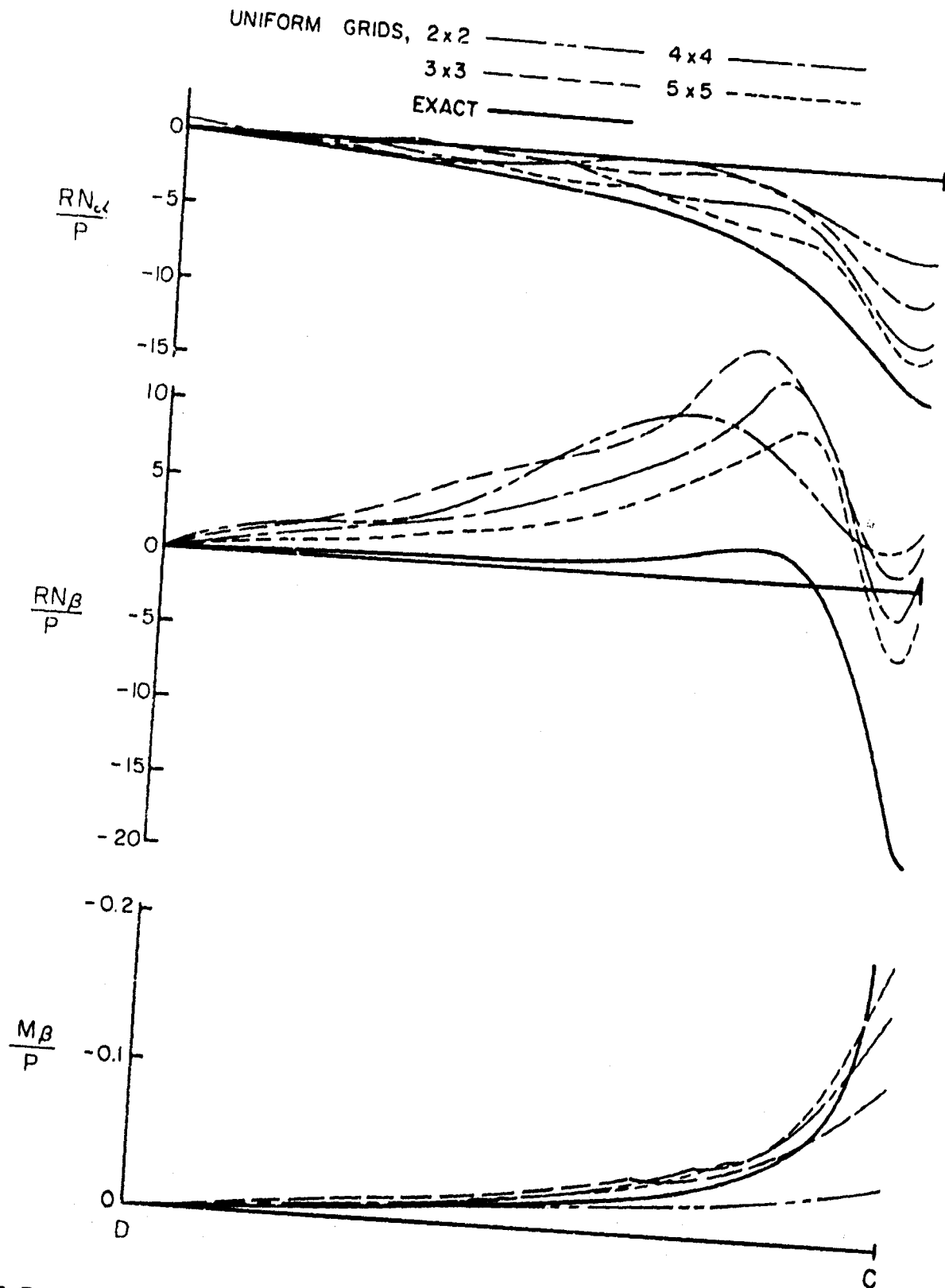
FIG.7c: MEMBRANE STRESS AND BENDING MOMENT DISTRIBUTIONS ALONG DC OF PINCHED CYLINDRICAL SHELL

UNIFORM GRIDS, 2 x 2 ——·—— 4 x 4 ——— ——

3 x 3 ——— ——— 5 x 5 --------

EXACT ———————

$$\frac{RN_{\alpha\beta}}{P}$$

A

D

$$\frac{M_{\alpha\beta}}{P}$$

A

D
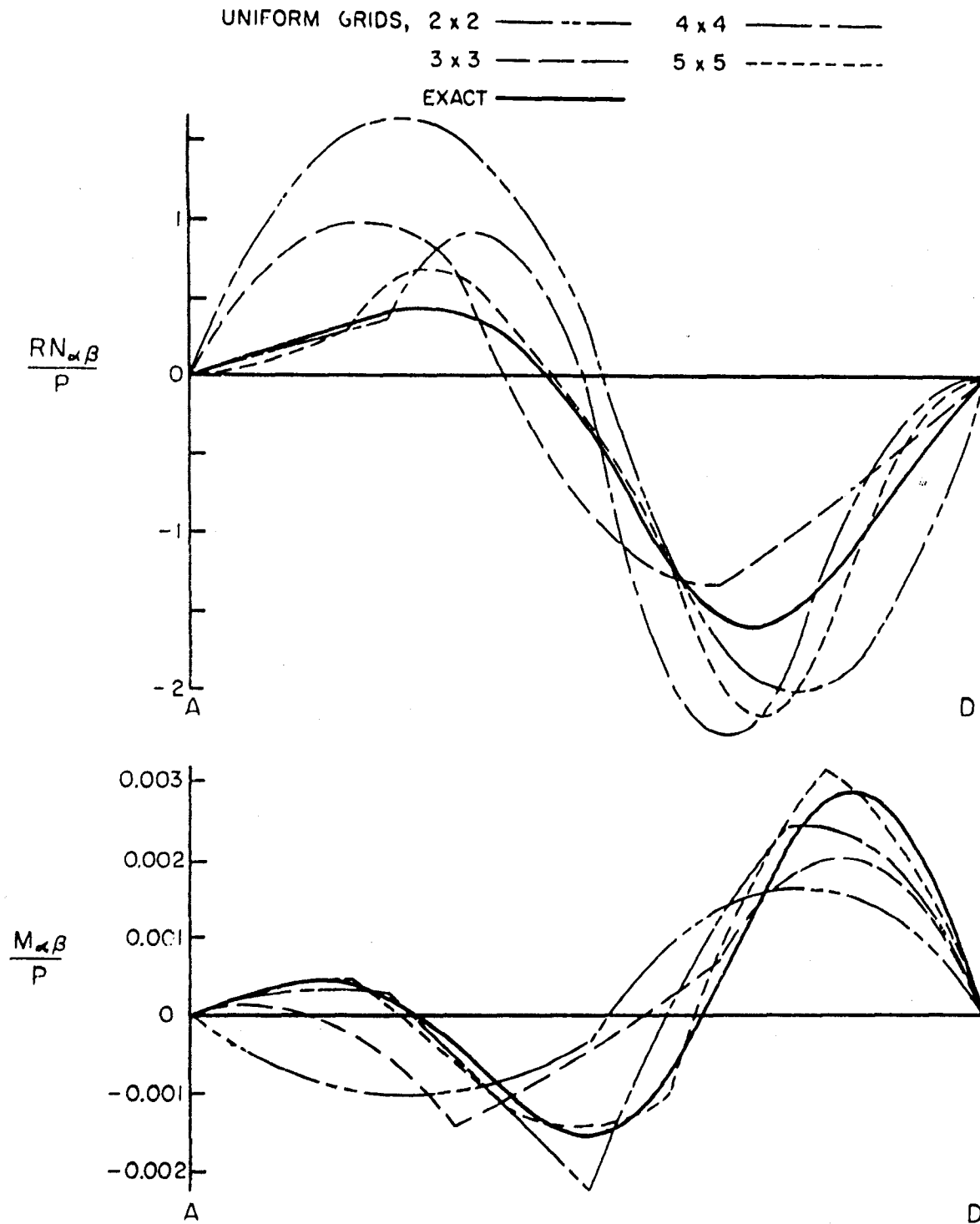
FIG. 7d : MEMBRANE SHEAR STRESS AND TWISTING MOMENT
DISTRIBUTIONS ALONG A D OF PINCHED CYLINDRICAL SHELL
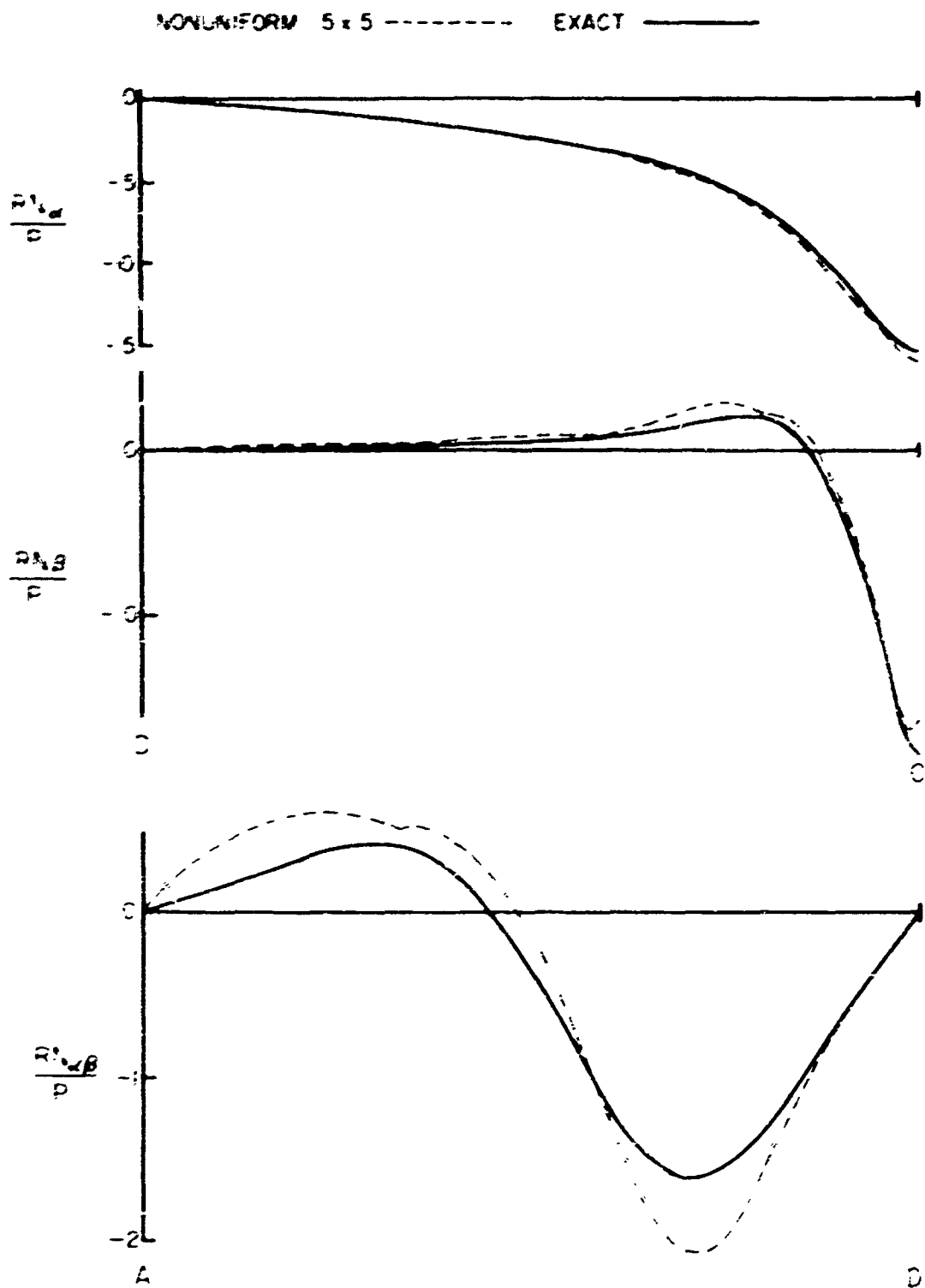
FIG 8 MEMBRANE STRESS DISTRIBUTIONS FOR PINCHED CYLINDRICAL
SHELL USING NON-UNIFORM 5 x 5 GRID OF ELEMENTS
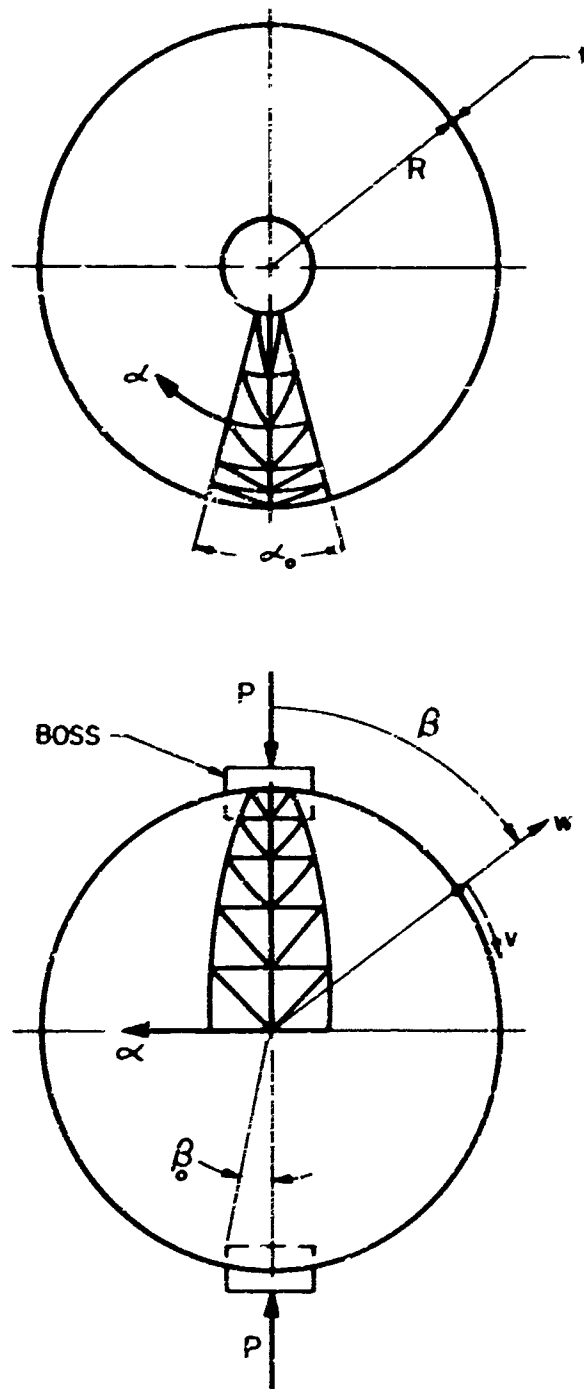
FIG. 9: PINCHED SPHERICAL SHELL CONFIGURATION

FINITE ELEMENTS   n = 3 ———·—
                       5 ————
                       7 ———·—
                       9 ··—·——
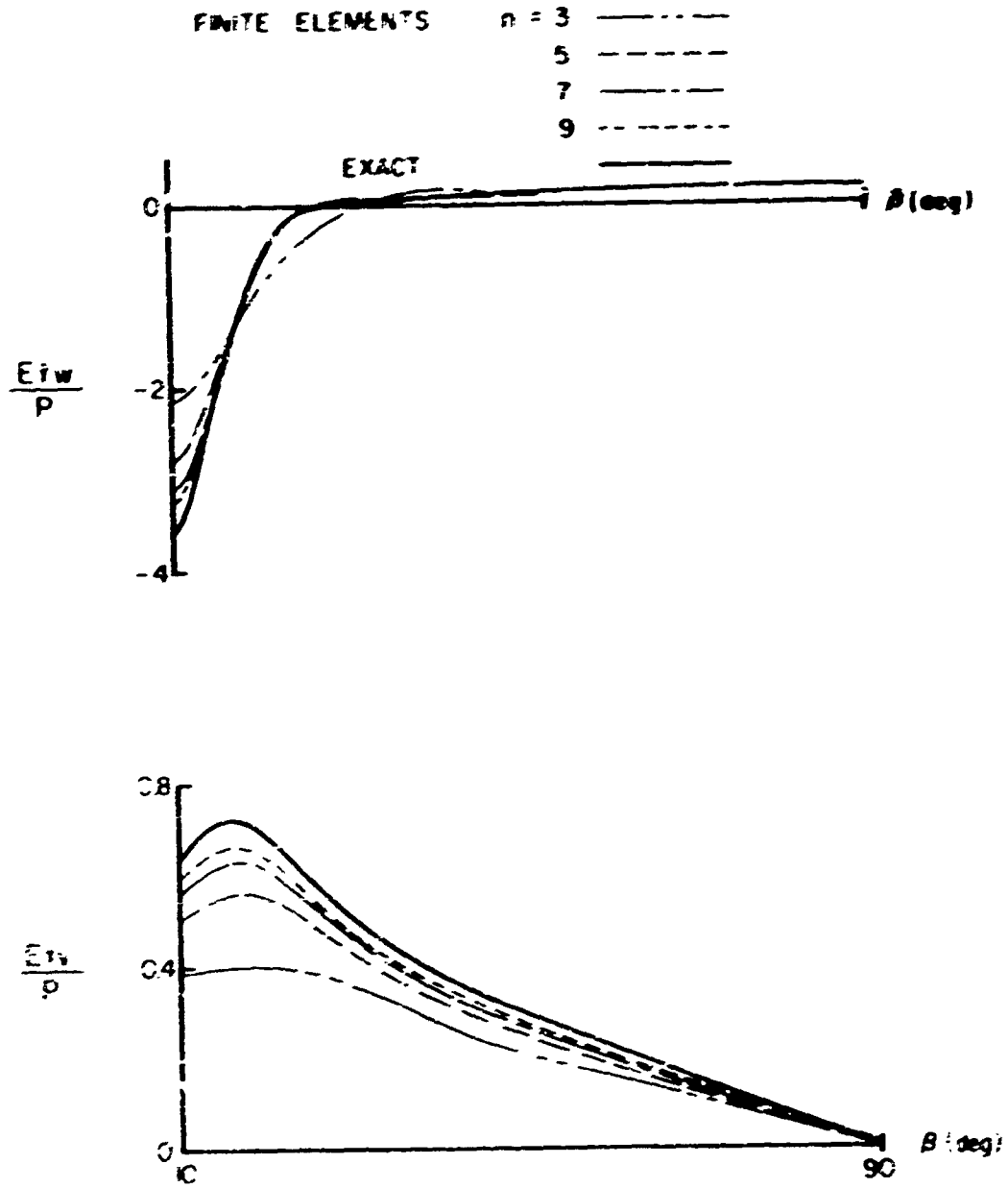
FIG.IO. DISPLACEMENT DISTRIBUTIONS FOR PINCHED SPHERICAL SHELL

APPENDIX A

NOMENCLATURE

Symbol	Definition
a_i	Displacement polynomial coefficients
$\{A\}$	Column vector of a_i
a, b, c	Finite element dimensions
E	Young's modulus
$[k]$, $[K]$	Stiffness matrices
L	Shell length
m_i, n_i, p_i, q_i, r_i, s_i	Exponents of ξ and η in displacement polynomials
M_α, M_β, $M_{\alpha\beta}$ N_α, N_β, $N_{\alpha\beta}$	Customary moment and membrane stress resultants
P	Magnitude of point load on shells
R	Shell radius of curvature
$[R]$	Rotation or transformation matrix
t	Shell thickness
$[T]$	Transformation matrix
u, v	Tangential displacements of shell
U	Strain energy
w	Normal displacement of shell
$\{w\}$	Column vector of generalized displacements
x, y, z X, Y, Z	Global cartesian co-ordinates
α, β	Shell co-ordinates
θ	Element rotation angle
ν	Poisson's ratio
ξ, η, ζ	Local cartesian co-ordinates
subscripts	Denote differentiation, e.g. $w_x = \partial w/\partial x$, etc.

PRODUCTION OF PRECISION FOAM PLASTIC PRODUCTS
BY PRESSURE MOLDING OF FOAM SLABS IN A HOT MOLD

D. A. Baker

Flight Research Laboratory

National Aeronautical Establishment

SUMMARY

This report describes a method of molding model Crash Position Indicators, which will be used in supersonic wind tunnel tests, from blocks of styrofoam. It also briefly describes methods that were tried before reaching a satisfactory one, and lists a few areas where this type of manufacture might prove valuable.

INTRODUCTION

In testing the Crash Position Indicator model aerofoils in the supersonic wind tunnel it was necessary to develop a method of manufacturing a lightweight aerofoil that could be made quickly, be tough enough to withstand the forces from supersonic wind tunnel speeds, and yet be light enough so that weight could be added to bring the centre of gravity to any required position and still keep the density of the aerofoil within the required region.

MOLDING METHODS AND MATERIALS

Five different molding methods and materials were tried. These are listed below.

"Pour In Place" Urethane Foam

This material formed a lightweight model but the edges of the model were too delicate and friable. It was difficult to remove the light density units from the mold, and proper venting of the mold was difficult.

Syntactic Foam

This material is made from microscopic hollow spheres of phenolic resin with a polyester resin as the binding material. It formed a good strong model in the density range of 15 to 20 pounds per cubic foot.

Polyethelene Molding Powders

Models were formed using polyethelene molding powder and the rotational molding method. This provided a hollow aerofoil with a thin tough surface, but it was

necessary to fill the cavity with foam in order to make it rigid enough for supersonic speeds. The total weight was prohibitive and the method dropped.

Expandable Polystyrene Beads (Dylite)

This material will expand and bond together when heated. It provided a lightweight model that could be kept well within the weight limits, but the edges of the beacon were quite weak.

Polystyrene Foam (Styrofoam)

Models were formed by pressure-molding blocks of styrofoam in a heated mold. This method proved to be a successful way of manufacturing a lightweight aerofoil with tough edges. The density of the aerofoil was easily controlled by controlling the size and density of the block of styrofoam used in the molding process. The density of the edges could be controlled by bevelling the edges of the block of foam (Fig. 1).

METHOD USED TO "HEAT FORM" POLYSTYRENE FOAM

The recommended method to "heat form" polystyrene foam is to soak the foam unit at a temperature slightly below the heat distortion temperature of 175°F, until the foam block is a uniform temperature throughout. The mold is heated to slightly above this temperature, to 190° - 200°F. The heated foam block is then placed in the mold and formed to shape by pressure.

This method was tried, but it was found that a beacon with a tougher skin and edge was obtained if the foam was left at room temperature and the mold temperature increased to 220° to 230°F and immediately quenched in cold water when the foam block was molded to shape. This method tended to compress the outer surface of the foam only, and produced a tough skin with an almost solid resin edge.

FOAM BLOCKS

The foam block, for a square beacon, was cut as shown in Figure 1. The size of the block of foam was made larger than the dimensions of the mold. Length and breadth were increased by 1/8 inch in order to take care of misalignment of the foam block in the mold. The height of the foam block varied with the density required in the finished model. It was found that the minimum height of foam had to be at least 1/16 inch greater than the depth of the mold to insure complete molding contact.

Two densities, 1.8 and 4.3 pounds per cubic foot, were tried in the molding process. The height of the block of foam varied from 1/2 to 1-1/4 inches. The densities of the aerofoil ranged from 3.86 to 21.5 pcf (Fig. 2).

MOLDS

Two types of molds were used in the production of the model aerofoils. The first type, Figure 3, was cast from Devcon C, which is a mixture of 80% aluminum

powder and 20% epoxy resin. This is a high temperature molding compound that will withstand 5000 psi at 400° F, with a shrinkage on curing of 0.0001 inch per inch. (Manufacturer's claim.)

The second type of mold was carved from solid aluminum. It had a better heat transfer than the plastic aluminum compound, and therefore provided a quicker production method. This type of mold was used on the later models. The model produced from the above mold is shown in Figure 4.

CONCLUSION

This method of molding provides a unique way of controlling the density throughout a molded product. The block of foam that is to be pressure-molded can be roughly shaped to produce required densities in different areas of the molded unit. The surface density can be controlled by the temperature of the mold. A thin layer of solid resin can be created on the surface, or it can remain a high-density foam surface, depending on the temperature of the mold. The sharp edges of the molded unit can be compressed to an almost solid resin or high-density foam depending on the thickness, at the edge, of the foam block that is being heat and pressure formed.

It lends itself particularly to the molding of any section that requires a strong thin edge, such as the trailing edge of streamlined struts, wing sections, tail sections, and elevators for model aircraft; or other units where light weight, strength, and toughness are requirements.

This method can also be used to mold lightweight filler sections for fibreglas propeller blades, ailerons, tail sections, etc., for full-scale aircraft.

It provides a void-free homogeneous foam unit with a solid resin or high-density foam skin from one molding operation.

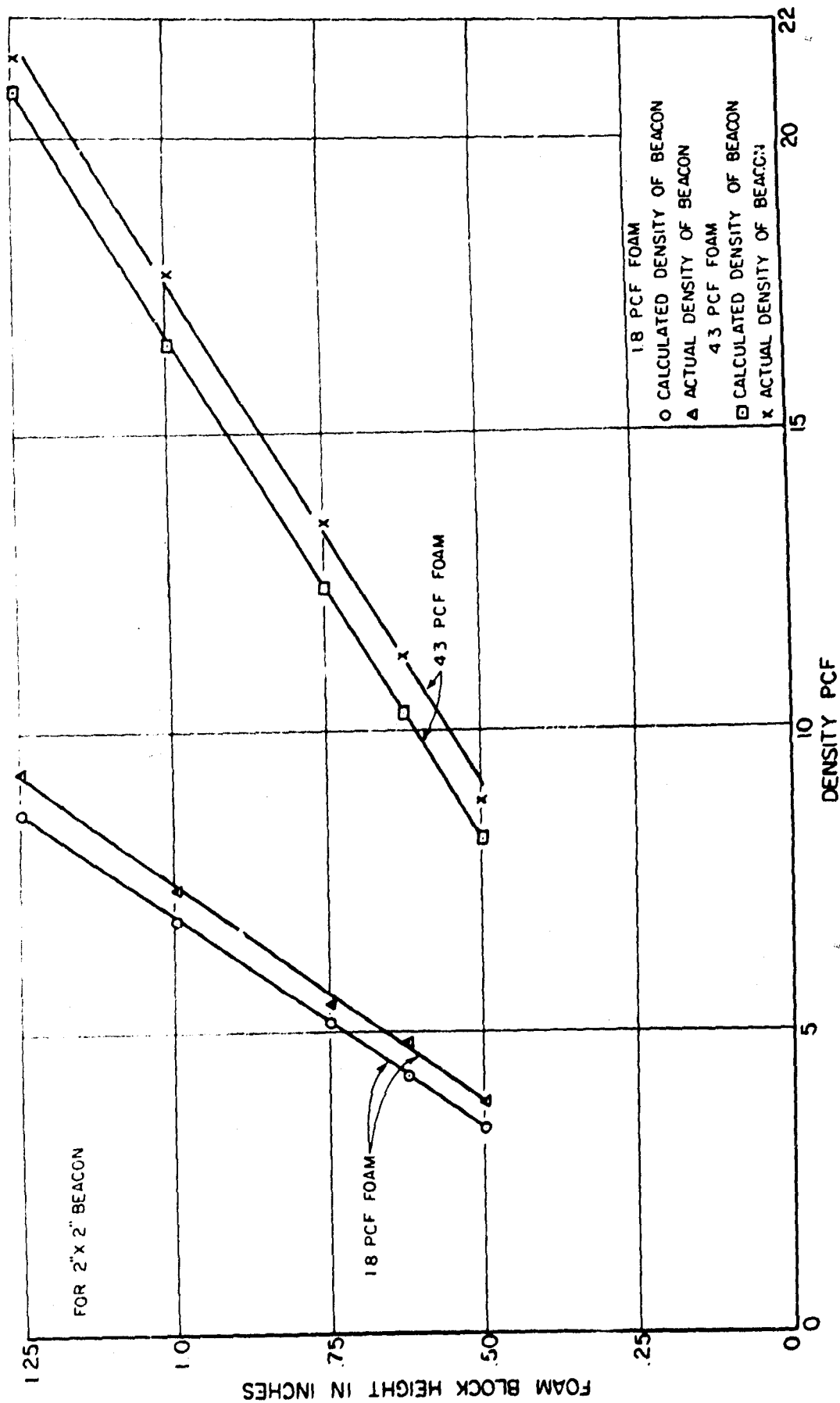FIG I FOAM BLOCK AND RESULTING C P I MODEL
(SURFACE MOUNT TYPE)

FIG. 2: MODEL DENSITY vs SIZE OF FOAM BLOCK CHART

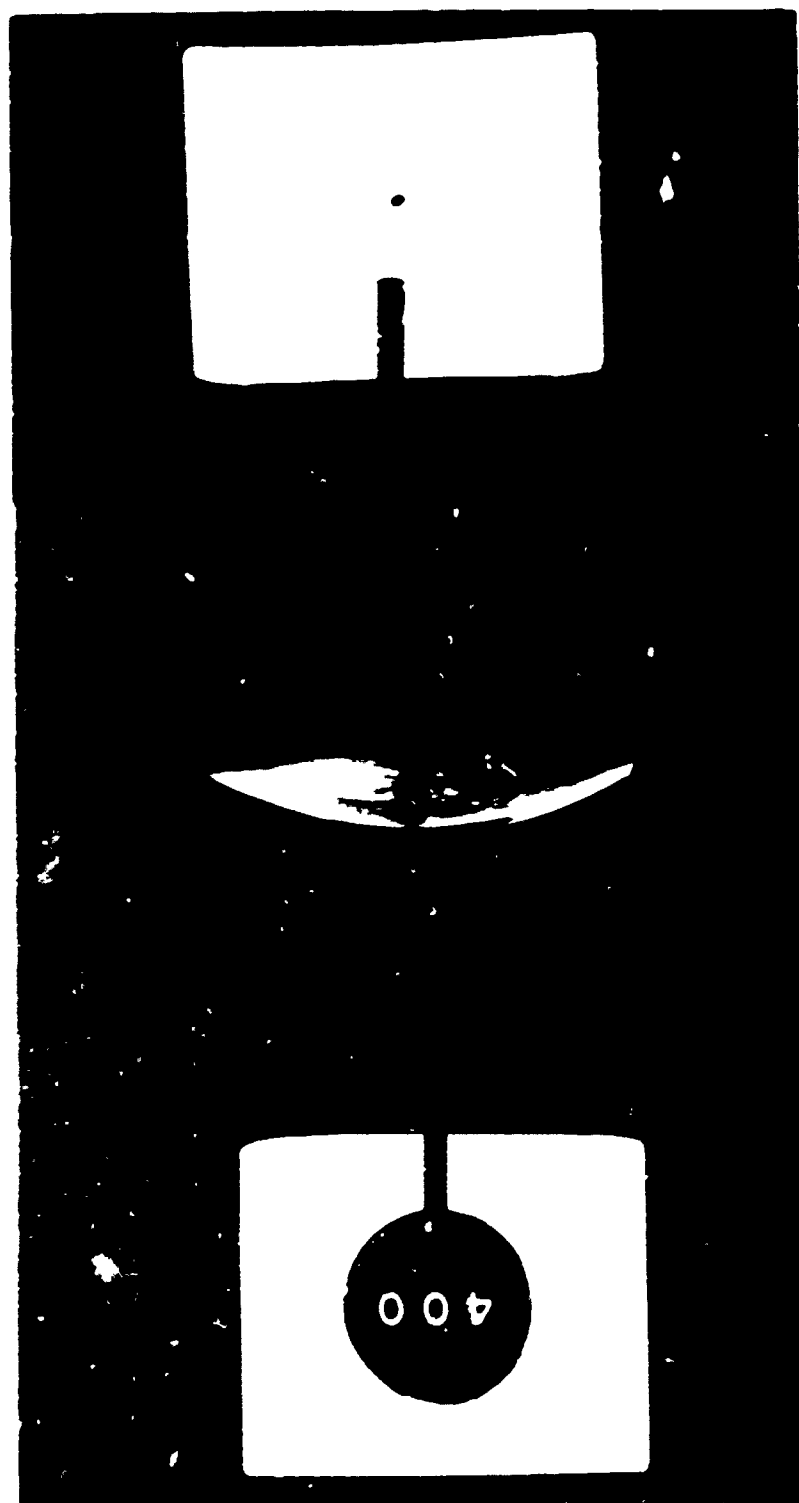FIG 5 DEVCON MOLD AND ALUMINUM TOP COVER FOR
SUPERSONIC MODEL OF C.P.I

FIG 4 MODEL C.P.1 FOR SUPERSONIC TESTS
(FLUSH MOUNT TYPE)

BLANK PAGE

NAE FLIGHT IMPACT SIMULATOR

J. W. Noonan and J. B. R. Heath

Structures and Materials Laboratory

National Aeronautical Establishment

1.0 INTRODUCTION

As aircraft become larger, fly faster, and continue to extend their field of operation, so too must test and development facilities match this extension of capability to maintain a high degree of safety in operation. Of all the hazards to flight safety the one categorized as "bird hazards to aircraft" has captured the imagination of almost everyone involved with aircraft and is currently receiving close and detailed attention by air regulatory bodies, airline operators, and military air commands. The progress reported at the recent World Conference on Bird Hazards to Aircraft held in Kingston, Ontario, in September, 1969, gave evidence that while a significant decrease in bird incidents involving aircraft in the vicinity of airports had been achieved, the incidence of en route encounters remained virtually unaffected and, in fact, showed signs of being on the increase. It would seem evident that the only measures offering any real assurance of reducing the en route hazard are those of "bird-proofing" of the aircraft.

Bird-proofing the aircraft consists in increasing the strength and the energy-absorbing capabilities of those vulnerable parts of the aircraft that are likely to be subjected to bird impacts, to a point where the statistical probability of a catastrophic failure owing to a bird strike is reduced to that which experience has dictated as an acceptable level. The areas considered to be vulnerable are the windshields, the leading edges of the empennage surfaces, and openings where ingestion into the engines can occur; wing structures are generally considered to have sufficient depth to sustain a bird strike without suffering serious damage. A great deal of useful design information can be generated by simulating bird impacts on various targets over an appropriate range of velocities and environmental conditions; force-time relations can be derived for a range of bird sizes; failure modes can be identified for different materials and combinations of materials and the ability to withstand penetration by bird sizes; and velocities spelled out in airworthiness regulations, where they exist, can be demonstrated.

The addition to the facilities of NAE of the Flight Impact Simulator, popularly known as the "bird gun", has provided a means for simulating bird strikes that is useful in providing information applicable to designing "bird-proof" aircraft and for determining the penetration velocity for critical locations on existing aircraft.

2.0 THE GUN

The core of the simulator is the pneumatic cannon or compressed air gun and, as it has been described in the NAE Report LTR-ST 281 from aspects of the operating principles and detailed design, a brief description here should be sufficient. The gun,

a photograph of which is shown in Figure 1 and a schematic diagram in Figure 2, is approximately 70 feet long and consists of a 60-foot³ reservoir, a transition section, a pressure step chamber that also functions as the breech, and a 40-foot barrel 10 inches in diameter; attached to the muzzle end is a sabot catcher. The supporting frame is pivoted on a horizontal axis at the reservoir end to permit elevation of the barrel to facilitate aiming at a target (Fig. 3).

3.0 THE SITE

The simulator is located on the grounds of the National Aeronautical Establishment at Uplands Airport and, as can be seen in the aerial photograph shown in Figure 4, it is housed in the end unit of a row of Butler-type buildings that lie in a northerly-southerly direction. At the north end of the building a concrete slab, 50 feet × 75 feet, in which steel tie-down rails are embedded forms the target area; a removable weather shelter protects the central part of the area. Approximately 150 feet from the end of the building a semi-circular earthen butt has been formed to contain flying debris resulting from the gun operations. As can be seen, the target area is readily accessible by service roads and can accommodate complete aircraft when the weather shelter is removed.

4.0 OPERATIONAL DETAILS

4.1 The Sabot

The 10-inch gun barrel permits a range of bird sizes to be used in the simulation of strikes. International airworthiness codes have established a 4-pound bird as a standard weight for impact tests; consequently the gun is extensively used for this bird weight. It is necessary to package the bird in a "sabot" that fits the barrel and will contain the bird without breaking up until it leaves the muzzle of the gun. Figure 5 shows the component parts of the sabot for a 4-pound bird. Because of the relatively large bore of 10 inches, the present sabot is only usable to a charge pressure of 50 psi; this produces a velocity of 420 knots and caters for almost all of the existing requirements.

4.2 Bird Types

Both synthetic and real birds are used in the simulator. The synthetic bird is made from a stable gel formulation consisting of cellulose gum (sodium carboxy-methylcellulose), aluminum acetate, and 98% water. The gel is cast in a cylindrical form about 5 inches in diameter and 9 inches long, the approximate dimensions of the real bird package, and packaged in a plastic envelope enclosed in a cotton bag. Figure 6 shows a real and a synthetic bird ready for packaging; no attempt has been made as yet to simulate any part of the bird's skeleton in the gel bird.

When real birds are used, they are selected from domestic fowl. electrocuted, packaged in a cotton bag and stored in a deep freeze unit until required for use. The birds are withdrawn 24 hours before use to allow them to reach room temperature.

4.3 Diaphragms

After an initial assessment of scribed 2S-O aluminum diaphragms and limited

testing of 0.0035-inch aluminum foil in single and multiple sheets, their use was discontinued in favour of the polyester film known as mylar. Diaphragms cut from this material proved to give sharp, repeatable rupture values over the fairly wide range of thicknesses in which the material is available. Figure 7 gives a table of rupture values for the 10-inch diaphragms, and Figure 8 illustrates short-term creep characteristics of the sheet material at room temperature for the 10-inch diameter diaphragm; it can be seen that the material can be held under pressure for a considerable time without the danger of an unscheduled firing taking place.

4.4 Gun Firing Sequence

After inserting the bird package and installing the diaphragms, the reservoir and step chamber are pressurized in the ratio of 2:1 to the required charge pressure, each diaphragm supporting 1/2 the reservoir pressure; depressing the operating button energizes a solenoid valve, allowing the pressure to bleed off from the step chamber, and the diaphragms are ruptured successively. The stored energy of the compressed air in the reservoir accelerates the bird package down the barrel, the sabot is arrested by the catcher at the muzzle, and only the bird travels to the target.

5.0 INSTRUMENTATION

5.1 Velocity Measurement

The velocity of the bird at impact is the single most important parameter to be measured and considerable care needs to be exercised in setting up a velocity measurement system. Prior to selecting a particular method, a number of different systems were tried. They were:

(i)   breaking of stretched wires set in the path of the bird to interrupt electrical circuits

(ii)   breaking of tapes set in the path of the bird causing light beams to impinge on photoelectric units

(iii)   interruption of a laser beam focused by an optical system on photoelectric units

(iv)   an optical system using a relatively wide and narrow light beam focused on photodiode units in conjunction with electronic counter-timer units.

Methods (i) and (ii) suffered from the same disadvantages, in that wires or tapes had to be installed before every firing. The wires or tapes had to be stretched to consistent values to achieve reproducible results and this was difficult to accomplish over the temperature range of operations from -25°F to +100°F. In addition, the holding frames had to be securely anchored to prevent movement.

Method (iii), in which a laser beam was focused through a beam splitter and a penta prism to produce two parallel beams normal to the bird path (both beams being focused on photoelectric cells to initiate and terminate a count of the time interval when interrupted by the passage of the bird) was undoubtedly a singularly accurate one, but was found to be unworkable from a practical standpoint. Problems of maintaining

alignment, and the extreme sensitivity of the device by which a false count could be generated by something as small as a raindrop, caused (iii) to be ruled out.

Method (iv) sounds complicated but is in actual fact extremely simple. It consists of an ordinary automotive-type sealed beam spotlight with a parabolic reflector that is housed in a box with the front face masked off to produce a wide thin beam, projected normally through the bird's path, to focus on a 2-inch collector lens that, in turn, is focused on a photodiode unit incorporated in an electronic trigger circuit. Two units are installed approximately 7 feet apart, and interruption of the light beams by the bird generates signals to operate a digitized electronic counter-timer to record the time elapsed between signals. When the count is terminated, the digital display of the time interval is locked in and cannot be affected by further events until the counter is reset to zero. Two completely separate systems are used, one in the horizontal and the other in the vertical plane. This redundancy was provided in case of a system malfunction. The outstanding feature of this system is that approximately 50% of the light reaching the collector lens must be interrupted before triggering a count signal, thus minimizing the chance of a false count by small stray objects; at the 50% obscuration level a signal is generated by interrupting the beam within a band of 0.005 inch in width. Other advantages are that nothing needs to be installed prior to each firing, and since the bird produces no reaction with the light beam, the frame holding the system has only to be lightly restrained. In 15 months of operation no failure of the system has occurred and maintenance has been confined to the occasional replacement of one of the spotlights. Figure 9 is a graphical representation of a unit of the system and Figure 10 shows the complete setup.

5.2 High Speed Photography

A 16-mm high speed camera of the revolving prism type is part of the normal instrumentation of the simulator. The maximum speed of the camera is 7000 frames per second, which, when projected at normal film speeds, slows down the action approximately 300 times. In normal practice the bird impact is photographed at 4000 frames per second, as increasing the film speed beyond this value requires a very substantial increase in the already high level of illumination. An electronic unit is used to control the camera start and its speed to insure the capture of the event on the film. Initiating a typical firing sequence by depressing the operating button causes (i) the camera to start about 0.5 second before the bird reaches the target, and (ii) the solenoid to bleed off the step chamber pressure approximately 0.2 second after initiation. Since in this particular sequence it takes 0.2 second from the time the diaphragm is ruptured and the bird impacts the target, the event is recorded when the camera has reached its predetermined speed. Study of the filmed events are of great value in assessing the behaviour of the target materials and the break-up of the bird at impact. Examples of high speed film coverage of (a) a 4-pound bird travelling at 317 knots in impact with the centre panel of a CF100 bullet-proof windshield are shown in Figure 11, and (b) an 8-pound bird travelling at 315 knots in impact with the leading edge of a DC8 vertical stabilizer, in Figure 12.

6.0 CALIBRATION

It is necessary to be able to predict the velocity of the bird before firing; the basis for this prediction is the relation established between the reservoir charge pressure and the velocity achieved for a given bird weight as measured by the velocity

measurement system. A series of test firings of 4-pound birds, up to a velocity of 700 ft/sec, was carried out. The air pressure in the reservoir was measured by a mercury manometer to within 0.05 in Hg (0.025 psi); the total package of sabot and bird, weighing approximately 7.0 pounds, was accelerated the length of the barrel, and after the sabot was arrested, the bird continued its flight through the measuring system, the centre of which was approximately 9 feet from the muzzle of the gun. This was the point at which the average velocity between the 7-foot spacing of the photodiode units was recorded. Synthetic gel birds and real bird carcasses were both used and no difference in velocity (that could be attributed to the difference in bird types) was established. Figure 13 gives the relation determined between reservoir pressure and bird velocity, as carried out under the conditions noted above, up to the limit of the capability of the present sabot.

7.0 DISCUSSION OF PERFORMANCE

The theoretical basis for the design of the gun was taken from a simple performance theory (Ref. 1) in which it is assumed that air stored in a reservoir of volume V_1 at pressure P_1 propels a bird package of weight W along the barrel of length L and area A by adiabatic expansion. From the equation of motion of the bird package of weight W when it has travelled a distance s along the barrel and the pressure has reached a value P_2 with an opposing pressure P_0 on the other side of the bird, the velocity u of the bird is

$$\frac{W}{g} \, u \, \frac{du}{ds} = (P_2 - P_0) \, A \tag{1}$$

$$P_2 V_2^{\gamma} = P_1 V_1^{\gamma} \tag{2}$$

$$P_2 = \frac{P_1 V_1^{\gamma}}{(V_1 + AS)^{\gamma}} \tag{3}$$

where γ = ratio of specific heats for air. By assuming that P_0 (atmospheric pressure) remains constant, and neglecting leakage and friction losses from (1) and (2)

$$\int_0^{V_c} u\,du = \left(\frac{gA}{W}\right) \int_0^L \left[\frac{P_1 V_1^{\gamma}}{(V_1 + AS)^{\gamma}} - P_0\right] ds \tag{4}$$

where V_c is taken as the velocity after travelling distance L, i.e. the theoretical muzzle velocity. Integrating gives

$$V_c^2 = \frac{2gAL}{W} \left[P_1 C_1 - P_0\right] \tag{5}$$

where

$$C_1 = \frac{K}{\gamma - 1} \left[1 - \left(\frac{1}{1 + \frac{1}{K}} \right)^{\gamma - 1} \right] \tag{5}$$

and

$$K = \frac{\text{reservoir volume}}{\text{gun barrel volume}} = \frac{V_1}{AL} \tag{7}$$

Taking V_o as the actual velocity attained, then $V_o = K_2 V_c$ where K_2 is a correction factor that varies with velocity and the particular gun design. For the NAE gun, the values of V_o obtained experimentally allowed K_2 to be determined, assuming negligible difference between muzzle velocity and the velocity as measured 9 feet from the muzzle. Figure 14 shows values of K_2 plotted against V_o over the range of velocities at which the gun has been operated; it is evident that the gun becomes less efficient at higher velocities. Extrapolation of the calibration curve shown in Figure 13 gives an indication that the maximum velocity achievable at a charge of 100 psig would be 900 ft/sec for the standard 4-pound bird as fired in the present sabot. The provision made for evacuating the air in the gun barrel should make it possible to achieve a V_o of 1000 ft/sec or higher. However, the present sabot is limited to a velocity of 700 ft/sec above which it is not completely arrested by the catcher and the possibility exists that portions of the sabot could reach the target. New sabot designs with greater energy-absorbing characteristics are under consideration, as are other means of dissipating the energy of the sabot to avoid contacting the target.

A significant amount of the energy of the air stored in the reservoir under pressure is expended in accelerating the 3-pound sabot in order to achieve the required bird velocity. It is interesting to note, however, that to minimize the sabot problem by reducing the barrel diameter to a smaller size and using the 4-pound bird without the sabot results in a lower predicted velocity for a given reservoir pressure. Considering the NAE gun where

$$W \text{ (bird + sabot)} = 7.0 \text{ lb}$$

$$L \text{ (barrel length)} = 40 \text{ ft}$$

$$A \text{ (barrel area)} = 78.54 \text{ in}^2$$

$$V_1 \text{ (reservoir volume)} = 60 \text{ ft}^3$$

$$P_1 \text{ (reservoir pressure)} = 45 \text{ psia}$$

$$P_0 \text{ (atmospheric pressure)} = 15 \text{ psia}$$

from (7)

$$K = \frac{V_1}{AL} = 2.75$$

from (6)

$$C_1 = 0.804$$

and from (5)

$$V_c = 783 \text{ ft/sec}$$

Reducing the barrel diameter to 6 inches and the weight of the bird package to 4 pounds, i.e.,

$$W = 4.0 \text{ lb}$$

$$A = 28.27 \text{ in}^2$$

$$K = \frac{V_1}{A L} = 7.65$$

and

$$C_1 = 0.921$$

$$V_c = 694 \text{ ft/sec}$$

At 45 psia (30 psig) the actual velocity V_a achieved with the 10-inch diameter barrel and the 7-pound bird package was 560 ft/sec and gave a value for K_2 of 0.715, which represents an increase over values for 6-inch diameter barrel configurations reported for other installations (Ref. 1, 3).

The operation of the simulator in conjunction with the current sabot design has proved to be accurate and efficient in the velocity range from 250 to 700 ft/sec, the range of most interest for bird impact simulation, and serves the purpose for which it was designed. Further development to extend the velocity to the 1000-ft/sec level will be undertaken in the order in which priorities are established.

8.0 TYPICAL IMPACT SIMULATIONS

Figure 15 shows the results of impacts on the leading edge of a DC8 horizontal stabilizer. The left-hand impact was made by a 4-pound gel bird travelling at 389 knots and the right-hand by a real bird carcass travelling at 357 knots. Superficially the two impacts look somewhat the same but, whereas the gel bird merely penetrated the leading edge skin, the real bird penetrated the leading edge skin, the main spar web, and some of the denser portions of the bird penetrated the rear spar; the fact that the gel bird was travelling at a greater velocity than the real bird indicates the magnitude of the problem of producing an acceptable synthetic substitute for the real bird.

Figure 16 shows a closeup view of the results of the 8-pound bird impact with the leading edge of a DC8 vertical stabilizer, shown at high speed in Figure 12. The bird was travelling at 315 knots and penetrated the triple leading edge skins, the main spar web, several canted ribs, and substantial portions of the bird contacted the rear spar. This particular shot was made in response to the FAA invitation to comment on

their proposal that the leading edges of the empennage surfaces of transport aircraft should be required to demonstrate the ability to sustain an 8-pound bird impact at cruise velocity at sea level (Ref. 2); comments have been forwarded to FAA. Figure 17 shows the results of the 4-pound bird in impact with the centre panel of a CF100 windshield, shown at high speed in Figure 11. The multi-layered glass and plastic panel were able to withstand penetration by the bird, but the cast magnesium frame was broken in three places; the most prominent break can be seen at the top left-hand side of the frame. The fifth frame from the top in the high speed photographs shown in Figure 11, is also worthy of note. It shows that the liquid-like flow of the bird on contact can cause high hydraulic forces to develop, and in this case bird fluids and tissue extruded between the top of the centre panel and the metal frame, even extruding through torn rivet holes on the inside, an indication of an extremely important detail to be taken into consideration at the design stage.

9.0 CONCLUSIONS

The NAE Flight Impact Simulator has been developed into a reliable impact loading tool operating through a velocity range from 250 to 700 ft/sec, using 4- and 8-pound birds as projectiles. Performance over this range has exceeded the designed value for K_2 of 0.58, i.e. the actual velocity $V_o = 0.58 \ V_c$ predicted originally has been exceeded by approximately 12%; a value of 0.70 has been achieved for K_2 and $V_o = 0.70 \ V_c$ at 700 ft/sec. The velocity can be predicted to within ·3% and measured to within ±0.5%. Further development to increase the velocity to 1000 ft/sec will be undertaken as allocation of priorities permits.

10.0 REFERENCES

1.   Perfect, D.A.   The Development of a Smooth Bore Gun for the Projection of Bird Carcasses
RAE Tech. Report No. 66008, January 1966.

2.   FAA Proposal, Dept. Transport Federal Aviation Administration Docket 9079: Notice 68-18, Sec. 25-631.

3.   Peake, D.J.   Two Laboratory Methods of Obtaining a Relative Velocity Between a Bird and a Structure.
NRC, Mech. Eng. Gas Dynamics Lab. Note GD-138, August 1963.

FIG. 1: COMPRESSED AIR GUN

HYDRAULIC SHOCK
ABSORBER

DIAPHRAGM No. 1

DIAPHRAGM No. 2

SABOT CATCHER

STEP
CHAMBER

LOCATION OF SABOT WITH
BIRD PRIOR TO FIRING
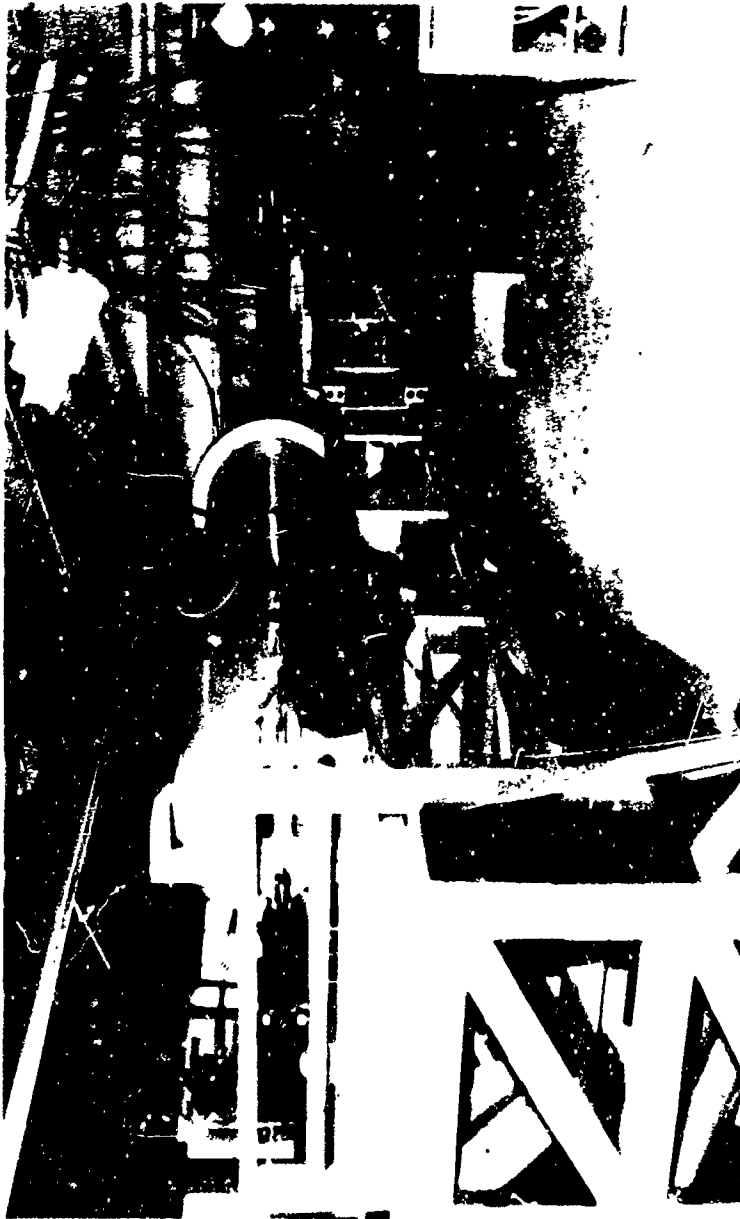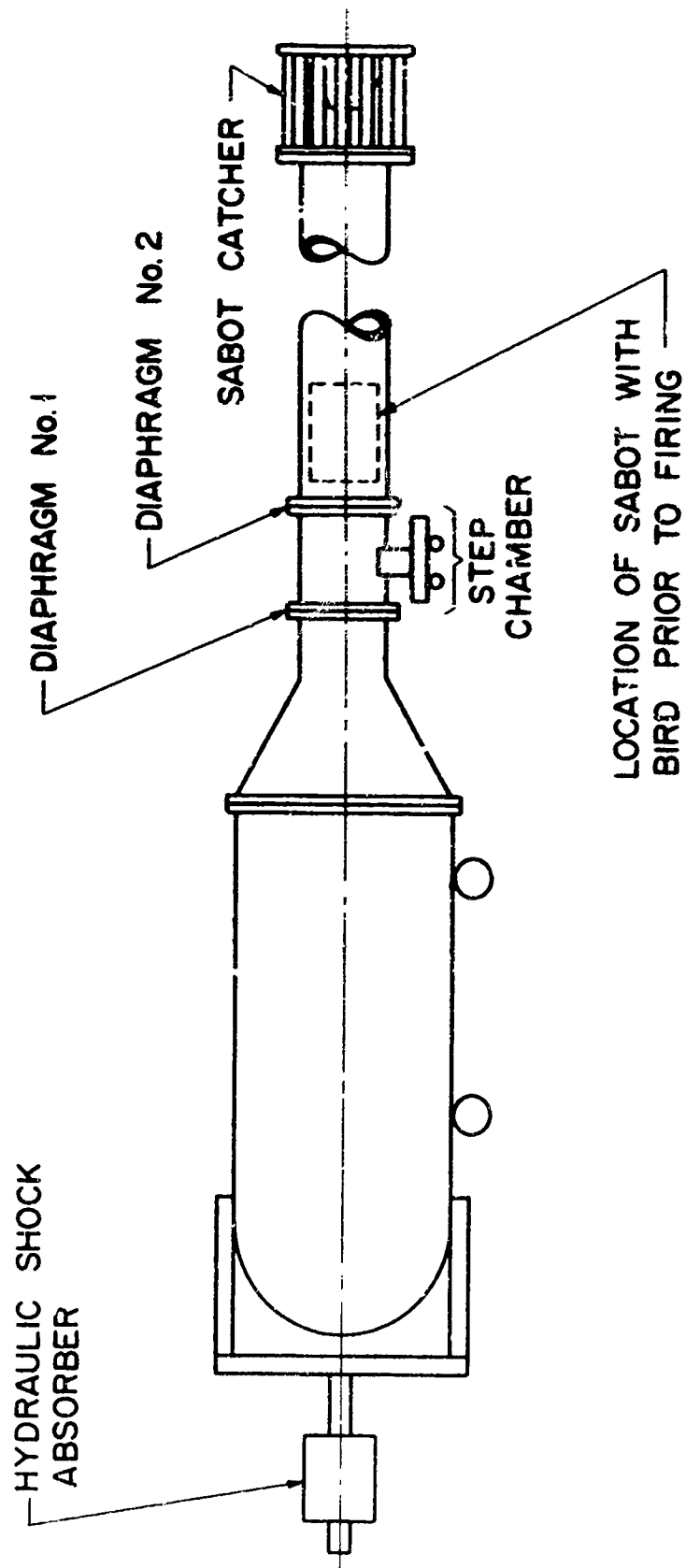
FIG. 2: SCHEMATIC DRAWING OF GUN
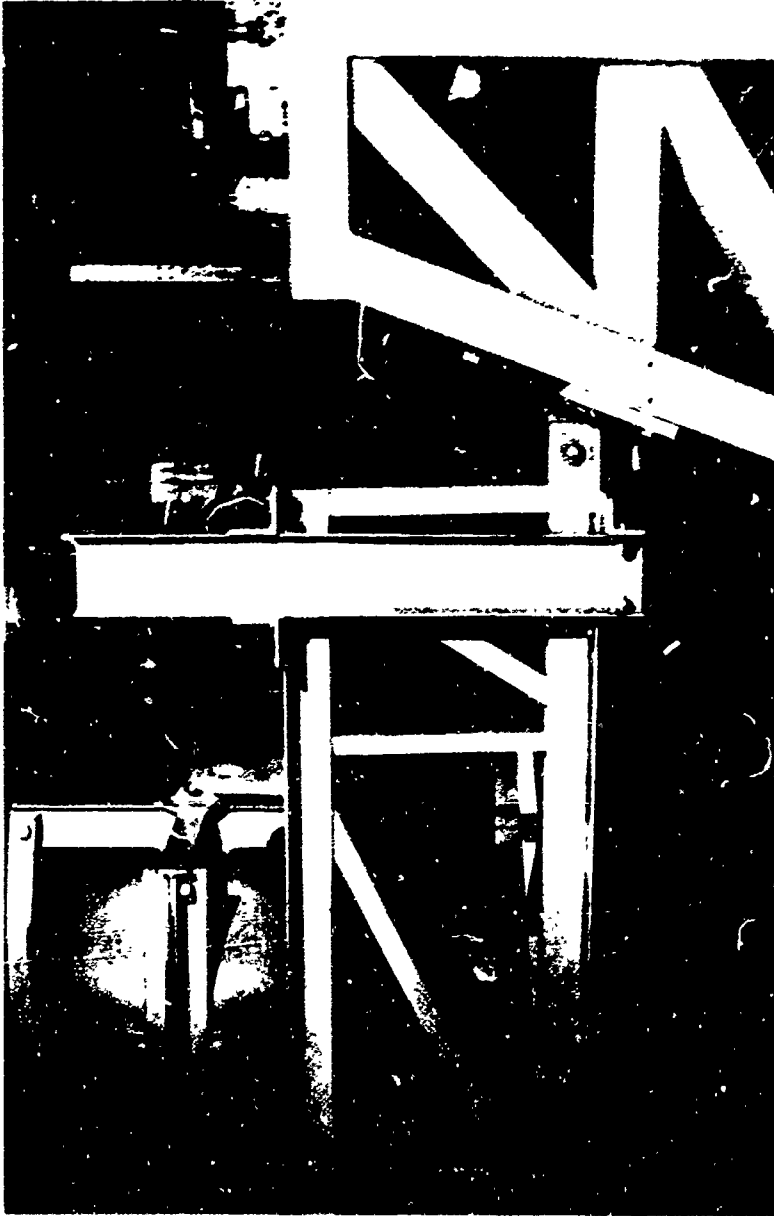
FIG. 3: GUN PIVOT TO FACILITATE AIMING
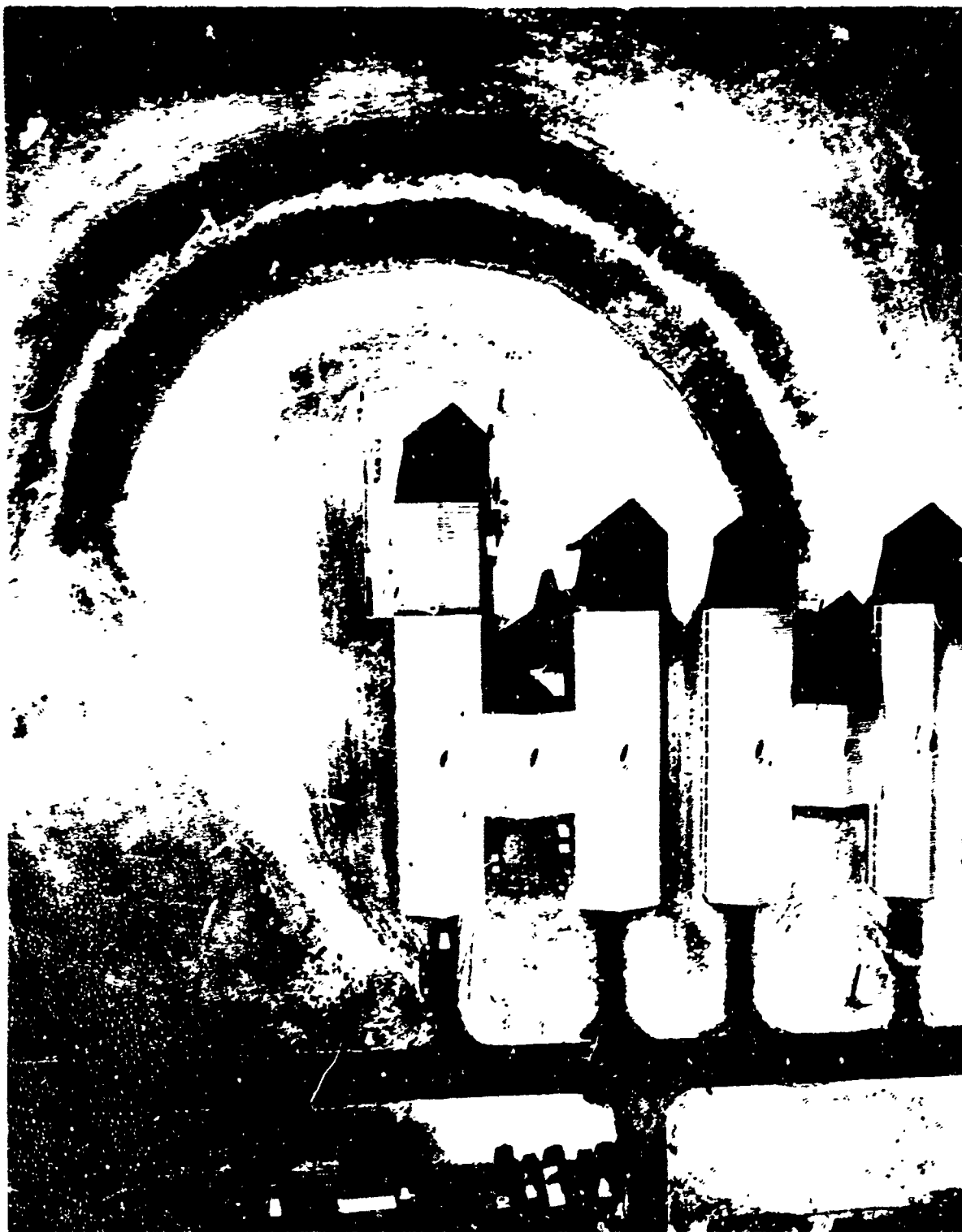
FIG. 4: AERIAL PHOTOGRAPH OF SITE
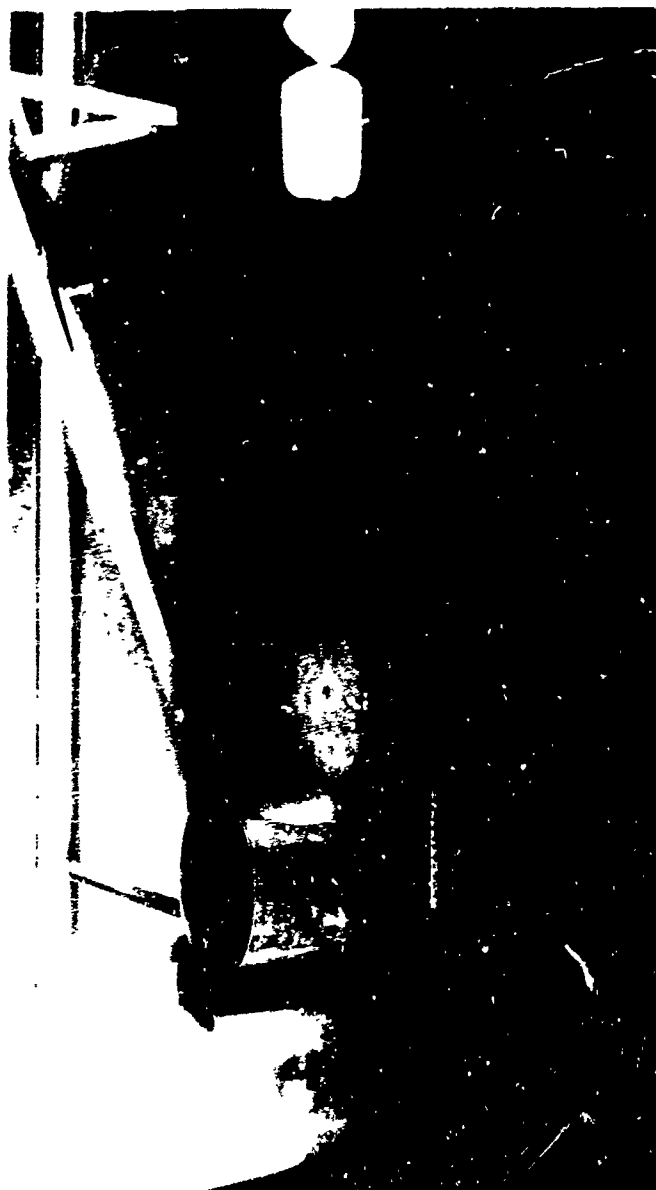
FIG.5: SABOT AND COMPONENT PARTS

FIG. 6: REAL AND SYNTHETIC BIRDS READY FOR
PACKAGING

DIAPHRAM THICKNESS (in)	PRESSURE TO RUPTURE (psi)	REMARKS
0.001	7.13	IN ALL CASES THE MINIMUM VALUE MEASURED IS REPORTED.
0.002	12.1	
0.003	16.4	VARIATION OF THESE VALUES CAN BE EXPRESSED
0.005	32.8	AS $+0.50$
0.0075	45.5	-0.00 psi

FIG.7: TABLE OF RUPTURE VALUES FOR 10-INCH DIAMETER MYLAR DIAPHRAGMS
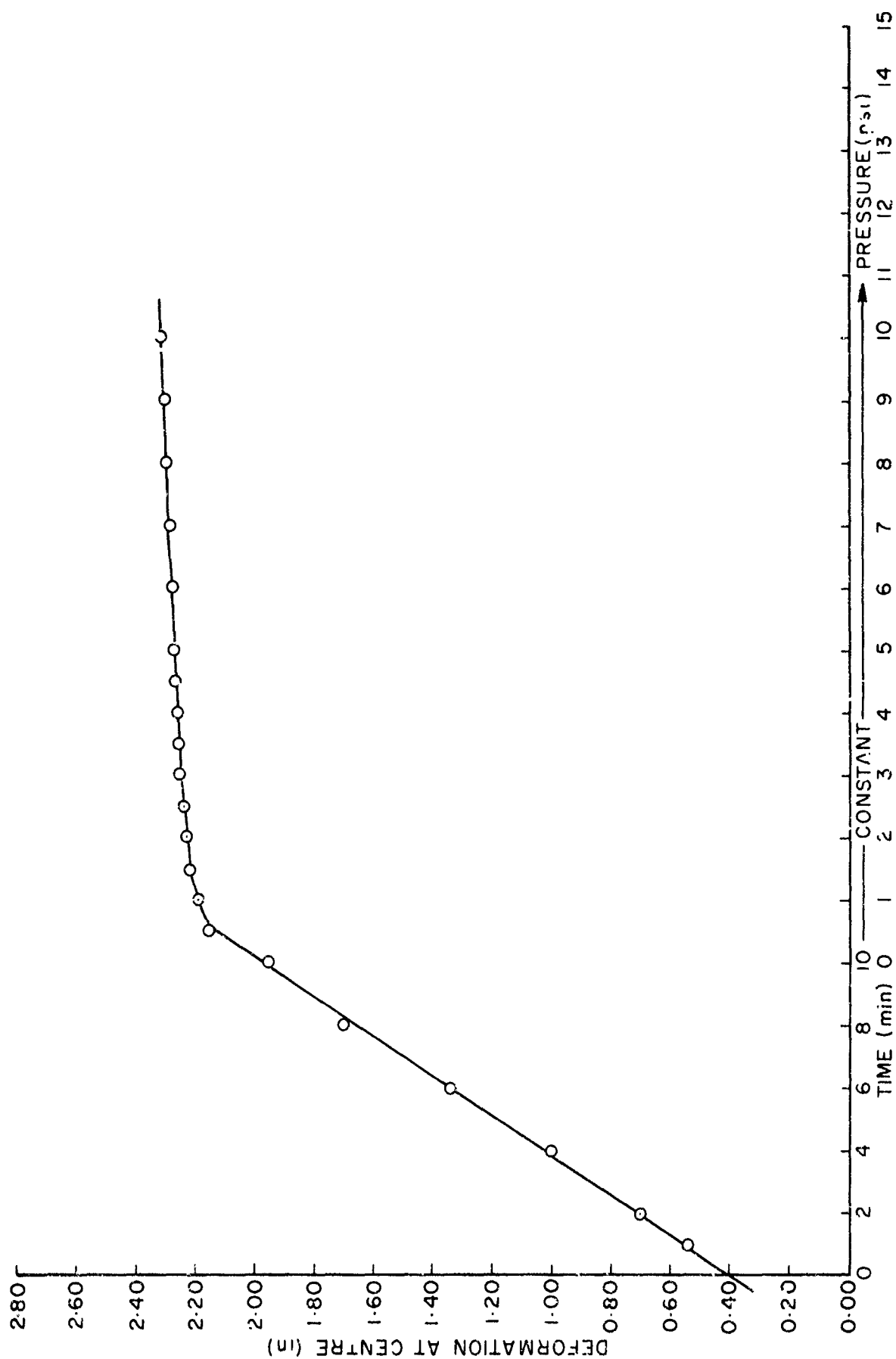
FIG.8: SHORT TERM CREEP CHARACTERISTICS OF 0·003-INCH MYLAR DIAPHRAGM
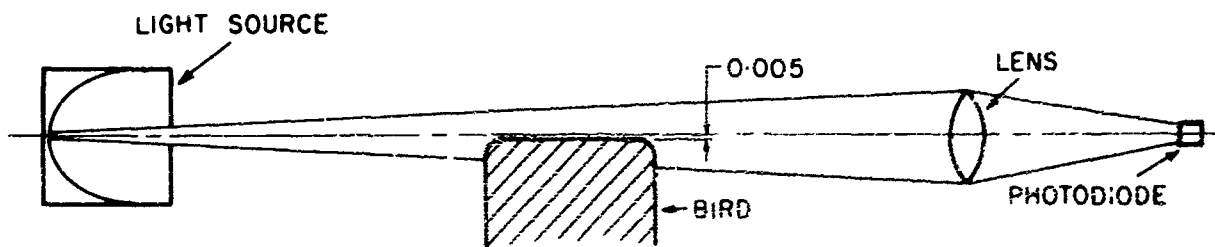
(a) TRIP BAND SHOWN IN VERTICAL PLANE
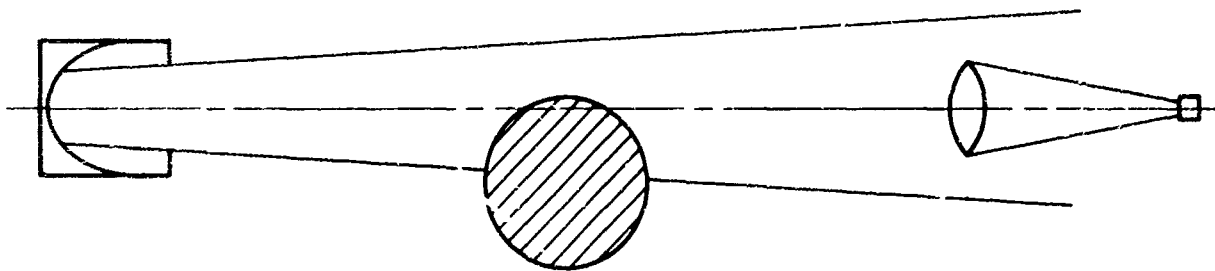
(b) MINIMUM OF 50 % LIGHT OBSCURED TO TRIGGER SIGNAL
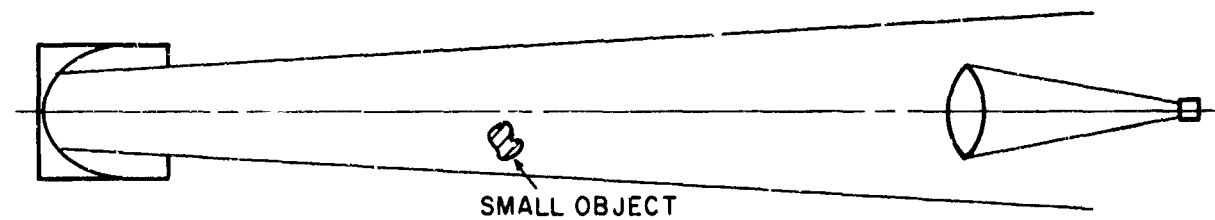
(c) LESS THAN 50 % DOES NOT TRIGGER SIGNAL

FIG. 9: VELOCITY MEASURING DEVICE
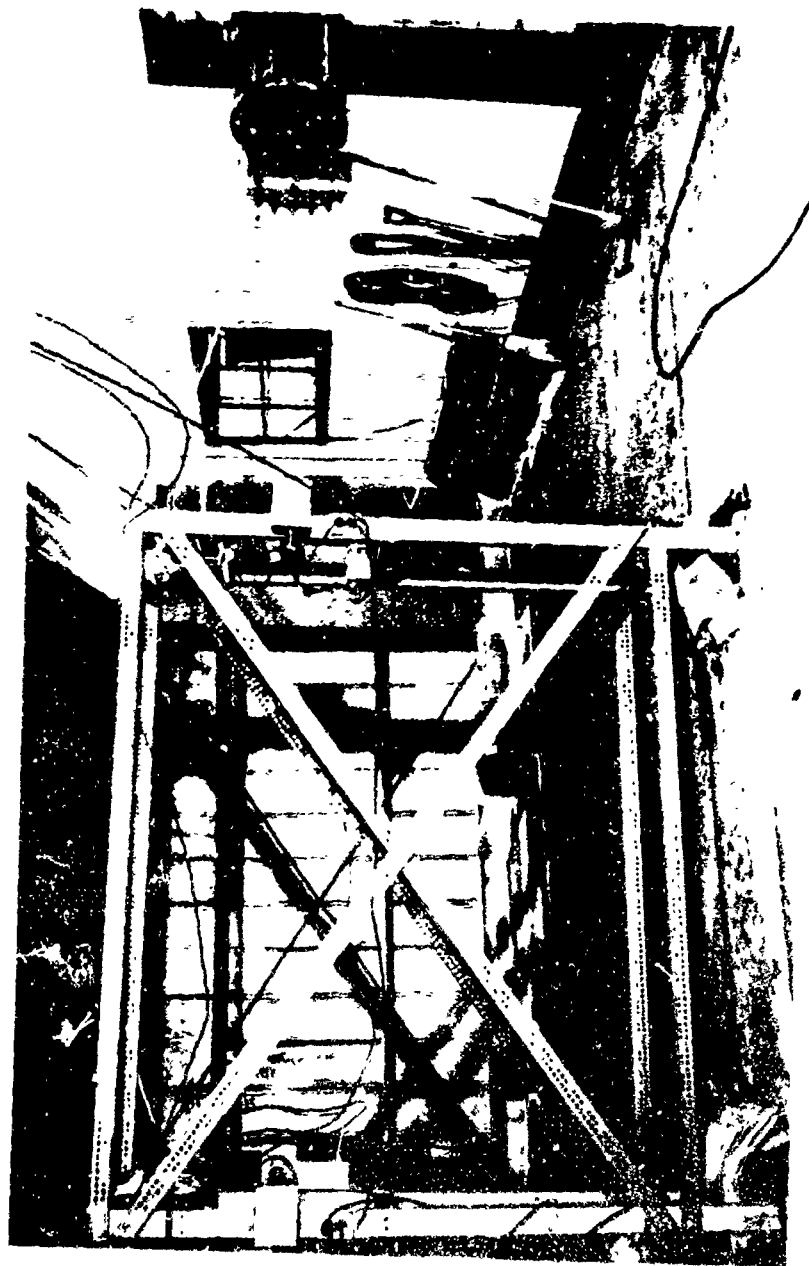
FIG. 10: PHOTO-ELECTRIC TIMING RACK
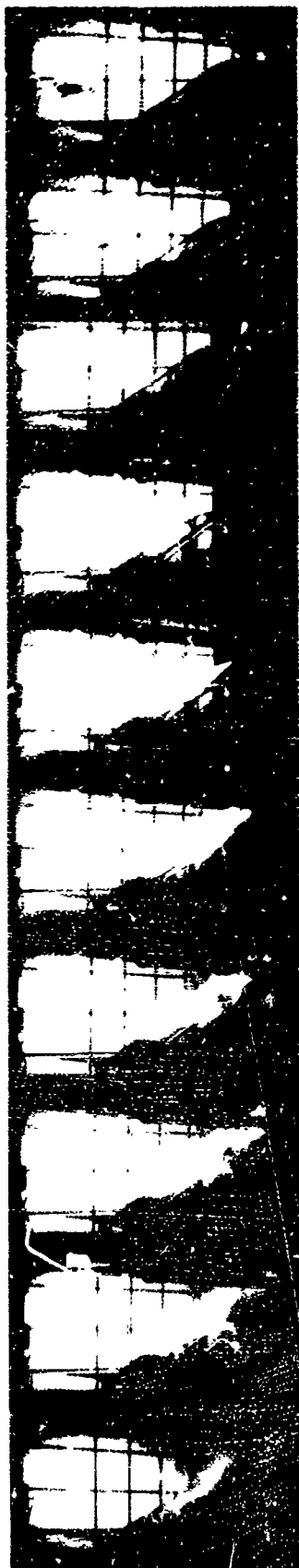
FIG.11: 4-POUND BIRD IN IMPACT WITH
CF100 WINDSHIELD AT 317 KNOTS
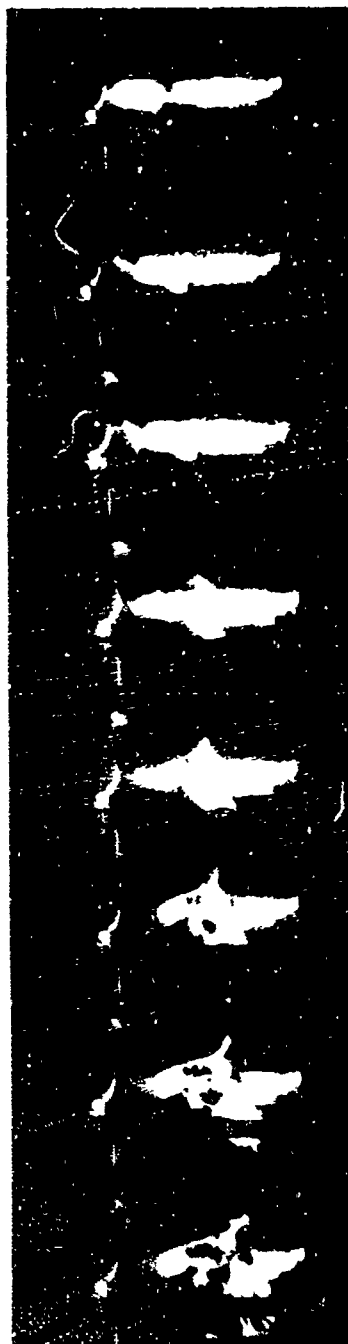
FIG.12: 6-POUND BIRD IN IMPACT
WITH DC8 VERTICAL STABILIZER
AT 315 KNOTS
(STABILIZER IN HORIZONTAL
POSITION)
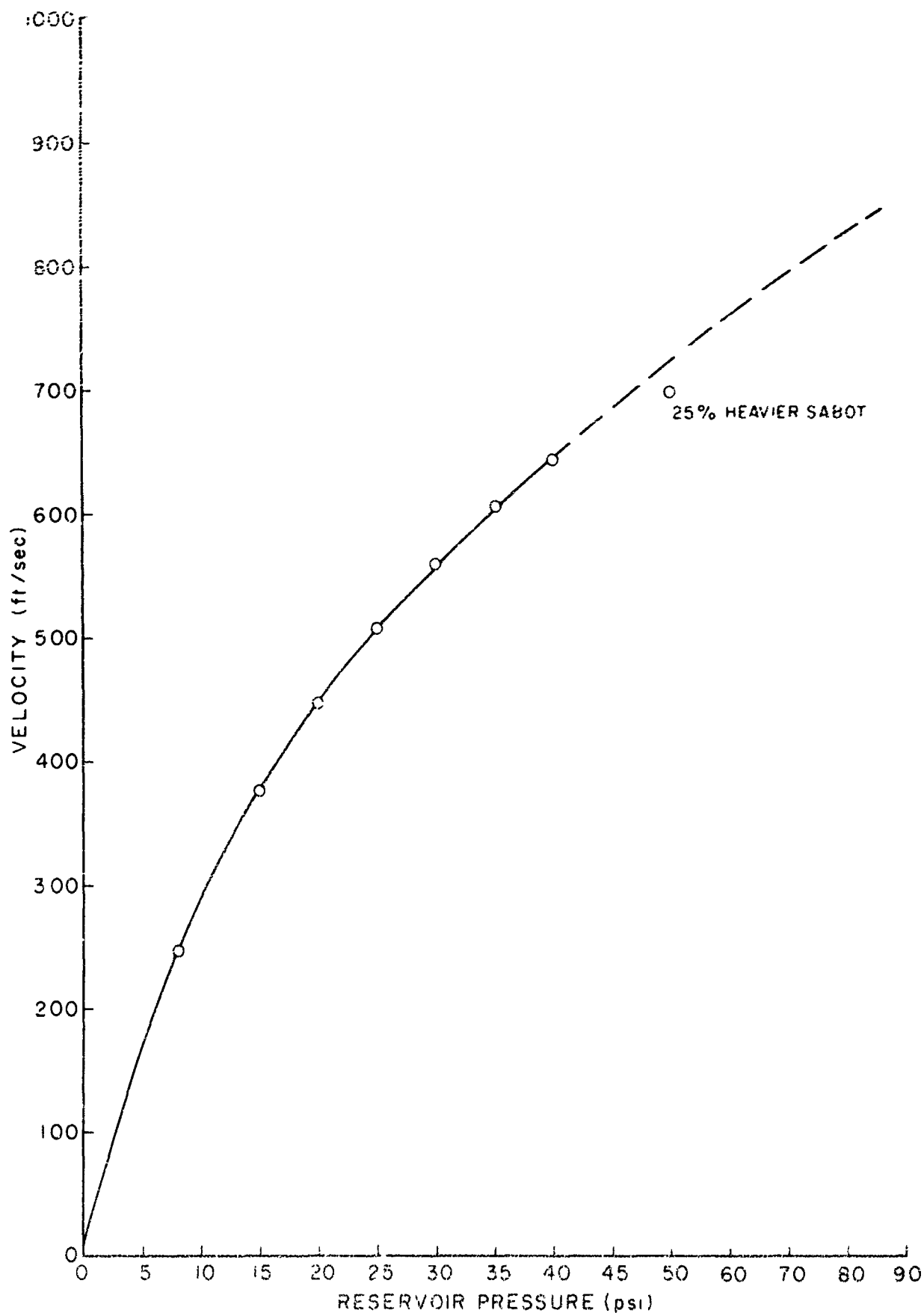
FIG.13. CALIBRATION CURVE FOR 4-POUND BIRD
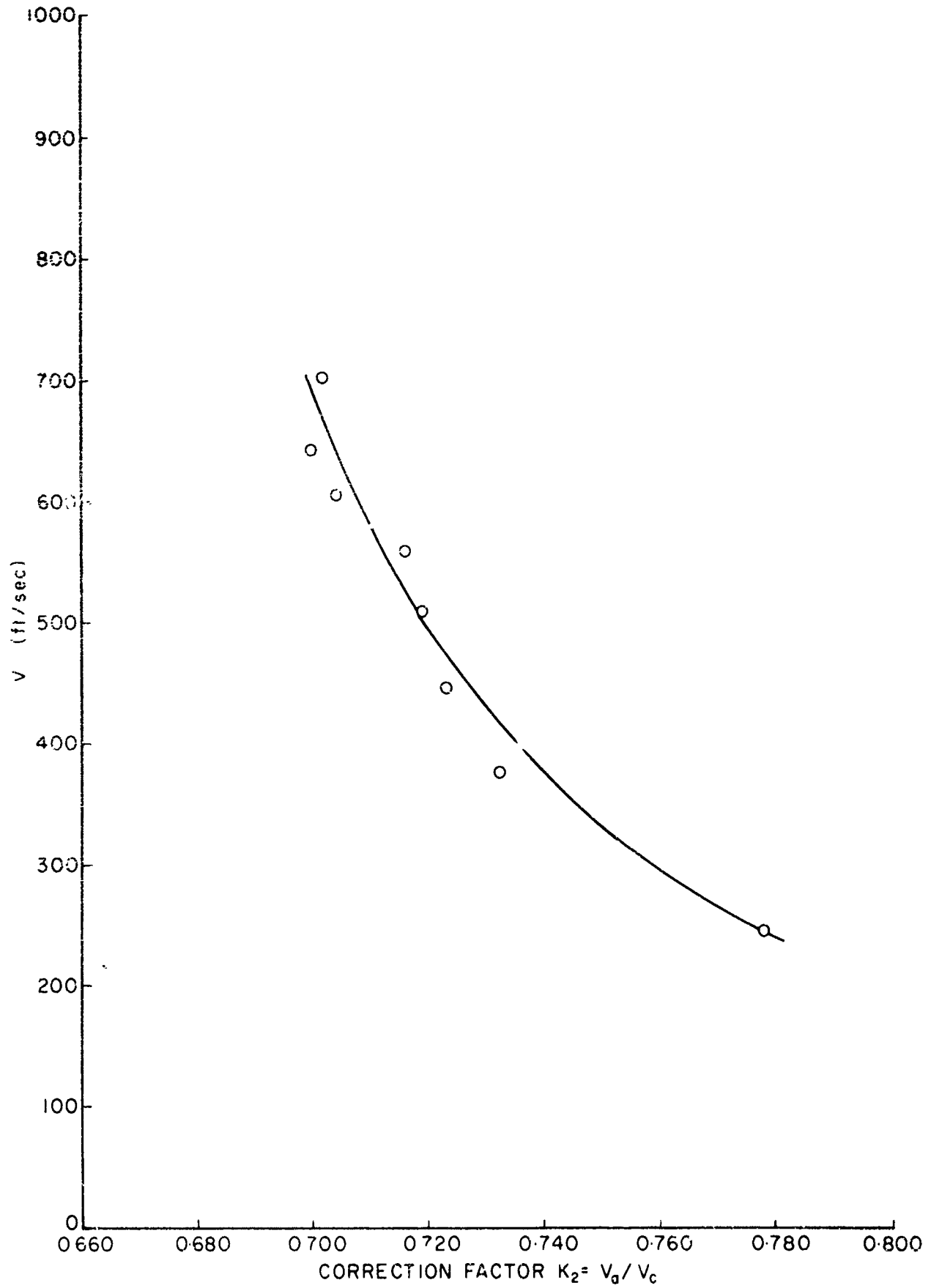
FIG. 14: RELATION OF CORRECTION FACTOR K_2 TO ACTUAL VELOCITY V_a

FIG. 16: 8-POUND BIRD IMPACT ON DC8
VERTICAL STABILIZER AT 315 KNOTS

FIG. 15: 4-POUND BIRD IMPACT ON DC 8
HORIZONTAL STABILIZER

FIG. 17: RESULT OF 4-POUND BIRD IMPACT
ON CF100 WINDSHIELD AT 317 KNOTS

CURRENT PROJECTS

Much of the work in progress in the laboratories of the National Aeronautical Establishment and the Division of Mechanical Engineering includes calibrations, routine analyses and the testing of proprietary products; in addition, a substantial volume of the work is devoted to applied research or investigations carried out under contract and on behalf of private industrial companies.

None of this work is reported in the following pages.

BLANK PAGE

AVAILABLE FACILITIES

This laboratory has analysis and simulation facilities available on an open-shop basis. Enquiries are especially encouraged for projects that may utilize the facilities in a novel and/or particularly effective manner. Such projects are given priority and are fully supported with assistance from laboratory personnel. The facilities are especially suited to system design studies and scientific data processing. Information is available upon request.

EQUIPMENT

1. An Electronic Associates 690 HYBRID COMPUTER consisting of the following:

   (a) EAI 640 digital computer

      - 16K memory
      - card reader
      - high speed printer
      - disc
      - digital plotter

   (b) EAI 680 analogue computer

      - 120 amplifiers
      - non-linear elements
      - x-y pen recorders
      - 6-channel strip chart recorder
      - large screen oscilloscope

   (c) EAI 693 interface

      - 18 digital-to-analogue converters
      - 32 analogue-to-digital converters
      - interrupts, sense lines, control lines

2. A Precision Instruments Model 400 FM tape recorder. IRIG standard (10 KHz) as well as extended bandwidth IRIG standard (20 KHz) record and playback electronics; 14 data tracks (1 inch tape) plus 2 voice channels or 7 data tracks (1/2 inch tape). 15/16 inches per second to 120 inches per second tape speed.

GENERAL STUDIES

Study of computing methods in optimal control.

Development of statistical analysis techniques for the analysis of analogue recorded data, including digital and hybrid implementations.

Study of hybrid computing techniques for parameter optimization in dynamic systems.

Study of the problem of decoupling multivariable systems by state variable feedback.

APPLICATIONS STUDIES

In collaboration with the Flight Research Laboratory of NAE, a study is being made of magnetic fields generated by surface waves and interval waves in oceans.

In collaboration with the Flight Research Laboratory of NAE, statistical analysis techniques are being developed for the analysis of clear air turbulence records.

In collaboration with Graham F. Crate Ltd. and Trans Canada Pipe Lines, a hybrid computer simulation of a natural gas pumping station is being developed. Numerous control schemes for operating the compressors in parallel are being investigated.

Development of digital programs for the analysis of data obtained by NRC's Biosciences Laboratory in the study of the effects of low temperature on rats.

In collaboration with the Mechanical Engineering Dept. of Queens University, a hybrid technique is being developed for the solution of the partial differential equation describing the gas pressures in the ducts of a two-stroke engine.

In collaboration with the Engine Laboratory of DME, a hybrid computer simulation of a free-piston-activated hydraulic pump is being studied. The simulation is being used to establish the engine geometry for efficient operation over wide hydraulic power levels.

Development of programs to use a magnetic disk as virtual memory for the EAI 640 computer

In collaboration with Canadian Aviation Electronics in Montreal, digitizing of data for a fully automatic compensation system for magnetic anomaly detection is being performed.

Development of programs to produce a parallel perspective drawing of a function of two variables, using the digital plotter. Also some study on the elimination of hidden lines in perspective drawings and on contour mapping of functions of two variables.

PRECEDING PAGE BLANK

Development of a curve-fitting digital computer program to allow fitting of analytic functions of many types to experimental data. The package provides on-line operator/computer dialogue as well as on-line plotting of results.

Digital programs for performing power spectral density, cross-spectral density, auto- and cross-correlation analyses, using a Fast Fourier Transform algorithm, are being developed for the Hydraulic Section of the Division of Mechanical Engineering.

In collaboration with the Canadian Pacific Railway, an appraisal study of the riding properties of the CPR 80-foot container cars is being conducted on the EAI 690 hybrid computer system.

APPLICATIONS STUDIES BY OTHERS

The Radio and Electrical Engineering Division is using the EAI 640 digital computer, digital-to-analogue and analogue-to-digital converters in processing data for the study of polarization of solar emission.

The Flight Research group of the NAE is using the EAI 640 digital computers, digital-to-analogue, analogue-to-digital converters and Calcomp plotter in obtaining power spectra of MAD (Magnetic Anomaly Detection) signals.

CONTROL SYSTEMS LABORATORY

INDUSTRIAL CONTROL PROBLEMS

Investigation of industrial systems applications of fluidic circuits.

In collaboration with the Department of Energy, Mines and Resources, an investigation of the process dynamics and control characteristics of an electric arc furnace for processing iron ore.

Dynamic modelling of electric arc and oxygen steelmaking processes.

Investigation of the process dynamics and control characteristics of a copper converter.

LARGE SYSTEMS STUDIES

Investigation of the possible influence of fresh water outflow on climate.

HUMAN FACTORS ENGINEERING

A general program of research and development in the Human Factors Engineering field that includes the following:

Investigation of the control characteristics of the human operator and the basic phenomena underlying tracking performance.

Investigation of the nature of sensory interaction in human perceptual-motor performance.

Investigation of the factors involved in the presentation and processing of information, particularly in relation to simulator design.

BIOLOGICAL ENGINEERING

A general program of research and development in the biological engineering field that includes the following:

Investigation of the implementation of feedback control in living organisms.

Investigation of data transmission processes, with particular reference to nerve conduction characteristics.

Investigation of auditory methods of monitoring electrophysiological signals in general and the electroencephalograph in particular.

Development of depth probes for the study of electrical activity in the deep structures of the human brain.

Development of stereo-taxic and other apparatus for neurosurgical procedures.

Development of a phase memory filter for electroencephalograph studies.

Investigation of muscle control by ordered electro-stimulation.

PATTERN RECOGNITION

Investigation of the fundamentals of pattern recognition.

Development of techniques for the identification of biological cell populations, fingerprints etc.

BIRD DISPERSAL BY MICROWAVE RADIATION

Investigation of the effect of low-intensity microwave radiation on the behaviour of birds on the ground and in the air, to determine the practicability of using microwave radiation for dispersing birds on airfields and from the flight path of an aircraft.

ENGINE LABORATORY

FREE PISTON ENGINES

Study of the free piston engine and its applications. Mathematical study of the dynamic and thermodynamic processes in the engine, using computer simulation techniques, with a view to elucidating starting and control phenomena. Experimental assessment of the operation and performance of the free piston engine in the laboratory. Study of the injection system most suitable for the peculiar requirements of the free piston engine, with possible application to all direct injection engines. The computer simulation technique has recently been extended to the study of hydraulic power take-off from a free piston engine through a pneumatic coupling.

DUCTED FAN AERODYNAMICS

Aerodynamic performance study of highly loaded ducted fans, with particular reference to inlet and outlet distortion phenomena as encountered typically by VTOL aircraft. Analytic study of the flow through a short compressor that operates with non-uniform inflow and outflow conditions. Experimentally assessed performance of a fan-in-wing model in a closed test section wind tunnel over a range of inflow ratios, angles of attack, and with a variety of inlet shapes.

V/STOL NOISE STUDIES

Study of the mechanism of the generation and suppression of noise produced by ducted fans for VTOL aircraft. Identification of the noise sources and relating the strength of the sources to the physical parameters of the system.

IN-FLIGHT THRUST METER FOR JET ENGINES

An investigation concerned with the development of a meter capable of indicating continuously the gross thrust of a jet engine, being carried out in conjunction with a Canadian electronics firm.

CENTRIFUGAL COMPRESSORS

Design and performance investigation of centrifugal compressors, including study of flow phenomena in oversize model impellers. Detailed study of devices for stabilizing the flow in the channels of a complete but simplified impeller. Test facilities have been expanded to permit improved correlation between flow patterns and performance.

AXIAL COMPRESSORS

Preliminary analytical and experimental studies of small axial compressors.

LOCOMOTIVE DIESEL ENGINE PROBLEMS

In co-operation with the Canadian National Railway and the Canadian Pacific Railway, an investigation of locomotive diesel engine problems, including those arising from the use of Athabasca Tar Sands crude oil as fuel. Studies of wear processes in the engine employing a specially developed, new method of spectrographic sampling of cylinder oil. Investigation of several new types of lubricating oil, oil filters, different kinds of cylinder liners etc. with respect to engine wear. Exploratory investigation and tests for planning a maintenance monitoring system on board diesel locomotives in service.

FOAMED-CLAY MATERIALS

Investigation of novel light-weight foamed-clay building materials, with respect to chemical composition and physical properties. Application is being made for patents on the process, after which it will be offered to Canadian Manufacturers.

J-85 JET ENGINE MOUNTED ON TEST BED
FOR FLIGHT THRUSTMETER PROGRAM

ENGINE LABORATORY
DIVISION OF MECHANICAL ENGINEERING

FLIGHT RESEARCH LABORATORY

DESIGN AND DEVELOPMENT TESTING OF A CRASH POSITION INDICATOR FOR HELICOPTERS

Experiments on models, supplemented by theoretical analyses, are being conducted for the purpose of evolving an improved crash position indicator for helicopters.

AIRBORNE REMOTE SENSING OF MAGNETIC PHENOMENA

Experimental and theoretical studies relating to the further development and use of magnetic airborne detection equipment. Equipment under development is installed on a North Star aircraft, which is used as a flying laboratory and for preliminary surveys requested by various Government Departments and other agencies.

A Beech Queenair aircraft is also being equipped and operated for the Department of Energy, Mines and Resources as a prototype for future general aeromagnetic surveys.

AIRBORNE REMOTE SENSING USING INFRA-RED TECHNIQUES

The same North Star aircraft is being used to investigate the potentialities of airborne infra-red techniques in hydrological surveying, soil, permafrost studies, and other possible applications.

INVESTIGATION OF FLYING QUALITIES AND CONTROL SYSTEM REQUIREMENTS APPLICABLE TO V/STOL AIRCRAFT

Airborne simulation techniques, using helicopters equipped to provide variable stability and control properties, are being employed to explore the effects of the numerous parameters involved and to produce data that are directly applicable for design purposes. Specific investigations are also being conducted for aircraft manufacturing firms and other agencies. Whenever possible direct comparisons are made between results obtained using the helicopter equipped as an airborne simulator and those obtained on actual VTOL and STOL aircraft. A Bell 47G3B1 helicopter with variable characteristics in four degrees of freedom is used for current research. A Bell 205A1 helicopter is being developed as an airborne simulator with variable characteristics in six degrees of freedom.

INVESTIGATIONS RELATING TO FOREST FIRE CONTROL BY AERIAL METHODS

Studies of various factors determining the effectiveness of aerial fire suppression methods, including theoretical and experimental work on the behaviour of liquids released into an airstream, operational analyses, and the investigation of aircraft design requirements. Data on aircraft behaviour and on liquid drop patterns are being obtained from flight experiments with a number of typical fire-bombing aircraft.

INVESTIGATION OF ATMOSPHERIC TURBULENCE

A T-33 aircraft, equipped to measure wind gust velocities, air temperature, wind speed, and other parameters of interest in turbulence research, is being used for several investigations. These include measurements at very low altitude, in clear air above the tropopause, in the neighbourhood of mountain wave activity, and near storms. Records are obtained on magnetic tape to facilitate data analysis. Clear air turbulence detection methods are also being investigated. The aircraft also participates in co-operative experiments with other Canadian and foreign research agencies. A second T-33 aircraft is used in a supporting role for these and other projects.

A USAF RB-57F aircraft has been instrumented and is gathering turbulence data on routine flights above 50,000 feet.

AIRCRAFT OPERATIONS

Various studies relating to aircraft operations are made from time to time. These may involve such matters as the provision of technical assistance during accident investigations, the analysis of particular aspects of aircraft behaviour in operations, or the preparation of recommendations on flight recorder requirements and specifications.

INDUSTRIAL ASSISTANCE

Assistance is given to aircraft manufacturers and other companies requiring the use of specialized flight test equipment or techniques.

FLIGHT INVESTIGATION OF SPRAY DROPLET RELEASE FROM AIRCRAFT

A Harvard aircraft is being equipped for spray nozzle flight experiments.
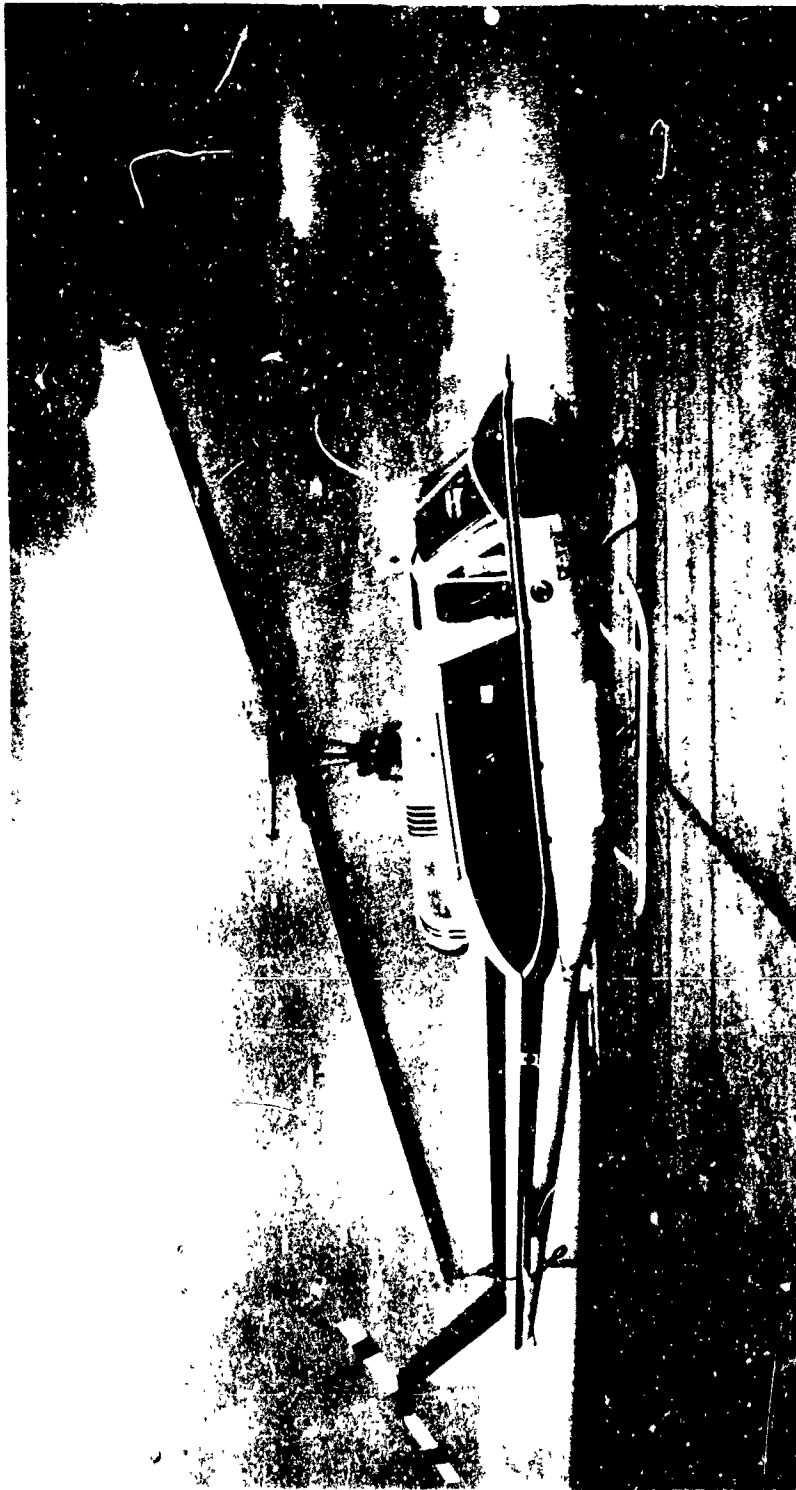
DURING THE NEXT TWO YEARS THIS AIRCRAFT WILL BE EXTENSIVELY
MODIFIED FOR USE AS AN AIRBORNE V/STOL AIRCRAFT SIMULATOR
WITH VARIABLE CHARACTERISTICS IN ALL SIX DEGREES OF FREEDOM.

BELL 205AI HELICOPTER PURCHASED IN SEPTEMBER 1969

FLIGHT RESEARCH LABORATORY
NATIONAL AERONAUTICAL ESTABLISHMENT

FUELS AND LUBRICANTS LABORATORY

HYDROGEN-OXYGEN ENGINES

Theoretical studies aimed at producing the best design features for hydrogen-oxygen engines in multi-stage vehicles.

Investigation of heat transfer in a 500-lb thrust rocket combustion chamber using a water-cooled chamber burning hydrogen and oxygen.

Testing of different types of rocket propellant injection plates.

Experiments on cryogenic tankage.

FUNDAMENTAL STUDIES OF FRICTION, LUBRICATION AND WEAR PROCESSES

Investigations of friction and wear processes including the mechanism of adhesion between non-conforming metal surfaces and the processes involved with transferred films of solid lubricants.

Theoretical and experimental studies of a modified type of hydrodynamic thrust bearing and a theoretical study of a novel form of gas bearing.

PRACTICAL STUDIES ON LUBRICATION, FRICTION AND WEAR

Assessment of wear in shotgun barrels with shot manufactured from different materials.

A co-operative program for the assessment of instrument oils and lubricant surface coatings in the bearings of miniature rotating electrical components.

COMBUSTION RESEARCH

Experiments on fuel spray evaporation.

EXTENSION AND DEVELOPMENT OF LABORATORY EVALUATION

Investigation of laboratory engine test procedures for evaluation of oxidation, dispersancy, and thermal stability characteristics of engine oils.

Development of laboratory full-scale axle procedures for the determination of the anti-score performance of hypoid gear oils.

PERFORMANCE ASPECTS OF FUELS, OILS, GREASES, AND BRAKE FLUID

Co-operative investigation covering used oil analysis and inspection of engines from Ottawa Transportation Commission buses to establish realistic oil and filter change periods.

Evaluation of used oils from railroad diesels to establish suitable test methods and condemning limits.

Development of a specification for high viscosity index hydraulic oils for marine use.

Examination and evaluation of some re-refined oils.

Investigation of laboratory methods for predicting flow properties of engine and gear oils under low temperature operating conditions.

Investigation of laboratory methods for predicting low temperature flow properties of diesel and heating fuels and assessment of their suitability.

Evaluation of methods for determining undissolved water content of aviation turbine fuels.

Low temperature performance of hydraulic oils in pump systems.

Investigation of lubricating oil performance in water-cooled 2-stroke engines.

Development of a laboratory method for evaluating the shear stability of multigrade motor oils.

Evaluation of additives for preventing carburetor icing in light aircraft reciprocating engines.

Determination of fuel system icing inhibitor in aviation turbine fuels.

Performance evaluations on domestic furnace fuel oil filters.

Diesel fuel system icing studies.

Investigation of the Performance of synthetic hypoid gear lubricants.

MISCELLANEOUS STUDIES

The preparation and cataloguing of infra-red spectra of compounds related to fuels, lubricants, and associated products.

The application of Atomic Absorption spectroscopy to the determination of metals in petroleum products.

Investigation of the stability of highly compressed fuel gases.

500-LB ROCKET THRUST CHAMBER FIRING

FUELS AND LUBRICANTS LABORATORY
DIVISION OF MECHANICAL ENGINEERING

GAS DYNAMICS LABORATORY

V/STOL PROPULSION SYSTEMS

A general study of V/STOL propulsion system methods with particular reference to requirements of economy and safety.

Investigation of a vectored lift/thrust engine arrangement involving a shrouded fan driven by a partial admission turbine.

Experimental investigation of a pod-mounted VTOL fan for studies including the effects of flow of distortion in cross-flow and shroud thrust effects.

Examination of V/STOL propulsion system intake arrangements involving lifting surface circulation control.

INDUSTRIAL GAS TURBINES

Investigation of gas turbine components, particularly for industrial applications.

INTERNAL AERODYNAMICS OF DUCTS

An experimental study of the internal aerodynamics of ducts, bends, and diffusers with particular reference to the effect of entry flow distortion in geometries involving changes of cross-sectional area, shape, and axial direction.

HEAT TRANSFER STUDIES

The study of heat transfer within a vertical sealed tube (thermo-syphon) in which working fluid is boiled in the lower section and condensed in the upper section. Several practical applications for this device are being studied.

HYDROSTATIC GAS BEARINGS

Studies of hydrostatic gas bearings to develop reliable methods of predicting bearing performance for a range of conditions and configurations, and to evolve suitable techniques for the satisfactory application of this type of bearing in situations where the special properties of gas bearings recommend their use.

ARC PRODUCED PLASMA STUDIES

A general investigation of the properties and flow behaviour of thermally ionized gases produced by arc heating on a continuous basis, together with the development of suitable diagnostic techniques for the study of such high temperature gases.

SHOCK PRODUCED PLASMA STUDIES

A general theoretical and experimental investigation of the production of high temperature plasma by means of shock waves generated by electromagnetic or gasdynamic means, and the development of diagnostic techniques suitable for a variety of shock geometries and the study of physical properties of such plasmas.

A theoretical and experimental study of strong converging and diverging shock waves, produced by chemical (explosive) and other means, and the development of experimental means to study the resulting transient plasma.

HIGH PRESSURE LIQUID JETS

Water jets ranging in size from 0.001" to 0.015", generated by pressures in the range of 10,000 to 100,000 psi, are capable of cutting materials such as paper, cloth, plastics, wood, masonry, and even some metals.

Laboratory work is directed towards commercial exploitation by various industries (e.g. paper, lumber, leather, garments, plastics, etc.) of this phenomenon, and to the detailed study of the phenomenon itself in order to improve the efficiency of the process and possibly to broaden the field of application.

INDUSTRIAL PROCESS INSTRUMENTATION AND APPARATUS

There is an appreciable effort, on a continuing basis, directed towards industrial assistance. This work is of an extremely varied nature and, in general, requires the special facilities and capabilities available in the laboratory. The following examples of work during the past year are typical: altitude performance of small gas turbine engine; hydraulic pump tests; cent-ifugal compressor tests for pipeline service; design and test of heaters for laying continuous rails on Canadian railways; assistance in air-bearing design for industrial applications; instrumentation for copper and iron smelter applications; design and experimental verification of pressure loss data for large air ducts in smelters; industrial and aero turbine development.

Current co-operative projects with manufacturers include:

(a)   Experimental development of gas turbine combustion chambers

(b)   Theoretical analysis, design, and development of a gas bearing spindle for the textile industry

(c)   Experimental assessment and development of cushion and propulsion schemes for track air cushion vehicles.

HIGH SPEED AERODYNAMICS LABORATORY

CONTROL OF A TURBULENT BOUNDARY LAYER IN A THREE-DIMENSIONAL SHOCK WAVE BOUNDARY LAYER INTERACTION

The 5-in × 5-in blowdown wind tunnel is being used to investigate the three-dimensional interaction between a glancing, oblique shock wave and a turbulent boundary-layer flow along a flat wall. In a second phase, the boundary-layer flow in the three-dimensional interaction region will be re-energized by tangential air blowing.

HYPERSONIC INTERNAL FLOW STUDIES

The fundamental aspects of internal flows are being investigated. In the theoretical phase of this project the inviscid flow fields of intakes with arbitrary lip profile at zero incidence are computed, using an imploding shock analogy and a multi-strip shock layer theory. Viscous interaction is also included. A mixed method using finite differences and the method of characteristics will be developed for the internal flow at angle of incidence. Laminar three-dimensional boundary-layer growth will also be investigated.

SCHLIEREN SYSTEM

All four transonic section windows have been installed and, using a matching source plate, made to correspond to the new optical path length. Good photographs have been taken through the transonic section under normal testing conditions, using the partially-completed controller.

Assembly of the reground supersonic windows is proceeding, a film identification numbering system is being added, and various aspects of the controller are being completed for a planned final installation in February.

NUMERICAL SOLUTIONS OF LAMINAR AND TURBULENT BOUNDARY LAYERS

The boundary-layer equations for a two-dimensional incompressible flow have been solved by a finite difference method. For the turbulent boundary layer, the mixing length hypothesis is used to relate the turbulent shear stress to the mean flow. The method is being extended to include the solutions of boundary-layer flows in a compressible fluid.

NUMERICAL SOLUTIONS OF THE FLOW FIELD FOR CONICAL BODIES IN A SUPERSONIC STREAM

A numerical procedure for solving the problem of steady supersonic inviscid flow around smooth conical bodies has been developed. The procedure solves the elliptic partial differential equation that define the conical flow between the body and the shock. Results have been obtained for circular cones up to relative incidences of about 1.4, including some cases for incidences beyond a critical value at which the entropy singularity is off the body surface. Also, results have been obtained for conical bodies with non-circular cross sections such as elliptic cones. Results for circular cones are presented in Agardograph No. 137, September 1969.

TWO-DIMENSIONAL TRANSONIC TEST FACILITY

This 15-in × 60-in facility, briefly described on a "would be" basis in previous issues of this bulletin, was installed and operated for the first time in October. An ambitious calibration program was originally planned, but, for various reasons, this had to be reduced to a bare minimum. However, enough test running was done to demonstrate that a new and workable facility has been commissioned. The calibration was conducted in three phases:

(i)   Empty tunnel wall pressure distribution measurements.

(ii)   Model pressure measurements on 10-in and 15-in chord NACA 64A410 airfoils.

(iii)   Balance measurements on the same models.

The calibration results are currently being analyzed. The main conclusions reached so far are:

1.   Good empty tunnel wall pressure distributions for $0.15 < M < 1.10$.

2.   Diffuser second throat provides adequate M-control.

3.   Side wall boundary-layer displacement thickness $\delta^* \sim 0.15"$ (at a station 15 inches ahead of balance centre lines).

4.   The side wall boundary layer suction arrangement can provide good stabilizing control over the wing flow adjacent to the walls. However, the present porous material produces an unnecessary large pressure drop, which reduces the useful M-Re range of the facility.

5.   The model pitch drive and sidewall balance arrangement is working well.

6.   Model measurements indicate that the present wall restraints are close to open jet.

7.   During high Reynolds number conditions the initial thermal shock during tunnel start-up is large enough to produce significant M-variation during a run.

8.   The open jet emerging from the insert sidewalls into the downstream diffuser section produces severe and unacceptable vibrations in the main strut-model support system used for driving a traversing wake probe.

After the present series of tests in the 2D insert are completed in January 1970, the facility will be dismantled to allow access to the full 5-ft × 5-ft transonic test section for other tests. The insert will not be installed again until the fall

of 1970 but will then include modifications in its design aimed at alleviating some of the problems encountered during its first test period.

THEORETICAL TWO-DIMENSIONAL TRANSONIC FLOW STUDIES

Computer programs for subcritical flow calculation (Sells and Catherall methods) have been adapted to IBM 360 system. Pressure distribution for several series of airfoils have been calculated, both for the calibration of the transonic insert (profile NACA 64A410) and for theoretical analysis of several contemporary airfoils. A study of accuracy of the original Sells method has been performed, some improvements have been introduced and some will be added in the near future.

The results of the "exact in mathematical formulat?n" Sells method have been compared with another exact method (Nieuwland's). It appears that for many quasi-elliptical airfoils there are significant differences in pressure distributions (near the peak). Another accuracy test was made using circular arc airfoil and Hayasi (Lockheed-Georgia) results. The Catherall method (incompressible flow) gives perfect agreement with Hayasi, while the standard Sells method gives results satisfactory for technical application.

Program for subcritical transonic flow with boundary layer has been developed (Lock-Sells-Powell-Wilby method) and several cases have been calculated. For moderate Reynolds number (20 × 10^6) the boundary-layer effects in subcritical flow decrease the lift by a few percent. However, this method predicts incorrect pressure distribution in the region of high subcritical local Mach numbers because of simplified compressibility corrections.

WIND TUNNEL CORRECTIONS

Linearized compressible flow analysis applied to the study of the two-dimensional perforated wall interference at subsonic speeds (method proposed by Baldwin, Turner, Knechtel) has been reviewed and completed. Calculated values of the interference velocity and its derivatives at the position of the model are interpreted (according to Rogers) as corrections to stream Mach number, angle of attack, lift coefficient, drag coefficient, and moment coefficient. In the existing program (written in Fortran IV) the strengths of representing singularities are calculated from the geometry of the model and the measured pressure-coefficient distribution. In the case of an unknown wall porosity parameter, the corrections are computed automatically for several values of porosity between closed wall and open jet. The results of this study are being applied to the analysis of the 2D-insert calibration data.

WIND TUNNEL TESTS IN THE 5-FOOT X 5-FOOT BLOWDOWN WIND TUNNEL FOR OUTSIDE ORGANIZATIONS

The Boeing Company (Seattle)

In November, two-dimensional transonic testing was carried out on the first of four (10-in chord, 15-in span) Boeing airfoils in the 2D transonic insert of the NAE 5-ft × 5-ft wind tunnel. Measurements included model balance forces, wake total pressure profiles, and wing surface pressure distributions. The tests were run at M = 0.615 - 0.725 at R$_z$ = 8, 20, and 35 × 10^6.

In order to supplement the poor data acquisition capability of the NAE data system, Boeing supplied an on-line analogue data system and an FM tape recording unit that were interfaced with the wind tunnel's regular data system. In addition, a controller unit was provided by Boeing to monitor and sequence all functions of the data acquisition process, including the wing pitch-pause program, wing pressure scans, wake traverses, and data taking signals. Owing to problems associated with interfacing and controller operations, as well as mechanical breakdowns in the wind tunnel, only a fraction of the intended program was completed.

Further testing of the Boeing airfoils will probably be continued in late 1970.

SAAB Sweden

A series of tests involving force and pressure measurements on various airfoil configurations have been carried out in the 2D transonic insert. The test program included flapped airfoils at low subsonic speed as well as "clean" airfoils at transonic speed.

HYDRAULICS LABORATORY

ST. LAWRENCE SHIP CHANNEL

Under the sponsorship of the Department of Transport, a study of navigation, water levels, tide and ice problems.

WAVE RECORDER DEVELOPMENT

Development of a staff gauge wave recorder, either to be mounted to a fixed mast in shallow water or floating in deep water. Evaluation of other types of wave recorders: accelerometers, pressure transducers, etc.

WAVE INTERACTION STUDY

An experimental investigation to study the development of a wave cascade resulting from the dynamic instability of a uniform progressive wave train of finite amplitude.

WAVE DIRECTION STUDY

Field investigation to study the direction of propagation of wave energy in a confused sea as a function of wind direction.

LOCK STUDY

General study of navigation locks and locking systems, with particular emphasis on winter operation.

SEDIMENT PROBLEMS

To define and analyze sediment problems in navigable waters.

VISAKHAPATNAN HARBOUR, INDIA

Model studies to find remedial measures for silting and beach erosion.

INSTRUMENTS LABORATORY

WAVE-MEASURING DEVICES

Modification of circuitry of absolute type wave sensor to accommodate a commercially available form of voltage-controlled oscillator.

ST. LAWRENCE RIVER MODEL CONTROL SYSTEM

Proof testing of the weir and pump control system completed. Programs for the control of the three weirs and pump system by digital computer being written.

NON-CONTACTING PROXIMITY GAUGE

Preparation of laboratory report.

AIRCRAFT BLIND LANDING SYSTEMS

Proposals for a simple system, particularly suited for use in remote areas, e.g., Northern Canada, summarized for internal distribution.

AIRCRAFT NOISE PROBLEM

Continued acquisition of components for a noise monitoring and recording system to be installed by the Department of Transport at a major Canadian airport.

Collaboration with the Department of Transport in regard to: (1) the formulation of International standards on airport noise, (2) the Department's presentation of the Canadian position at the November, 1969, ICAO special meeting on aircraft noise.

COMBUSTIBILITY STUDIES

Development of technique for the measurement of the power dissipated in an exploding wire.

WAVE-MAKING EQUIPMENT

Design of control system for synchronization (with variable relative phasing) of two existing wave makers to be used simultaneously in one hydraulic model.

MECHANICAL AIDS TO SURGERY

Evaluation of a prototype semi-automatic staple loader for the production form of the NRC/Vogelfanger vascular suturing instrument.

Development and assembly of components for a hydraulically powered lower limb orthosis.

Laboratory endurance tests on an experimental form of artificial venous valve.

FREIGHT CAR STUDIES AND CAR DYNAMICS

Continuation of performance measurement in loaded cars, of various forms of draft gears not previously available to the laboratory.

Strength proving tests on a new CPR design of coal hopper car.

Engineering drawings of a system for the mechanical restraint of newsprint completed. Copies sent to the CPR.

General discussions with the Canadian Railways, of the truck hunting problem with a view to the formulation of a shared research program. Assistance to the CPR in the preparation and instrumentation of a caboose to be used for field measurements.

Initial evaluation by simulation, of a second commercially available impact cushioner for train running.

NAVIGATION SYSTEM TESTING

Continued development of an on-line computer-based system for in-flight testing and control of navigation systems. Design and construction of associated interface instrumentation and software.

LOW SPEED AERODYNAMICS LABORATORY

AERONAUTICAL WIND TUNNEL TESTS FOR OUTSIDE ORGANIZATIONS

Tests were carried out in the 6-ft × 9-ft horizontal wind tunnel for deHavilland Aircraft of Canada, Limited.

NON-AERONAUTICAL WIND TUNNEL AND WATER TUNNEL TESTS

Force measurements for several proposed bridge sections for the new Burrard Inlet crossing were completed in the vertical wind tunnel and a program of dynamic tests was begun.

THE NRC 30-FOOT V/STOL WIND TUNNEL

Seven major construction and equipment supply contracts have essentially been completed, and commissioning and calibration of the facilities is in progress. The tunnel has been operated up to full speed and preliminary aerodynamic calibrations were obtained.

FLUIDICS

Development work on fluidic velocity sensors for oceanographic research has started.

THE AERODYNAMICS OF PROPELLER-DRIVEN V/STOL LIFTING SYSTEMS

A light-weight model consisting of a wing in the slipstream of a single propeller is being used to determine the power spectrum of response to artificially generated wind tunnel turbulence. Strain-gauge balances measure five components of propeller force and moment, and wing lift, drag, and rolling moment.

WIND TUNNEL SIMULATION OF SURFACE WIND STRUCTURE

Experimental comparison in the 3-ft pilot wind tunnel, of different methods of generating thick boundary layers similar in shear and turbulence characteristics to natural winds in the lower 1000 ft of the atmosphere.

THE EXTERNALLY BLOWN JET FLAP

A project has been initiated, both in the 6-ft × 9-ft and flow visualization water tunnels, to investigate the characteristics of the externally blown jet flap. This employs the exhaust from a simulated fan-jet engine, which is directed through the flap assembly of a typical double-slotted, flapped aerofoil. The resulting flow interaction produces high local lift coefficients, and large deflection angles. The wing models, which are under construction, are both two-dimensional, but with a single simulated engine nacelle.

LOW TEMPERATURE LABORATORY

LOW TEMPERATURE PROBLEMS IN RAILWAY OPERATIONS

Analytical and experimental work, conducted under the auspices of the Associate Committee on Railway Problems, Sub-Committee on Climatic Problems, including the low temperature performance of air brake systems, aftercooler, design and development, an investigation into rail switch malfunctions under severe climatic conditions, evaluation of various rail switch heater systems. Methods of cooling continuous welded rail to obtain a suitable temperature for rail laying and anchoring are being studied.

HELICOPTER DE-ICING

A study of helicopter icing protection involving the evaluation of various systems (thermal, fluid, and self-shedding materials) and the development of de-icing control systems including ice detectors.

AIRCRAFT INSTRUMENTATION

The investigation of possible modes of failure for aircraft pitot heads under icing and snow conditions.

MISCELLANEOUS ICING INVESTIGATIONS

Analytical and experimental investigations of a non-routine nature, and the investigation of certain aspects of icing simulation and measurement.

TRAWLER ICING

In collaboration with the Department of Transport, an investigation of the icing of fishing trawlers and other vessels under conditions of freezing sea spray, and of methods of combatting the problem.

LOW TEMPERATURE APPLICATIONS IN MEDICAL ENGINEERING

An investigation into boundary-layer thermal flow measurement in pulsatile non-Newtonian flow.

Design of a shunt valve for cerebrospinal fluid in hydrocephalus. The device can be adjusted after implantation without surgical intervention.

Development of a capsule for telemetry of intracranial pressure. A special feature is its permanent, radio-transparent, moisture-impermeable casing.

SHIP LABORATORY

CABLE FAIRINGS
Drag measurements continued on various configurations.

WEATHERSHIP SEAKEEPING
Various model anti-pitching fins and bulbs tested.

WAVE AND STRESS ANALYSIS
Further work was carried out in improving existing methods and developing new electronic and computer techniques. A number of sea records were processed.

TANKER
New model prepared for steering assessment. Radio-controlled manoeuvring experiments completed with two stern configurations.

ICE BREAKING IN ARCTIC
Observations and some measurements taken on board Canadian icebreaker accompanying "Manhattan" now being analyzed.

YACHT DESIGN
The effect of various parameters on the performance of large sailing yachts are being investigated theoretically. It is expected that a limited experimental program will result.

STRUCTURES AND MATERIALS LABORATORY

FATIGUE OF METALS

Fatigue strength of welded maraging steel plate; characteristics of structural grade steel bolts under fatigue loading; effects of environment on fatigue strength of lt ht alloys; development of test methods for variable amplitude loads and investigation of effects of such loads; certification tests on aircraft components.

RESPONSE OF STRUCTURES TO HIGH INTENSITY NOISE

Study of excitation and structure response mechanisms; study of panel damping characteristics and critical response modes; investigation of fatigue damage laws; industrial hardware evaluation; investigation of jet exhaust noise.

HIGH TEMPERATURE AIRCRAFT HYDRAULICS

Study of bulk modulus of hydraulic fluids, including emulsions and mixtures in relation to temperature and pressure; studies of seal performance and high pressure, high velocity jet phenomena.

OPERATIONAL LOADS AND LIFE OF AIRCRAFT STRUCTURES

Instrumentation of aircraft for the measurement of flight loads and accelerations; fatigue life monitoring and analysis of load and acceleration spectra; full-scale fatigue spectrum testing of airframes and components; investigation of rough ground operations.

FRACTURE MECHANICS AND FRACTOLOGY

Investigation of crack formation and propagation in gradient stress fields; correlative electron microscope studies of fracture surfaces; notch sensitivity and fracture toughness; resistance of materials to high strain rate and impact loading.

RESEARCH ON PROTECTIVE COATINGS FOR REFRACTORY METALS

Investigation of coating compounds for protection of refractory metal substrates at high temperatures; methods and techniques of coating deposition; study of interface diffusion rates and products; development of methods of evaluation of physical properties of coated test coupons.

MECHANICS AND THEORY OF STRUCTURES

Preparation of formulae and charts for vibrations of an elastically suspended rigid body; study of coupled flexural-torsional vibration of a uniform cantilever beam; development of transmission matrices; extension of beam theory to include effects of transverse curvature; study of dynamics of a cable under transverse impact.

CONSTRUCTION AND DEVELOPMENT OF FLIGHT IMPACT SIMULATOR

Development of Canadian facility; analysis of national needs and co-ordination of utilization; hardware evaluations.

CALIBRATION AND CERTIFICATION OF FORCE MEASURING DEVICES

Facilities available for the calibration of government, university, and industrial equipment include deadweight force standards up to 100,000 lb, back-to-back calibration of accelerometers, and limited calibration of fluid pressure-type transducers.

COMPOSITE AND NON-METALLIC MATERIALS

Studies of resins, crosslinking compounds, and polymerization initiators; material properties and uses of polymers and reinforcements for composites; procedures for application and fabrication; structural efficiencies.

FINITE ELEMENT METHODS

Development of refined finite elements for plate bending and plane stress; development and application of a cylindrical shell finite element; application of finite elements to flutter problems; development of a general triangular shell element.

 It's a full-page scientific figure showing sound wave movement in a screeching jet, rotated sideways.
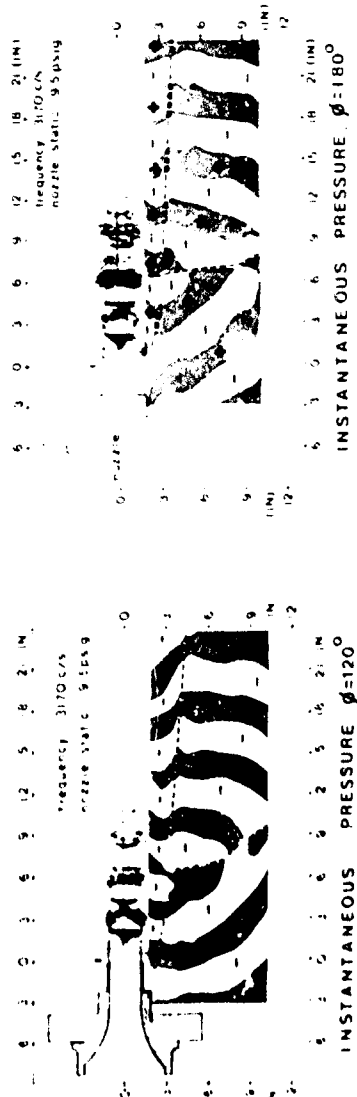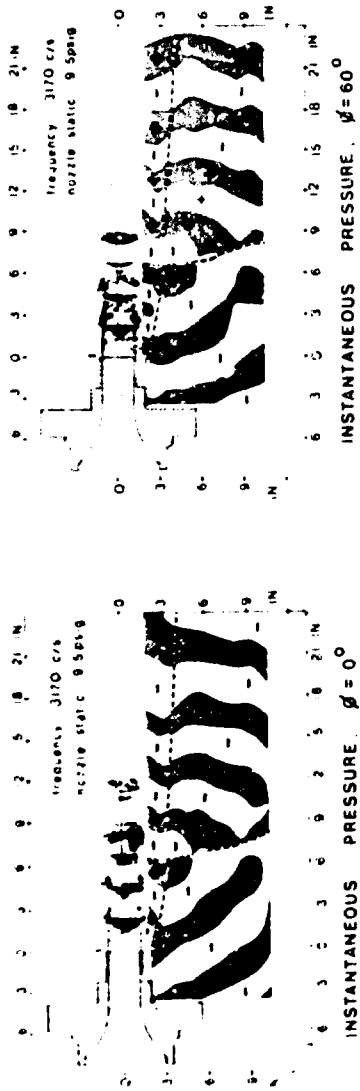
MOVEMENT OF SOUND WAVES DURING HALF CYCLE
OF SCREECHING JET

STRUCTURES AND MATERIALS LABORATORY
NATIONAL AERONAUTICAL ESTABLISHMENT
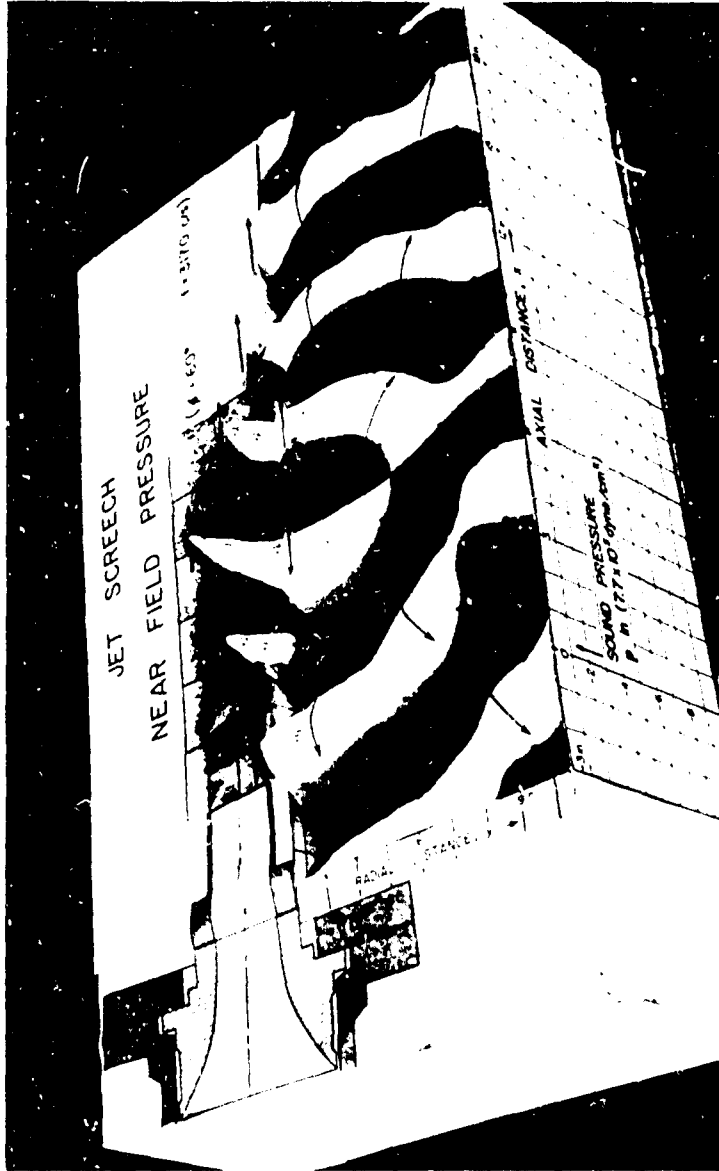
PRESSURE DISTRIBUTIONS NEAR SCREECHING JET

STRUCTURES AND MATERIALS LABORATORY
NATIONAL AERONAUTICAL ESTABLISHMENT

UNSTEADY AERODYNAMICS LABORATORY

STUDY OF VISCOUS HYPERSONIC FLOW ON A STEADY PLATE

Surface pressure distributions and flow field surveys at hypersonic Mach numbers on a flat plate at incidence, including the use of anemometry and glow-discharge techniques

STUDY OF OSCILLATORY PHENOMENA IN HYPERSONIC FLOW

Theoretical and experimental investigation of the effects of viscosity and leading-edge bluntness on aerodynamic characteristics of two-dimensional oscillating aerofoils. Pressure distribution and flow field measurements; determination of static and dynamic stability derivatives; optical studies. All experiments performed in helium at Mach numbers 9 and 18.

PRESSURE MEASUREMENTS ON OSCILLATING WINGS IN SUPERSONIC FLOW

Measurements of the mean surface pressure and of the amplitude and phase of the oscillatory pressure on a 5 percent thick delta wing at Mach number 1.8 in air

HELIUM HYPERSONIC WIND TUNNEL

Two 11-inch diameter contoured nozzles (on long term loan from the U S.) for Mach numbers 10 and 18 now available Also available, a heater to provide small (100°F) increases in the stagnation temperature of the flow, and a variable incidence sector support for static force, moment, and pressure measurements on sting-mounted models

DYNAMIC EXPERIMENTS ON ELLIPTIC CONES

Measurement of oscillatory characteristics of a series of elliptic cones at Mach number 11 in helium

AXISYMMETRIC FREE JETS

A method-of-characteristics solution of the flow field in the core of a free helium jet issuing into a vacuum

SUBLIMATION STUDIES

Study of surface recession rates and of boundary layer pitot profiles on carbon-dioxide flat-plate models in the helium wind tunnel.

ANALYTICAL STUDIES OF UNSTEADY FLOWS

Analysis of inviscid unsteady flow fields over elliptic cones in supersonic flows and over parabolic-arc aerofoils in hypersonic flows.

GAS PHASE REACTION KINETICS

A physico-chemical study of the reactions of some constituents of the upper atmosphere, such as oxygen, nitrogen, and hydrogen atoms, to provide laboratory data in support of rocket experiments on upper atmospheric composition. Proposal available for a new method for the absolute determination of the atomic concentration of oxygen and nitrogen in the 90-120 km region.

COSMIC RADIATION

Review of possible hazards for high altitude flight owing to cosmic radiation.

PUBLICATIONS

The following unclassified reports were released during the quarter:

AERONAUTICAL REPORTS

LR-529   APPLICATION OF THE HIGH PRECISION TRIANGULAR PLATE-BENDING ELEMENT TO PROBLEMS WITH CURVED BOUNDARIES.

M. W. Chernuka, G. R. Cowper, G. M. Lindberg and M. D. Olson, National Aeronautical Establishment, October 1969.

The application of the high precision triangular plate-bending element to problems with curved boundaries is considered. Appropriate edge conditions for nodal points on these boundaries are derived. The error inherent in representing a curved boundary by a series of straight segments is found to be the limiting factor on accuracy, while the effect of approximations in the boundary conditions is minor. To overcome the first type of error, the high precision element is modified to include one curved edge. Substantial improvements in accuracy are obtained, as demonstrated in example calculations for circular and elliptical plates.

MECHANICAL ENGINEERING REPORTS

ME-232   A TECHNIQUE FOR MEASURING, RECORDING AND ANALYZING TORSIONAL OSCILLATIONS OF CRANK-SHAFTS OF RECIPROCATING ENGINES

T. H Hammell and J E Carvish, Division of Mechanical Engineering June 1969.

Tests were made on three types of transducers, and a variable capacitor unit that frequency modulates a carrier wave was considered best for general use The inherently good signal-to-noise ratio, plus the ability to calibrate statically in the field, were considered particularly attractive

It was found that dynamic calibration of the transducer should be carried out periodically, and a good Hookes couple is ideal for this purpose.

Several instrumentation check methods are outlined that may be followed to assure consistency in the data produced.

ML-4   SLEEP DEPRIVATION EFFECTS ON RESPONSES TO SIGNALS OF UNEQUAL PROBABILITY IN AN ARTI-FICIALLY ELECTRICALLY CHARGED ENVIRONMENT

L Buck, C B. Gibbs and R Leonardo, Division of Mechanical Engineering, October 1969.

Young male subjects made repeated runs on a step-tracking task over a period of 48 hours during which they were deprived of sleep. Successive runs showed a reaction time (but not error rate) increase that was inversely related to signal probability, and a movement time increase that was related to distance travelled. Both effects were more evident on machine-paced than subject-paced tracking. There was no evidence that performance deterioration could be modified by the use of a patented anti-fatigue device.

MP-53   DIMENSIONAL CHANGES IN SHOT GUN BARRELS CAUSED BY THE FIRING OF HARD METAL PELLETS.

C. Dayson and T. Maloney, Division of Mechanical Engineering, July 1969.

This report describes progress to date on the development of a means of assessing the wear and deformation of shot gun barrels caused by the firing of non-toxic but relatively hard metal pellets. The results of an initial series of tests on hard metal pellets, some of which were coated with non-metallic anti-wear coatings, are also presented. These indicate that the enlargement of the bore of the barrel at the muzzle constriction (choke) was, in this case, primarily due to the "hammering out" action of the hard pellets, with the wear of the bore being a secondary effect. The pellet coatings tested proved to be ineffective as a means of preventing either form of damage.

MS-119   AUTOMOBILE DEFROSTER PERFORMANCE DURING A CANADIAN WINTER.

G. F. W. McCaffrey, National Aeronautical Establishment, June 1968.

Considerable dissatisfaction has been expressed, by drivers, regarding the performance of defroster systems in Canadian winter driving conditions. In an attempt to obtain some data on this problem a group of six typical automobiles was subjected to a standardized test of defroster performance and, subsequently, monitored during normal driving from November 1967 to March 1968.

MECHANICAL ENGINEERING REPORTS (Cont'd)

MS-126   A Cr-Ti-Si DIFFUSION COATING FOR THE NIOBIUM ALLOY B66: AN INVESTIGATION OF SOME COATING PARAMETERS.

J.M Trenouth and M.S. Grzedzielski, National Aeronautical Establishment, December 1969

Chromium-titanium and chromium-titanium-silicon diffusion coatings were formed on specimens of the niobium alloy B66 by vacuum pack cementation. Some of the coating parameters for formation of the chromium-titanium diffusion coating were investigated with respect to the amount and structure of the coating formed. The rate of formation of this coating was found to be diffusion-dependent. Consequently the rate was strongly dependent on the processing parameters of time and temperature, and essentially independent of vapour-phase conditions such as activator concentration and pressure (evacuation rate). The rate of formation, and the structure and composition of the resulting coating were a function of the pack alloy and hence of the coating atmosphere composition. For coatings formed in a 60/40 w/o Cr/Ti alloy pack, the overall formation rate was calculated to be $K_{C-T} = 2.14 \times 10^6 \exp\left(-\frac{36 \times 10^3}{RT}\right) \mu\ h^{1/2}$ The formation rates for the two zones of the coating (overlay and diffusion zone) were determined to be $K_{Overlay} = 1.07 \times 10^7 \exp\left(-\frac{42 \times 10^3}{RT}\right) \mu/h^{1/2}$ and $K_{Diffusion\ zone} = 1.58 \times 10^5 \exp\left(-\frac{30 \times 10^3}{RT}\right) \mu/h^{1/2}$. The amount of diffusion alloying of silicon with previously formed chromium-titanium coatings was independent of the chromium-titanium coating conditions and thickness As a result of this constant silicide layer thickness on different thicknesses of the chromium-titanium coating, varying structures of the final chromium-titanium-silicon coating were obtained.

MS-127   THE INFLUENCE OF SODIUM SULPHATE AND SODIUM CHLORIDE ON THE OXIDATION RESISTANCE OF A Cr-Ti-Si COATING ON ALLOY B66.

E.P. Whelan and J.M. Trenouth, National Aeronautical Establishment, December 1969.

An investigation has been made of the influence of Na_2SO_4 and NaCl on the oxidation resistance of Cr-Ti-Si coatings deposited by pack cementation on the niobium alloy B66.

Coated specimens were contaminated by Na_2SO_4 salt concentrations of approximately 1 mg/cm^2, and oxidised at 1100°C, 1200°C, and 1300°C. Oxidised contaminated specimens exhibited initial mass gains considerably greater than those of identical uncontaminated specimens. The contaminated surface became brown, glassy, and bubbly within 10 minutes of being exposed to the oxidising environment.

Microstructures of oxidised contaminated specimens indicated that the protective silicide coating zones oxidised at a more rapid rate than did those of uncontaminated specimens, and that an array of particles, possibly titanium oxides or nitrides, formed in the diffusion zone in less than 100 minutes at 1300°C. Electron probe microanalysis did not detect any sodium or sulphur in the oxide or substrate after 300 minutes exposure at 1300°C. Oxidation prior to Na_2SO_4 contamination did not increase the subsequent corrosion resistance of the coatings

A preliminary investigation indicated that NaCl also influenced the oxidation resistance of coated specimens in a deleterious manner.

MISCELLANEOUS PAPERS

BUCK, L   How Does Drinking Impair Driving? (Comment l'alcool affaiblit les reflexes au volant). Royal Canadian Mounted Police Gazette, 31(10), 18-22, October 1969   (English and French editions)

CHAN, Y.Y.   Parametric Approximation for Incompressible Laminar Boundary Layers with Suction and Injection. CASI Transactions Vol 2, No. 2, September 1969.

CHAN, Y.Y.   An Experimental Study of a Yawed Circular Cone in Hypersonic Flows   AIAA Journal, Vol 7, No. 10, October 1969

COWPER, G.R., KOSKO, E., LINDBERG, G.M. and OLSON, M.D   Static and Dynamic Applications of a High-Precision Plate Bending Element. AIAA Journal, Vol. 7, No. 10, October 1969, pp. 1957-1965

DEBLOIS, J.D   Changing Time - Cinematography at Speeds Other Than Normal. To be published in the Proceedings of the 1969 Symposium of the Canadian Science Film Association.

FISZDON, W., IYENGAR, S. and ORLIK-RUCKEMANN, K J.   On Unsteady Effects of Viscosity on the Hypersonic Flow Past a Slowly Oscillating Wedge with Attached Shock Wave. National Research Council of Canada, NAE Lab. Tech. Report LTR-UA-11, September 1969.

GARDNER, I   Colorimetric Determination of Ethylene Glycol Monomethyl Ether in Aviation Turbine Fuel. Journal of the Institute of Petroleum, Vol. 55, No. 546, November 1969.

LEE, B.H.K   A Modified Shock Layer Theory for Hypersonic Internal Flows. CASI Transactions Vol. 2, No. 2, September 1969, pp. 67-74.

LEE, B.H.K   The Production of Strong Shocks in a Multi-Stage Gaseous Detonation Driven Shock Tube. CASI Transactions Vol. 2, No. 2, September 1969, pp. 75-80.

MEYER, R F. and GRAHAM, G D.   A Non-Axisymmetric Hypersonic Blast Wave Analogy. CASI Transactions, September 1969.

MISCELLANEOUS PAPERS (Cont'd)

MUFTI, I.H. CHOW, C.K. and STOCK, F.T. Solution of Ill-Conditioned Linear Two-Point Boundary Value Problems by the Riccati Transformation. SIAM Review, Vol. 11, No. 4, October 1969.

ORLIK-RÜCKEMANN, K J. Simple Formulas for Unsteady Pressure on Slender Wedges and Cones in Hypersonic Flow. J. Spacecraft and Rockets, Vol. 6, No. 10, October 1969, pp. 1209-1211.

PEAKE, D.J. Three-Dimensional Flow Separations on Upswept Rear Fuselages. CASI Journal, December 1969.

ROMERO-SIERRA, C., TANNER, J.A. and VILLA, F. EMG Changes in the Limb Muscles of Chickens Subjected to Microwave Radiation. National Research Council of Canada, DME Lab. Tech. Report LTR-CS-16, November 1969.

ROMERO-SIERRA, C., HUSBAND, C. and TANNER, J.A. Effects of Microwave Radiation on Parakeets in Flight. National Research Council of Canada, DME Lab. Tech. Report LTR-CS-18, November 1969.

TANNER, J.A., ROMERO-SIERRA, C. and DAVIE, S.J. A Preliminary Investigation of the Effect of Pulsed Microwaves on the Feeding Behaviour of Chickens. National Research Council of Canada, DME Lab. Tech. Report LTR-CS-20, December 1969.

VAN DAM, W., TANNER, J.A and ROMERO-SIERRA, C. A Preliminary Investigation of Piezoelectric Effects in Bird Feathers National Research Council of Canada, DME Lab. Tech. Report LTR-CS-19, December 1969.

VILLA, F., ROMERO-SIERRA, C. and TANNER, J.A. Techniques for Extracting Bioelectric Signals from Birds Subjected to Microwave Radiation. National Research Council of Canada, DME Lab. Tech. Report LTR-CS-15, November 1969.

WARDLAW, R L. and PONDER, C.A. An Example of the Use of Wind Tunnels for Investigating the Aerodynamic Stability of Bridges. Proceedings Canadian Good Roads Association Convention, September-October 1969.

WOODSIDE, C.M Pellet Steelmaking Modelling and Control - Interim Report No. 1, National Research Council of Canada, DME Lab. Tech. Report LTR-CS-14, December 1969.

UNPUBLISHED PAPERS AND LECTURES

BAKER, R and GRAEFE P W.U. Ocean Wave Profiles and Spectra Measurements Using an Airborne Magnetometer. Presented at Annual Meeting of the Canadian Committee on Oceanography and Second International Oceanographic Symposia, Empress Hotel, Victoria, B C., 17-21 November 1969.

COWPER, G.R. Finite Element Methods for the Stress Analyst. Lecture presented to the Society for Experimental Stress Analysis, in Ottawa, Ontario, 2 December 1969.

DAYSON, C. A New Type of Stepped Thrust Bearing. Presented at Graduate Student Seminar, University of Alberta, Edmonton, Alberta, 8 September 1969.

DEBLOIS, J.D. The Motion Picture Camera in Scientific Investigation. Presented at the Second Annual Conference on Bio-Medical Photography at Rochester Institute of Technology, Rochester, New York, 25 October 1969.

DEBLOIS, J.D. High Speed Camera Techniques. Presented at the Canadian Society of Cinematographers, Ottawa Meeting, 29 November 1969.

GODBY, E.A., HOOD, P.J.* and BOWER, M.* Aeromagnetic Reconnaissance of Baffin Bay, the Labrador Sea and the North Atlantic Ocean. Presented at Annual Meeting of the Canadian Committee on Oceanography and Second International Oceanographic Symposia, Empress Hotel, Victoria, B.C., 17-21 November 1969.

INCE, S. Winter Navigation Problems on the St. Lawrence River. Seminar at the University of Toronto, Toronto, Ontario, November 1969.

KASVAND, T. Computing Machines and Intelligence. Lecture (in Estonian) presented to the Academic People (Estonians) and guests from Latvian and Lithuanian Societies for the 50th Anniversary of the Estonian National University of Tartu, 1 December 1969.

KASVAND, T. Computers. Lecture (in Estonian) presented to the Estonian Society in Ottawa, Ontario, 1 November 1969.

LINDBERG, G M. and OLSON, M.D. Development of High Precision Triangular Plate Bending and Shallow Shell Finite Elements. Seminar given at University of Waterloo, Waterloo, Ontario, 25 November 1969.

LINDBERG, G.M. and OLSON, M.D. Applications of Finite Element Techniques. Lecture presented to the Society for Experimental Stress Analysis, in Toronto, Ontario, 25 November 1969.

MILNER, M. Studies of Human Locomotion and Programmed Stimulation of Skeletal Muscle. Lecture presented to Prosthetics and Orthotics Research and Development Unit, Manitoba Rehabilitation Hospital; Research Group, Shriner's Hospital for Crippled Children, Medical Staff, University of Manitoba, Winnipeg, Manitoba, 7 November 1969.

MILNER, M. A Bio-Engineer Looks at Human Locomotion. Lecture presented to Emory University Regional Rehabilitation, Research and Training Center, Atlanta, Georgia, U.S.A, 4 December 1969.

---

* D.E.M.R Geological Survey of Canada.

MILNER, M. Introduction to Bio-Engineering. Engineering 94.570, a graduate course of study presented to the Engineering Department at Carleton University, Ottawa, Ontario, September-December 1969.

PELLEG, J. Diffusion of ^{44}Ti into Niobium Single Crystals. TMS-AIME Fall Meeting, Philadelphia, Pa., U.S.A., October 1969. Paper presented by Dr. E.P. Whelan in the absence of Dr. J. Pelleg.

STEVENSON, H.T. A Review and Recent Developments in Crash Position Indicator - Soft Landing Systems. Presented to the Canadian Aeronautics and Space Institute, Ottawa Branch, Ottawa, Ontario, 10 December 1969.

TARNEY, J.W. Some Developments Involving the Uses for Unbounded Turbulent Jets in Fluidic Sensors. Talk given to the staff of the SACLANT ASW Research Center, La Spezia, Italy, 22 September 1969.

WHELAN, E.P. and DAINTY, R.V. The Oxidation Resistance of Commercial Aluminide Coatings on the Superalloys INCO 713C and IN 100. Paper presented by Dr. E.P. Whelan at TMS-AIME Fall Meeting, Philadelphia, Pa., U.S.A., 16 October 1969.

AERONAUTICAL LIBRARY

Statistical Summary of Library Operations for the Quarter
October - December 1969

Documents accessioned (including duplicates)	3,728
Documents accessioned (first copies only)	3,329
Cards added to the catalogue	13,021
Books received	237
Bound periodicals received	167
Loans to NRC staff (including Periodical circulation and Xerox and Microfiche copies supplied in lieu of loans)	7,765
Loans and distribution to outsiders	2,339
Total circulation	10,104

Statistical Summary for 1968 and 1969

	1968	1969
Documents accessioned (including duplicates)	15,268	16,886
Documents accessioned (first copies only)	11,461	12,495
Cards added to the catalogue	62,853	57,800
Books received	1,557	1,587
Bound periodicals received	337	648
Loans to NRC staff (including Periodical circulation and Xerox and Microfiche copies supplied in lieu of loans)	30,505	30,042
Loans and distribution to outsiders	7,648	9,138
Total circulation	38,153	39,180

NOTE: These summaries include statistics for the Uplands Branch of the Aeronautical Library.

PROPRIETARY PROJECTS DURING 1969

Part of the work of the two Divisions covers proprietary projects, and, for this reason, has not been reported in these Bulletins.

Following is a list of Industrial Organizations, Government Departments and Universities for whom work was done during 1969.

INDUSTRIAL ORGANIZATIONS

Aero Photo Inc., Quebec, P.Q.

Aerospace Exhibits Limited, Montreal, P.Q.

Air Canada, Montreal, P.Q.

Aircraft Industries of Canada Ltd., St.Jean, P.Q.

Allatt Auto Supply, Toronto, Ont.

Automatic Electric Co., Brockville, Ont.

Avian Aircraft Ltd., Georgetown, Ont.

Babcock-Wilcox Canada Ltd., Galt, Ont.

Back-Simpson Ltd., London. Ont.

Barnes Engineering Co., Stamford, Conn., U.S.A.

Battelle Memor. 'l Institute, Columbus, Ohio

Bell Helicopter Co., Fort Worth, Texas, U.S.A.

Bobtex Corporation Ltd., Montreal, P.Q.

Boeing Company, Seattle, Washington, U.S.A.

Boeing of Canada Ltd., Arnprior, Ont.

Bourns (Canada) Ltd., Toronto, Ont.

B.P. Canada Ltd., Oakville, Ont.

B.P. Canada Ltd., Montreal, P.Q.

Bristol Aerospace Industries, Montreal, P.Q.

Bristol Aerospace Ltd., Winnipeg, Man.

Bristow Instruments Company, Edmonton, Alta.

CAE Industries Ltd., St.Laurent, P.Q.

CAMAT Transportation Consultants Inc., Montreal, P.Q.

Canadair Ltd., Montreal, P.Q.

Canadian Aero Services Limited, Ottawa, Ont.

Canadian Amateur Ski Association, Montreal, P.Q.

Canadian Aniline & Extract Co., Hamilton, Ont.

Canadian Aviation Electronics, Montreal, P.Q.

Canadian Broadcasting Co., Ottawa, Ont.

Canadian Car Pacific, Vancouver, B.C.

Canadian Gas Association, Toronto, Ont.

Canadian General Electric Co., Ltd., St.Andrews East, P.Q.

Canadian General Electric, Port Hawkesbury, N.S.

Canadian Industries Limited, McMasterville, P.Q.

Canadian Ingersol-Rand Co., Montreal, P.Q.

Canadian International Paper Company, Gatineau, P.Q.

Canadian Liquid Air, Montreal, P.Q.

Canadian National Railways, Montreal, P.Q.

Canadian Pacific Airlines, Vancouver, B.C.

Canadian Pacific Railway Co., Montreal, P.Q.

Canadian Petrofina, Pointe-Aux-Trembles, P.Q.

Canadian Vickers Limited, Montreal, P.Q.

Canadian Westinghouse Co., Ltd., Hamilton, Ont.

Canadian Yacht Consortium, Halifax, N.S.

Canive Ltd., Hagersville, Ont.

Capital Air Surveys Limited, Ottawa, Ont.

Centennial Auto Parts, Ottawa, Ont.

Central Design and Drafting Ltd., Montreal, P.Q.

Century Air & Ground Services, Montreal, P.Q.

Cessna Aircraft, Wichita, Kansas

Champlain Power Products Ltd., Toronto, Ont.

Charbonneau, Mr. G., L'Original, Ont.

Cities Service Oil Co., Cranbury, N.J.

City of Ottawa, Ottawa, Ont.

Coast-Eldridge Professional Services Division, Vancouver, B.C.

La Compagnie Photo-Air Laurentides, Quebec, P.Q.

Computing Devices of Canada Ltd., Ottawa, Ont.

Consolidated Bathurst Paper Co., Grandmere, P.Q.

Cook Electric Co., Chicago, Ill., U.S.A.

Cornell Aeronautical Laboratory Inc., Buffalo, N.Y., U.S.A.

D. Corrigan & Co., Hamilton, Ont.

G.F. Crate Ltd., Toronto, Ont.

Crawley Films Limited, Ottawa, Ont.

DeHavilland Aircraft of Canada Ltd., Downsview, Ont.

DeHavilland Aircraft of Canada Ltd., Longueuil, P.Q.

Dowty Equipment of Canada Ltd., Ajax Ont.

Dufresne Piling Company, Ottawa, Ont.

DuPont of Canada Ltd., Montreal, P.Q.

Dustbane Ltd., Ottawa, Ont.

Eastern Air Lines Inc., New York, N.Y., U.S.A.

Eastman Kodak Co., Rochester, N.Y.

EMI Electronics Ltd., Dartmouth, N.S.

Enjay Additives Laboratory, Linden, N.J.

Esso Research and Engineering, Linden, N.J.

Fathom Oceanology Limited, Port Credit, Ont.

Ferranti-Packard Ltd., Toronto, Ont.

Field Aviation Ltd., Malton, Ont.

Fleet Manufacturing Ltd., Fort Erie, Ont.

Furnace Engineering, Montreal, P.Q.

Garrett Mfg. Ltd., Rexdale, Ont.

General Dynamics, Convair Division, San Diego, Calif., U.S.A.

General Electric Co., Cincinnati, Ohio

General Motors of Canada, Ottawa, Ont.

German and Milne, Naval Architects and Marine Surveyors, Montreal, P.Q.

Golden Eagle Can. Ltd., Montreal, P.Q.

Grace, W.R. Hatco Div., Fords, N.J.

Great Can. Oil Sands, Fort McMurray, Alta.

Gulf Oil Canada Ltd., Sheridan Park, Ont.

Hamel, Malouin & Assoc. Drummondville, P.Q.

Hauts-Monts Inc., Quebec, P.Q.

The Hospital for Sick Children, Toronto, Ont.

Howe India Private Limited, New Delhi, India

Hugh Carsons, Ottawa, Ont.

Huntec, Division of Kenting Exploration Services Ltd., Toronto, Ont.

Hydradrive Engines Ltd., Toronto, Ont.

Hydro-Electric Power Commission of Ontario, Toronto, Ont.

Ian Martin Associates, Ottawa, Ont.

Imperial Oil Enterprises Ltd., Charlottetown, P.E.I.

Imperial Oil Enterprises Ltd., Darmouth, N.S.

Imperial Oil Enterprises Ltd., Lewisporte, Nfld.

Imperial Oil Enterprises Ltd., Montreal, P.Q.

Imperial Oil Enterprises Ltd., Sarnia, Ont.

Imperial Oil Limited, Toronto, Ont.

Industrial Metal Co. of Canada, Toronto, Ont.

International Cellulose Research Ltd., Hawkesbury, Ont.

International Paper Co., Gatineau, P.Q.

Iron Ore Co. of Canada, Labrador City, Nfld.

Johnson, Matthey & Mallory Ltd., Toronto, Ont.

Kenting Aviation Limited, Malton, Ont.

Knox, Mr. James, Ottawa, Ont.

Laurentian Air Services Ltd., Ottawa, Ont.

Leigh Instruments Ltd., Carleton Place, Ont.

Leigh Systems Inc., Syracuse, N.Y., U.S.A.

Lockheed Aircraft Corp., Burbank, California, U.S.A.

Lockheed Missiles & Space Co., Sunnyvale, Calif.

Lockwood Survey Corp. Ltd., Toronto, Ont.

Lockwood Survey Corp. Ltd., Vancouver, B.C.

Lubrizol Corp., Cleveland, Ohio

Machair Survey Limited, Calgary, Alta.

MacMillan Bloedell and Powell River Co., Vancouver, B.C.

Mechron Engineering Products, Ottawa, Ont.

Merck, Sharpe & Dohme Can. Ltd., Pointe Claire, P.Q.

Miltronics Ltd., Peterborough, Ont.

Mobil Res. & Development Co., Paulsboro, N.J.

Montreal Transportation Commission, Montreal, P.Q.

Muirhead Instruments Ltd., Stratford, Ont.

National Aeronautics and Space Administration (USA)

Noranda Copper Refining Industries Ltd., Montreal, P.Q.

North American Rockwell Corp., Tulsa Division, Tulsa, Oklahoma

Northern Electric Co. Ltd., Belleville, Ont.

Orenda Ltd., Malton, Ont.

Ottawa Civic Hospital, Ottawa, Ont.

Ottawa Transportation Commission, Ottawa, Ont.

Philips Electronics Industries Ltd., Toronto, Ont.

Preci-Tools Limited, Montreal, P.Q.

Public Fuel Transmission Systems, Ottawa, Ont.

Quebec Cartier Mining Co., Port Cartier, P.Q.

Quebec Hardwoods Inc., Hull, P.Q.

Quebec North Shore & Labrador Railway Co., Sept Iles, P.Q.

Rails Co., New Jersey

Range Aerial Survey Limited, Calgary, Alta.

Research Engineering Associates, Toronto, Ont.

Rio Algom Mines Ltd., Toronto, Ont.

Rolls-Royce (Derby) Ltd., Derby, England

Rolls-Royce (Montreal) Ltd., Montreal, P.Q.

Ron Engineering & Construction Ltd., Ottawa, Ont.

SAAB Aktiebolag, Sweden

Saguenay Terminals Limited, Port Alfred, P.Q.

Sandia Corporation, Albuquerque, New Mexico

Saunders Aircraft Corp. Ltd., Dorval, P.Q.

Schofield & de Vries, Breslau, Ont.

Separator Engineering Ltd., Montreal, P.Q.

Shell Canada Ltd., Montreal, P.Q.

Shell Canada Ltd., St. Boniface, Manitoba

Shell Canada Ltd., Toronto, Ont.

Societe Nucletron Inc., St. Leonard, P.Q.

Space Research Institute, Montreal, P.Q.

Spar Aerospace Company, Toronto, Ont.

Spartan Air Services Ltd., Ottawa, Ont.

Sperry Gyroscope Company, Montreal, P.Q

The Steel Company of Canada Ltd., Hamilton, Ont.

Sud Aviation, Marignane, France

Sun Oil Canada Ltd., Toronto, Ont.

Survair Limited, Ottawa, Ont.

Sutton Perry Ltd., Ottawa, Ont.

Swan Wooster - CAB, Vancouver, B.C.

Terry Industries Limited, Dorval, P.Q.

Texaco Canada Ltd., Montreal, P.Q.

Texaco Inc., Beacon, N.Y.

Toronto Coppersmithing Co. Ltd., Toronto, Ont.

Toronto General Hospital, Toronto, Ont.

Trans Canada Pipelines, Toronto, Ont.

Tretolite Division of Petrolite Corp., Clarkson, Ont.

Turbo Chemical Co., Edmonton, Alta.

Underwriters Adjustment Bureau, Hull, P.Q.

Underwriters' Laboratories of Canada, Scarborough, Ont.

Union Carbide Ltd., Don Mills, Ont.

United Aircraft of Canada Ltd., Longueuil, P.Q.

Vale Enterprises, Montreal, P.Q.

Vapor Heating Limited, Montreal, P.Q.

Varian Associates of Canada Ltd., Georgetown, Ont.

Wabash Mines, Point Noir, P.Q.

Western Caissons Limited, Laval, P.Q.

Westinghouse Electric, Philadelphia, Pa.

Worthington (Canada) Ltd., Brantford, Ont.

GOVERNMENT DEPARTMENTS

Atomic Energy Control Board, Ottawa, Ont.

Atomic Energy of Canada Limited, Ottawa, Ont.

Atomic Energy of Canada Ltd., Winnipeg, Manitoba

The Bank of Canada, Ottawa, Ont.

British Columbia Research Council, Vancouver, B.C.

Canada Centre for Inland Waters, Burlington, Ont.

Canadian Broadcasting Corporation, Ottawa, Ont.

Canadian Government Specifications Board, Ottawa, Ont.

Consumer & Corporate Affairs, Dept. of Trade & Practices, Toronto, Ont.

Defence Research Board, CARDE, Ottawa, Ont.

Defence Research Establishment, Halifax, N.S.

Defence Research Establishment, Valcartier, P.Q.

Department of Agriculture, Ottawa, Ont.

Department of Defence Production, Ottawa, Ont.

Department of Energy, Mines and Resources, Ottawa, Ont.

Department of Fisheries & Forestry, Ottawa, Ont.

Department of Forestry & Rural Development, Ottawa, Ont.

Department of Indian Affairs, Northern Development, Ottawa, Ont.

Department of Industry, Trade & Commerce, Ottawa, Ont.

Department of Justice, Ottawa, Ont.

Department of National Defence, Ottawa, Ont.

Department of National Health & Welfare, Ottawa, Ont.

Department of Public Works, Ottawa, Ont.

Department of Transport, Meteorological Branch, Toronto, Ont.

Department of Transport, Ottawa, Ont.

Department of Transport, Prescott, Ont.

Engineering Research Service, Central Experimental Farm, Ottawa, Ont.

Forest Products Laboratory, Ottawa, Ont.

Hydro-Quebec, Montreal, P.Q.

Ministry of Technology, Aeroplane & Armament Experimental Establishment,
Boscombe Down, Salisbury, England

Museum of Science and Technology, Ottawa, Ont.

National Severe Storms Laboratory, Norman, Okla., U.S.A.

Ontario Department of Lands & Forests, Ottawa, Ont.

Ontario Department of Lands & Forests, Toronto, Ont.

Ontario Provincial Government, Gasoline Tax Branch, Toronto, Ont.

Ontario Provincial Police, Perth, Ont.

Research Council of Alberta, Edmonton, Alta.

Royal Canadian Mounted Police, Ottawa, Ont.

Supreme Court of Ontario, Toronto, Ont.

United States Air Force, Wright-Patterson Flight Dynamics Group Dayton, Ohio, U.S.A.

United States Army, Paulsboro, N.J.

U.S. Department of the Navy, U.S. Naval Air Station, Patuxent River, Maryland

UNIVERSITIES

Carleton University, Ottawa, Ont.

Cornell University, Ithaca, N.Y.

Ecole Polytechnique, Montreal, P.Q.

Laval University, Quebec, P.Q.

McGill University, Montreal, P.Q.

Queen's University, Kingston, Ont.

State University of New York, Albany, N.Y., U.S.A.

University of Alberta, Edmonton, Alta.

University of British Columbia, Vancouver, B.C.

University of Ottawa, Ottawa, Ont.

University of Sherbrooke Sherbrooke, P.Q.

University of Surrey, Surrey, England

University of Toronto, Toronto, Ont.

University of Waterloo, Waterloo, Ont.